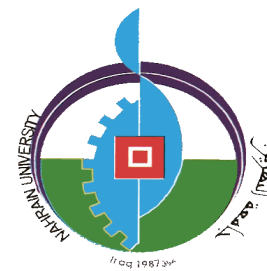Ministry of Higher Education &
Scientific Research
University of AL-Nahrain
College of Engineering

FABRICATION OF FIBER BRAGG GRATINGS USING INFILTRATED HOLLOW CORE PHOTONIC CRYSTAL FIBERS

A Thesis

Submitted to the College of Engineering of

Al-Nahrain University in Partial Fulfillment

of the Requirernents for the Degree of Master of Science

in

Laser and Optoelectronics Engineering

by

Farah Salim Hanash Ali

(B.Sc, 2014)

Rabia'a Ul-Thani   1438

January   2017

Superviser Certification

I certify that this thesis entitled **"Fabrication of Fiber Bragg Gratings Using Infiltrated Hollow Core Photonic Crystal Fibers"** was prepared under my supervision at College of Engineering / Al-Nahrain University in partial fulfillment of the requirements for the degree of **Master of Science in Laser and Optoelectronics Engineering.**

Asst. Prof. Dr. Anwaar A. Al-Dergazly

Supervisor

2 /2/2017

In view of the available recommendation, I forward this thesis for debate by the **Examining Committee.**

Prof. Dr. Bassam G. Rasheed

Head of the Laser and Optoelectronics Engineering Department

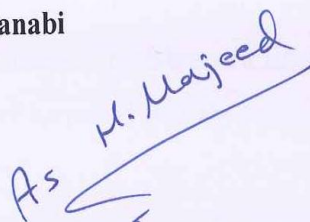5 /2/2017

Committee Certificate

We certify, as an Examining Committee, that we have read this thesis entitled "**Fabrication of Fiber Bragg Gratings Using Infiltrated Hollow Core Photonic Crystal Fibers** " and examined the student "**Farah Salim Hanash Ali**" in it's content and what related to it, and found it adequte for the standard of a thesis for the degree of **Master of Science in Laser and Optoelectronics Engineering**.

Prof. Dr. Abd Al-Hadi Al-Janabi

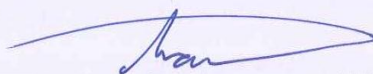**(Chairman)**

2 /2/2017

Asst. Prof. Dr. Tahreer Safa'a Mansour

(Member)

2 /2/2017

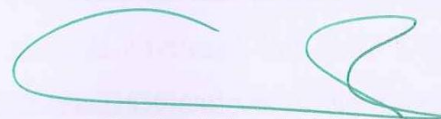**Dr.Asmaa Hameed Majeed**

(Member)

8 /2/2017

Asst. Prof. Dr. Anwaar A. Al-Dergazly

(Supervisor and Member)

2/2/2017

Approved by the College of Engineering / Al-Nahrain University

Prof. Dr. Jassim Abbood Abbas Aldabbagh

Dean of the College of Engineering

/ /2017

ABSTRACT

In this work, four fibers Bragg gratings were fabricated by infiltration different volumes of liquids (star line Glass Mechanix optical adhesive material, olive oil diluted with ethanol) into the hollow core photonic crystal fiber (HC19-1550 (Thorlab company)). The amplitude splitting interferometric technique with a high resolution specially designed translation stage was used for the fabrication process. This stage is capable of moving the fibers in micrometer resolution steps. The fabrication was carried out using blue laser operated at wavelength of 405 nm. The infiltrated four photonic crystal fibers were exposed to the blue laser beam of 405 nm forming periodic fringes for Bragg grating generation. These fringes were generated from the interference of two splitted laser beams. The fabricated Bragg fiber was about 3.8 cm in length and the average grating period was about 0.224 μm.

The four fibers were analyzed by an optical microscope which displayed the areas that were cured using blue laser. The fabricated fibers also were tested by putting laser beam at one end of the fiber and determining the transmittance at the other fiber end by optical signal analyzer (Thorlabs-CCS200). The resulted Bragg grating fibers have 653.3 nm Bragg reflected wavelength. The results also showed that fiber with higher volume of olive oil has the highest reflection peak about 96.09647 % with the greatest FWHM (full width at a half maximum) about 0.74 nm.

Three of the fabricated fibers (B, C and D) that contained olive oil were prepared for testing magnetic field sensor. The results showed that all the fibers shifted to near infrared range. The results also showed that fiber with higher volume of olive oil has the greatest magnetic wavelength shift about 653.4 nm, the highest fiber sensitivity about 0.000494623656 nm/ Gauss, the highest reflection peak about 96.91827 %, and the greatest FWHM about 0.98 nm.

List of Contents

CHAPTER FOUR: Application of Fiber Bragg Grating in Magnetic Sensing Technology

CHAPTER FIVE: Conclusions and Future Work

Notations

Symbols

NA	The numerical aperture
n_{Core}	Fiber core refractive index
n_{Clad}	Fiber cladding refractive index
$\theta_{Inc.}$	The incident angle
V	The normalized frequency
λ	Incident light wavelength
r	The core radius
Λ	The grating Period
θ	The angle between the scattering planes and the incident planes
n	Integer
$\hbar\omega_f$	The reflected radiation frequency
$\hbar\omega_i$	The incident frequency
k_i	The incident wave vector
K	The grating wave vector
k_f	The scattering radiation wave vector
π	Pi
n_{eff}	The effective refractive index of the fiber core
λ_B	The Bragg Wavelength
N	The number of grating planes
l	Bragg grating Length
$n(x)$	Index of refraction profile
Δn	The amplitude of the refractive index perturbation
x	The distance along the fiber longitudinal axis
$R(l,\lambda)_{Max.}$	The grating reflectivity
Ω	The coupling coefficient

Δk	The wave vector detuning
k	The propagation constant
$\eta(V)$	Function of the normalized frequency
λ_{UV}	The inscription UV laser beam
θ	Half the angle separation between the two beams when recombining
m	Diffracted beam orders
Λ_{PM}	The relief pattern period or phase mask period
θ_m	The angle of diffraction
θ_i	The incident angle of the UV inscription beam
h	The height of the liquid
σ	The surface tension
θ_C	The contact angle
ρ	The density of liquid
g	Acceleration gravity
r_C	The capillary radius
V_0	The velocity of the liquid in the capillary tube
η	The coefficient of viscosity
T	The time that the liquid takes to rise inside the capillary tube
V_C	Capillary tube volume
φ	The rotation angle of the polarized light
L	The path length
B	The magnetic field component
$V_{Constant}$	Verdet constant

Abbreviations

UV	Ultraviolet
HPDLC	Holographic polymer dispersed liquid crystal
LC	Liquid crystal
FBGs	Fiber Bragg gratings
NIR	Near infrared
FWHM	Full width at a half maximum
FBG	Fiber Bragg grating
PCF	Photonic crystal fiber
PCFs	Photonic crystal fibers
H_2	Hydrogen
Ge	Germanium
PMMA	Poly methyl methacrylate
mPOFs	Micro structured Polymer Optical Fibers
SI	Step index
GI	Graded index
IG-PCF	The index guided photonic crystal fiber
PBG-PCF	Photonic bandgap photonic crystal fiber
PBG	Photonic bandgap
NOA	Norland Optical Adhesives
POFBGs	polymer optical fiber Bragg gratings
POF	Polymer optical fiber
WDM	Wavelength division multiplexing
UV-VIS-IR	Ultraviolet-Visible-Infrared
PC	Personal computer
PWM	Pulse width modulation
CW	Continuous wave
TTL	Time to live
OSA	Optical signal analyzer

CCD	Charge coupled device
TMM	Transfer matrix method
DGM	Digital Gauss-meter

List of Tables

List of Figures

X

XI

CHAPTER ONE

Introduction

1.1 Introduction

The discovery of optical fibers has developed the field of telecommunications. Over the past three decades, the developments in optical fiber has certainly improved and reshaped fiber optic technology. In addition to applications in telecommunications, optical fibers are also used in the fields of fiber optics sensors, fiber lasers, and fiber amplifiers. Despite the enhancements in optical fiber manufacturing and progressions in the field in general, basic optical components have been a challenge to integrate with fiber optics, such as mirrors, wavelength filters, and partial reflectors. In recent times, all these have been improved with the ability to change the core refractive index in an optical fiber using optical absorption of ultraviolet (UV) light. This photosensitivity of optical fibers allows the fabrication of grating planes in the core of fibers. These gratings planes are obtained by permanently varying the refractive index in a periodic form along the core of the fiber. A periodic variation of the refractive index in the fiber core acts like a wavelength selective mirror that satisfies the Bragg condition i.e. it forms a fiber Bragg grating. The grating period and length of the grating, together with the strength of the variation of the refractive index, limited whether the grating had a high or low reflection over a wide or narrow range of wavelengths [1].

The first explanations of the refractive index variations in germanosilica fibers were noticed and reported by Hill and co-workers [2-3] in 1978. They designed a permanent grating written in the core of the fibers by launching it into the fiber the argon ion laser line at 488 nm. This specific grating had a very weak index variation, which was valued to be of the order of 10^{-6} causing in a narrow band reflection filter at the inscription wavelength. Photosensitivity in optical fibers remained dormant for years after its discovering it by Hill et al. [2] essentially as a

result of limitations of the fabricating technique. However, an improved interest has grown with the demonstration of the side fabricating technique by Meltz et al. [4] nearly ten years later. In the past few years, international groups achieved developments in direct optical fabrication of high quality gratings into the core of optical fibers by different techniques such as the amplitude splitting interferometry, wave front splitting interferometry, phase mask, and point by point exposure to ultraviolet laser light. Photosensitivity of optical fibers has, certainly, opened a new area in the field of fiber-optic based devices [5-7].Inventing new Bragg grating structures leads to their way in the fields of telecommunication and sensor devices.

1.2 Liquid Crystal Bragg Grating

Electrical and magnetic fields are effecting on liquid crystals and these effects have several applications , therefore it's used as Bragg grating when mixing with photo polymer phases to form holographic polymer dispersed liquid crystal (HPDLC), and HPDLC refractive index can be spatially and periodically varied. This refractive index variation offers a great promise for electrically, magnetically and optically switchable holographic devices. HPDLC structure is typically formed by using interferometric photoirradiation. This irradiation induces polymerization and subsequent phase separation in a mix of a photoreactive monomer and liquid crystal (LC). During the exposure, in the regions of the mix that receive more intense irradiation, the monomer is polymerized more efficiently, while LC molecules are pushed out into the regions that receive a smaller amount of intense irradiation. Hence, LC molecules are considered to be spontaneously oriented along the grating vector to form an LC-rich phase. When the applied external voltage goes beyond the critical voltage, LC molecules go in the same direction of the electric field and vary the refractive index [8]. Figure (1.1) shows the fabrication process of HPDLC.

2
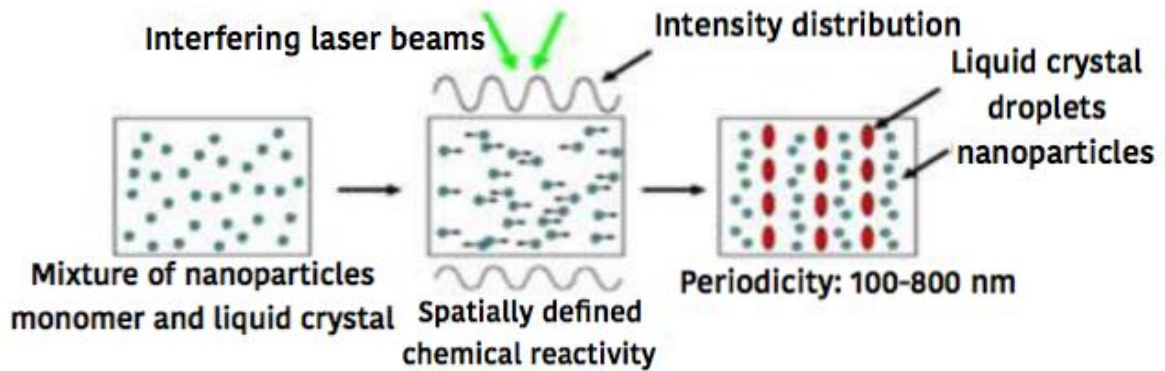
Figure (1.1): HPDLC fabrication process [9].

The strong polarization state in the diffraction grating is considered to arise from the highly ordered orientation of LC molecules in the droplets. Droplets morphology and distribution are strongly effect the orientation order of the LC molecules, particularly when the droplet dimension is some tens or hundreds of nanometres [10, 11].

1.3 Literature Survey

Several researches study fabrication techniques of fiber Bragg grating using Photonic crystal fiber and optical adhesive material and test it in sensing applications. Some of these researches are:

In 2006, E. Wikszak et. al. [12], had fabricated fiber Bragg gratings (FBGs) using a phase mask technique with near infrared (NIR) femtosecond laser pulses into a non-photosensitive Erbium doped fiber. A grating length of 40 mm with a grating period of 1.075 μm was realized. Transmission losses was measured and it's about −18.9 dB at λ=1554.5 nm with a full width at a half maximum (FWHM) bandwidth of 0.15 nm. The fiber containing the fabricated fiber Bragg grating (FBG) using pumping, fiber laser with an output power of 38 mW was possible to achieve.

In 2007, Y. Lai et. al. [13], had fabricated fiber Bragg gratings with a point by point technique by a femtosecond laser. Fiber Bragg gratings with spectral quality and first-order Bragg resonances within the C-band are realized

by optimizing the fabrication process. The birefringence about (1.2×10-4) and a degree of polarization dependent index variation are perceived in these gratings. Applications of these gratings in resonators are also demonstrated.

In 2008, **B. Guan et. al. [14]**, fiber Bragg gratings were fabricated by use of two photon ultra violet excitation and characterized for temperature responses, axial strain, and hydrostatic pressure in pure-silica polarization-maintaining photonic crystal fiber.

In 2009, **Y. Wang et. al. [15],** fiber Bragg gratings (FBGs) were fabricated in pure-silica and Ge-doped photonic crystal fibers (PCFs) with a dual-beam interference technique and a femtosecond or excimer laser. High flexibility was observed by such a technique because it allows the fabrication of FBGs for different Bragg wavelengths. Effects of H_2 (Hydrogen)-loading and Ge (Germanium) doping on the efficiency of grating inscription were investigated by determining the improvement of Bragg wavelength and attenuation in the transmission spectrum with an increased exposure dose.
H_2-loading dramatically improved the laser-induced index variation not only in Ge-doped PCFs but also in pure-silica PCFs. A reversible Bragg wavelength shift during femtosecond pulse irradiation was observed, which showed an internal temperature rise of about 77 °C.

In 2010, **Z. Zhang et. al. [16],** had fabricated fiber Bragg grating with Bragg wavelength of 962 nm in trans-4-stilbenemethanol doped poly(methyl methacrylate) polymer optical fibers by a phase mask technique with 17% zeroth-order diffraction for the fabrication wavelength of 325 nm. The zeroth-order diffraction effect of the phase masks on fiber Bragg grating in polymer optical fiber was observed by perceiving micrographs of the gratings.

In 2011, **Y. Wang et. al. [17],** had fabricated fiber Bragg gratings (FBGs) in two various types of small-core Ge-doped photonic crystal fibers with a UV laser. FBGs sensing applications were methodically investigated by means of

demonstrating the Bragg wavelengths responses to temperature, strain, bending, and transverse-loading.

In 2012, C. M. Rollinson et. al. [18], had fabricated fiber Bragg gratings using the phase mask technique. The reflectance peaks from fiber Bragg gratings have been studied to obtain the relative importance of the grating features. Spectra measurements of two different fibers with two different phase masks allowed the contribution from grating features of half the periodicity of a phase mask and of the periodicity of a phase mask at the Bragg reflected wavelength to be obtained. The dominance of the phase mask periodicity was qualified to either the small diameter of the fiber core that limited the diffraction pattern extent, or to the improved ±2 diffraction orders using a custom made phase mask.

In 2013, T. Elsmann et. al. [19], had fabricated fiber Bragg gratings with interferometer technique by femtosecond laser pulses of 400 nm wavelength. The interferometer technique for the fabrication process makes multiplexing practicable.

In 2014, I. Bundalo et. al. [20], fiber Bragg grating (FBG) had written in Poly methyl methacrylate (PMMA) Micro structured Polymer Optical Fibers (mPOFs) using UV Phase Mask technique with writing times shorter than 10 min was demonstrated. The shortest writing time was 6 minutes and 50 seconds and the longest writing time was 8 min and 50 sec. The FBGs were written in a 125 μm PMMA mPOF having three rings of holes; Bragg reflection peaks were centred at 632.6 nm and have high reflection as high as 26 dB. It also confirmed how the writing dynamics depends on the intensity of the writing beam.

In 2015, A. Engad et. al. [21], FBG using hollow core PCF filled with liquid mixture of olive oil and optical adhesive was designed and constructed using two-beam interferometric technique. Diode laser 405 nm used to write on fiber to make FBG with Bragg reflected wavelength (λ_B) of 806 nm. The optical adhesive material properties and ability to work as Bragg grating are studied too.

It concluded from these studies that Bragg grating can be fabricated in a PCF. Polymers optical adhesives after exposing to laser radiation can be used to

fabricate Bragg grating and the PCF can be filled with olive oil material as liquid photonic crystal.

In this research, FBGs will be fabricated in hollow core PCFs (HC19-1550 (Thorlab company)) filled with different volumes of liquid mixture consisting from olive oil, ethanol and optical adhesive material using amplitude splitting interferometric technique, and then testing these PCFs for magnetic sensing application.

1.4 Aims of the Project:

This project aims to:

- Design and construct a liquid crystal fiber Bragg grating.
- Study the application of the fabricated fiber Bragg grating for magnetic sensing technology.

CHAPTER TWO

Theory of Fiber Bragg Grating

In this chapter, several basic concepts of optical fibers, photonic crystal fibers, fiber Bragg gratings principles are introduced. The photosensitivity in polymers, fiber Bragg grating fabrication techniques, olive oil, capillary action and FBG magnetic field sensor are then conducte.

2.1 Optical Fibers

An optical fiber is a cylinder shaped dielectric waveguide. The fiber consists of a core with an index of refraction n_{Core} and a surrounding cladding layer with an index of refraction n_{Clad} (Figure 2.1). If the refractive index of the core is larger than the refractive index of the cladding material, the light will be guided in the fiber core as a result of total internal reflection at the core cladding interface. The numerical aperture NA, which is the acceptance angle of the fiber, is defined by these two indices, and it is given by :

$$NA = \sqrt{n_{Core}^2 - n_{Clad}^2} \qquad\qquad 2.1$$

If the incident angle ($\theta_{Inc.}$) is within the NA, light coupled into the fiber core is guided . If the incident angle ($\theta_{Inc.}$) is larger, then the light ray will leave the core of the fiber into the cladding.

$$NA = n_{Core} \times sin\,\theta_{Inc.} \qquad\qquad 2.2$$

Core and cladding boundary may either be abrupt, in step index (SI) fiber, or gradual, in graded index (GI) fiber.

As a waveguide, the optical fiber supports one or more transverse modes by which light can be directed along the fiber. Modes number (or the mode volume) is related to the normalized frequency,V, which is a measure to know if the fiber is

7

single mode fiber ($V < 2.405$) or multimode fiber. The V number is given by equation 2.3 [22]:
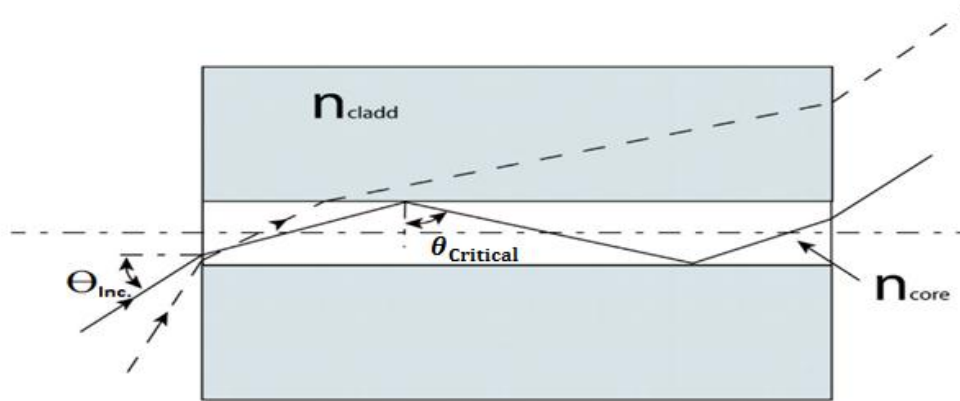
Figure (2.1): Fiber Principles [22].

$$V = \frac{2 \times \pi \times r}{\lambda} \times NA \qquad\qquad 2.3$$

where λ is incident light wavelength, r is the core radius.

2.2 Photonic Crystal Fiber

Photonic crystal fiber is distinguished by a periodic arrangement of air holes along the fiber length, centred either on a solid core called index guiding photonic crystal fiber (IG-PCF) or a hollow core called photonic bandgap photonic crystal fiber (PBG-PCF). The main difference between conventional fibers and PCFs depends on the fact is that the PCFs waveguide properties are not from spatially varying glass composition like in conventional fibers, but from very tiny arrangement and closely spaced air holes which directed through the whole fiber length. In contrast with conventional fibers, PCFs can be prepared of a single material and have some geometric parameters that can be manipulated presenting large design flexibility. Moreover, these PCFs present also the opportunity of light guiding in a hollow core, opening new viewpoints in fields for instance fiber lasers, nonlinear fiber optics, particle guidance, supercontinuum

8

generation, and fiber sensors. So, there is a high concentration of the scientific community on using PCFs in different field [23].

The main difference between PCFs types is that IG-PCF has a solid core that is surrounded by micro structured periodic air holes in the clad of the fiber. These air holes decrease cladding refractive index. IG-PCF guides the light in the solid core by total internal reflection like the conventional fibers as shown in figure (2.2 a). In PBG-PCF the light guided in the hollow core that is surrounded by a micro structured periodic cladding based on a photonic bandgap (PBG) effect which make the core refractive index lower than the cladding refractive index as shown in figure (2.2 b) [24] .
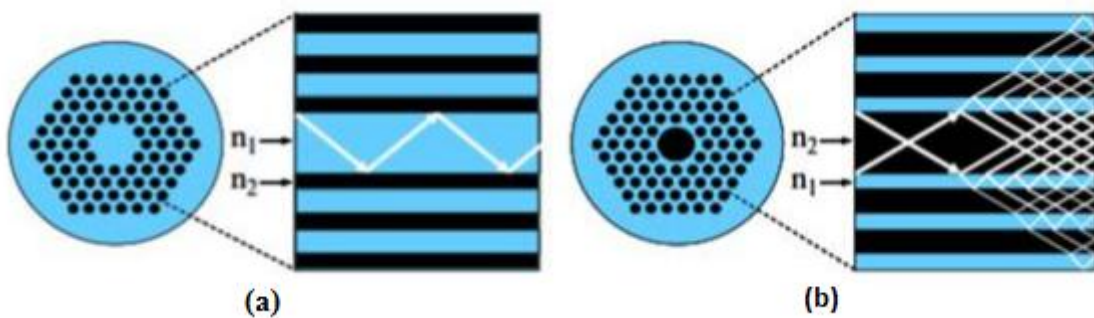
Figure (2.2): (a) solid core PCF, (b) hollow core PCF [25].

2.3 Fiber Bragg Gratings Principles

Gratings in a fiber are fabrication result of periodic perturbations within the fiber core. The perturbations known as grating planes are generally formed by exposing the fiber core to a UV light interference pattern, which increases the core refractive index (n_{Core}) at the points of exposure. In the simplest form, the grating planes are perpendicular to the fiber length and have a constant grating period as the assumption is made and it's shown in figure (2.3) [26].

9
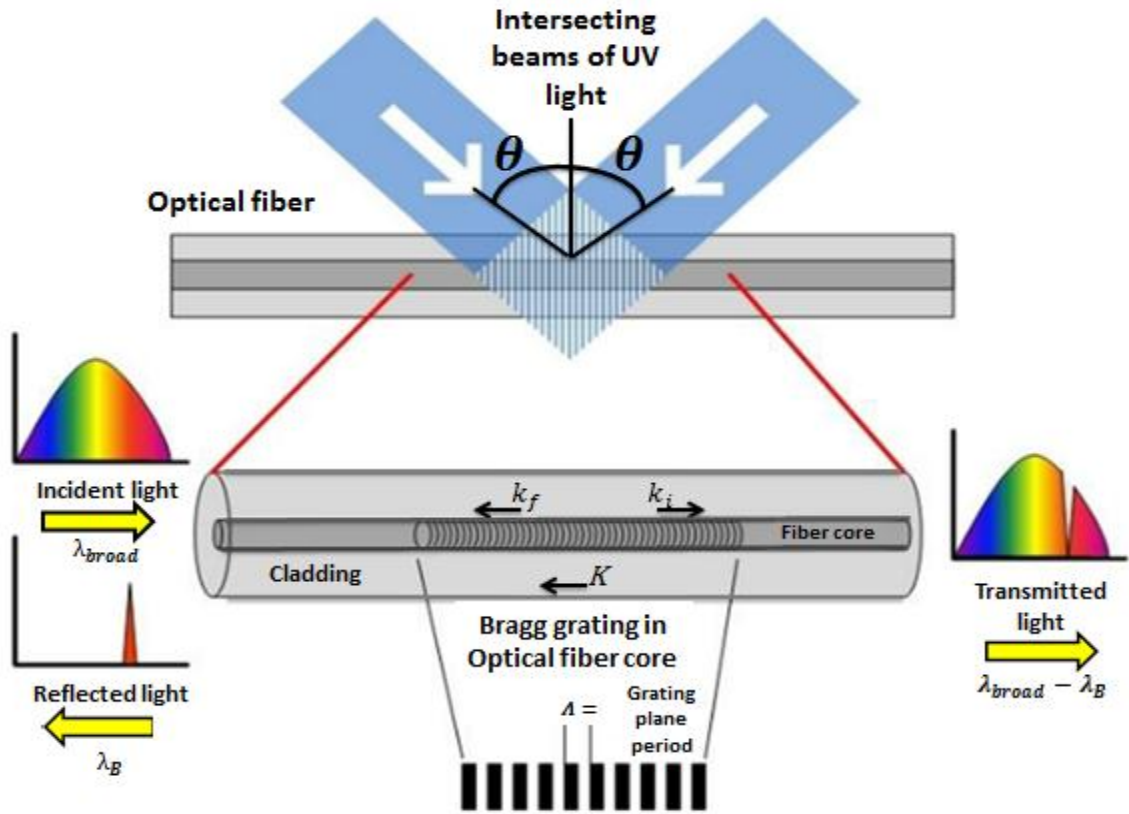
Figure (2.3): Illustration of uniform Bragg grating inside a fiber [27].

Phase match between the incident light that is directed along the fiber and the grating planes is required in order to reflect the light back within the core of the waveguide along counter propagating modes to meet the Bragg condition and it's defined by equation 2.4 [26]:

$$2 \times \Lambda \times sin\theta = n \times \lambda \qquad\qquad 2.4$$

where Λ is the grating planes period, θ is the angle between the scattering planes and the incident light , n is an integer and λ is the incident light wavelength.

No reflection from the Bragg grating can be detected, if the Bragg condition is not met i.e. the incident irradiation light is out of phase with the grating planes. However, if the Bragg condition is satisfied, the light that is reflected from each grating plane is in phase and constructively interferes, as a result together are added in a reverse backwards way to the incident irradiation light generating a reflected back signal called reflected Bragg response. This reflected Bragg response has a

10

center wavelength known as the Bragg reflected wavelength (λ_B) that is identified by the Bragg grating parameters. The grating planes are shown in the illustration of figure (2.3) as steps of index variation; however a factual illustration would look like nearer to a sinusoidal variation of refractive index along the waveguide core. The Bragg condition is met if energy and momentum is preserved. Energy preservation ($\hbar\omega_f = \hbar\omega_i$) needs that the reflected radiation frequency to be equal to the incident frequency. Momentum preservation requests that the summation of the incident wave vector (k_i) and the grating wave vector (K) is equivalent to the scattered radiation wave vector (k_f) as given in equation 2.5 [26]:

$$k_i + K = k_f \qquad\qquad 2.5$$

When the grating wave vector (K) is perpendicular to the grating planes, then it will be equivalent to $2 \times \pi / \Lambda$. Incident wave vector and diffracted wave vector are the same in the magnitude but reverse in the direction, so the momentum preservation condition will be as follow [26]:

$$2 \times \left(\frac{2 \times \pi \times n_{eff}}{\lambda_B} \right) = \frac{2 \times \pi}{\Lambda} \qquad\qquad 2.6$$

Equation 2.6 is simplified to give Bragg condition for the first order as follow:

$$\lambda_B = 2 \times n_{eff} \times \Lambda \qquad\qquad 2.7$$

Where λ_B is the Bragg wavelength, which is the center wavelength of the reflected response and n_{eff} is the effective refractive index of the fiber core along Bragg grating length [26].

Equation 2.8 is used to obtain the number of grating planes N [28]:

$$N = \frac{l}{\Lambda} \qquad\qquad 2.8$$

where: l is Bragg grating length.

For a uniform FBG inscribed in the optical fiber core with a index of refraction n_{eff}, the index of refraction profile $n(x)$ is given as follow [29]:

$$n(x) = n_{eff} + \Delta n \ cos \left(\frac{2 \times \pi \times x}{\Lambda} \right) \qquad 2.9$$

where Δn is the amplitude of the refractive index perturbation and x is the distance along the fiber longitudinal axis. The grating reflectivity with constant amplitude modulation and period can be described as follow [29]:

$$R(l, \lambda)_{MAX.} = \frac{\Omega^2 \ \times \ sinh^2(s \times l)}{\Delta k^2 \ \times \ sinh^2(s \times l) \ + \ s^2 \ \times \ cosh^2(s \times l)} \qquad 2.10$$

where $R(l, \lambda)_{MAX.}$ is the reflectivity, which is a function of Bragg grating length l and incident light wavelength λ, Ω is the coupling coefficient, $\Delta k = k - \pi/\lambda$ is the wave vector detuning, $k = 2 \times \pi \times n_{eff}/\lambda$ is the propagation constant, and $s = \sqrt{\Omega^2 - \Delta k^2}$. The coupling coefficient Ω for the sinusoidal variation of index perturbation along the fiber longitudinal axis has been found as follow:

$$\Omega = \frac{\pi \ \times \ \Delta n \ \times \eta(V)}{\lambda} \qquad 2.11$$

where $\eta(V)$ is a function of the normalized frequency V of the optical fiber that represents the fraction of the fiber mode power contained in the fiber core, $\eta(V) \approx 1 - V^{-2}$ [29]. The normalized frequency V was given previously in Equation 2.3.

At the Bragg wavelength, there is no wave vector detuning i.e. Δk equals zero, so the reflectivity becomes [29]:

$$R(l, \lambda)_{MAX.} = tanh^2(\Omega \times l) \qquad 2.12$$
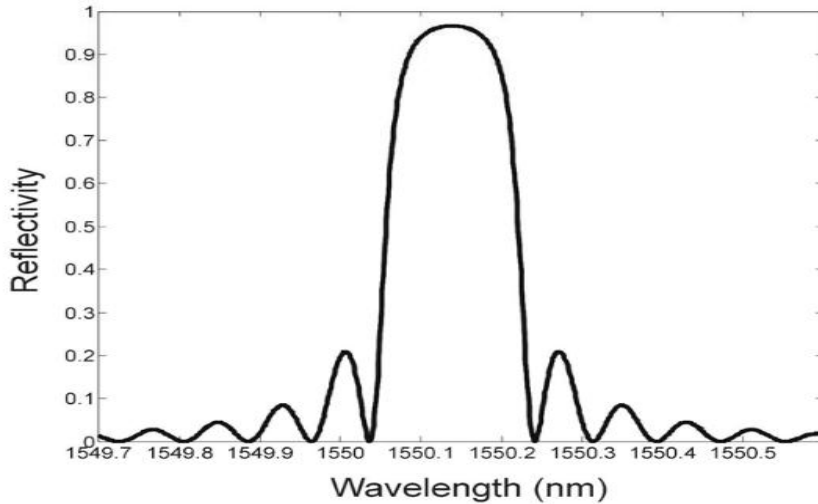
Figure (2.4): The simulation of reflection spectrum of FBG as a function of wavelength detuning [29].

The reflection increases by increasing the variation of the refractive index and Bragg grating length. A simulation of reflection spectrum of FBG as a function of the wavelength detuning is given in figure (2.4), in which the resonance side lobes are caused by multiple reflections and from opposed ends of the Bragg grating zone [29].

Inscription of Bragg grating in a highly photosensitive fiber shows an obvious transmission feature on the short wavelength side of the Bragg transmitted peak figure (2.5). This feature is noticeable in the transmission spectrum only and only the central peak is visible in the reflection spectrum, which is happen as a result of the light leaving the fiber from the side. Radiation-mode coupling as a loss mechanism on core-mode transmission has been suggested to explain this phenomenon . For the cylindrical cladding air boundary, the transmission spectrum of Bragg grating has many sharp peaks which modulate the radiation mode coupling. The energy of the light in Bragg grating will be coupled at shorter wavelengths to other modes, some will be absorbed or reflected, and the rest will leave the optical fiber. These interactions are shown in the spectrum at wavelengths that are shorter than the Bragg central wavelength as a series of several transmission dips [30-31].

13
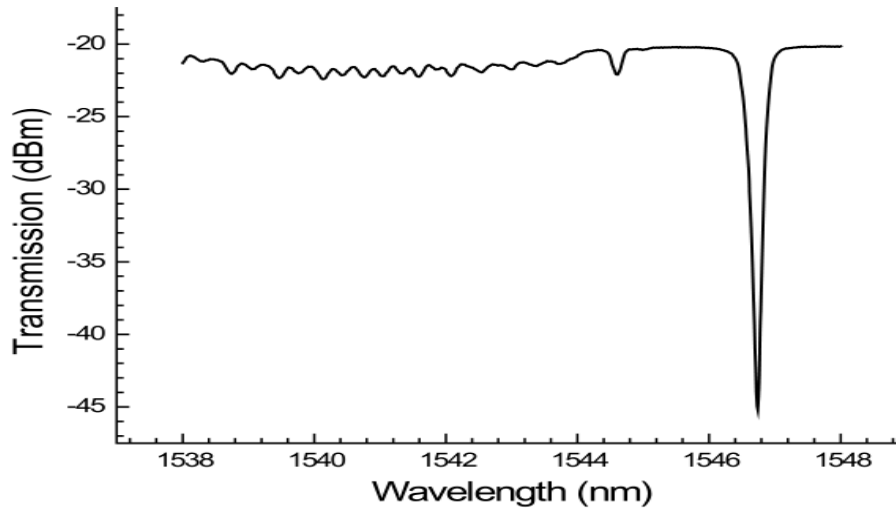
Figure (2.5): A typical FBG transmission spectrum [31].

2.4 Photosensitivity in Polymer Adhesives

The term photosensitivity refers to the variation of the optical properties when it exposed to light irradiation of specific wavelength and intensity. It can be considered in an optical fiber as a measure of the amount of the variation of the index of refraction in the core of the fiber when it exposed to light irradiation. In fibers, photosensitivity has significant importance in FBGs fabrication for telecommunications and sensors applications. Polymer Adhesives systems, which use UV light range from 315nm to 400nm or visible light range from 400nm to 460nm, to begin curing are very attractive systems to the industrialization engineers, allowing components assembly and then curing on command by exposing to the UV light. Many successful applications have been marketed for 30 years by curing of UV light [32].

Curing by UV radiation is the most effective technique for producing highly cross-linked-polymer materials. Because of the advantage of this technique in solvent free formulation gives excellent physical properties and fast reaction rates. This technology was used in many industrial applications, such as printing plates, optical fibers, electronic components and fast drying varnishes and ink [33].

14

Moreover, systems that are UV cured are based on cure polymerization adding, where by adding a cationic or free radical to a double bond of carbon-carbon or ring of an oxirane, this chain reaction leads to the polymer generation. Crosslinking reaction is rise by the combination of multifunctional and monofunctional monomers, which contribute to the strength formulations and heat resistance. In photoinitiators compounds adding case, UV light cure consists from a polymerization of multifunctional monomers that are transformed to a polymer network (tridimensional) as stated as in next reaction scheme (2.6) [34]:
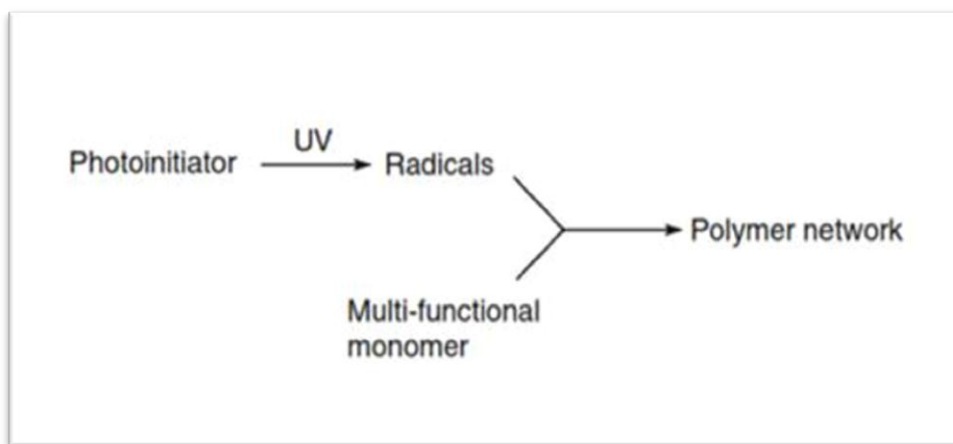
Figure (2.6): UV light cure in case of photoinitiators compounds adding [34].

In order to absorb UV light and make splitting in the reactive species, a photoinitiator was used (free radical or protonic acid), which initiated a reaction of the crosslinking polymerization respectively consistent with a cationic or radical mechanism [34].

The steps of chain termination and propagation basically will be similar in the polymerization when radicals or ions initiating have been produced, except for the larger initiation rate that is produced using UV intense light. A liquid polymer resin could convert within a fraction of a second into a solid polymer. UV curing technology has a unique advantage which is providing an accurate control of the setting process temporally and spatially, which will occur on order, in the illuminated areas selectively [35]. Figure (2.7) shows two types of photoinitiator .

Radical photoinitiation

Cationic photoinitiation
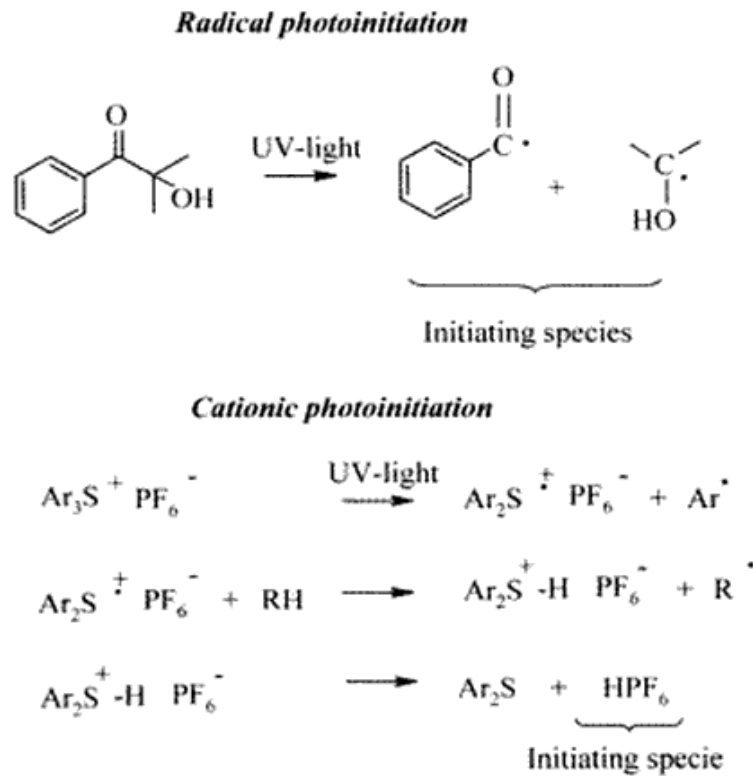
Figure (2.7): Free cationic and radical photoinitiators and their activation reaction [36].

UV irradiation curing adhesives, which are used for glass to glass bonding, have several types such as Norland Optical Adhesives type NOA 68, NOA 72, NOA 74, CF-thin Poly-Lite windshield resin type, star line Glass mechanix type and DYMAX. These polymers adhesives can be used for fabricating photonic crystal Bragg grating [37] by mixing two different materials of different quantities for example liquid-crystal material mixed with polymer adhesive material [38] this is done in order to get large variation in refractive index between the mixed materials.

2.5 Fiber Bragg Grating Fabrication Techniques

This section refers to the different methods of fabricating FBGs; all were first applied in silica fiber. The fabrication methods can be classified as two classes:

internally inscription and externally inscription methods. Because of the impracticalities, the internal inscription method is not usually active . It is presented first owing to its importance in the history of FBGs. Then, externally inscription methods will be detailed later, externally inscription methods such as amplitude splitting interferometry, wavefront splitting interferometry, phase mask and point by point inscription. Externally inscription methods are considered a practical method to design FBGs; the practicality of each method is explained for polymer optical fiber Bragg gratings POFBGs inscription [27].

2.5.1. Internally Inscription FBGs Technique

This technique demonstrated the fabrication of internally inscription FBGs by Hill et. al. in 1978 [2-3]. The periodic variations were made by directing a single mode laser argon ion type operating at 488 nm or 514.5 nm wavelengths, into fiber core made of germanium doped with silica. The laser directed through the fiber core interfered with 4% of reflected backword light from the other end of the optical fiber. A standing wave within the fiber core is formed due to the interference. At the high intensity of the laser interference pattern, the index of refraction of the fiber core was eternally varied and then created periodic variations of the index of refraction along the fiber. Internally FBG inscription isn't a useful solution mainly in polymer optical fiber (POF). Reflected Bragg wavelength will be limited only to the inscription wavelength, so in the case of fabrication of fiber Bragg grating in POF, Bragg reflected wavelength will be approximately 325 nm. So, the absorption of the polymer at this wavelength will limit the transmission of laser light into core to a few centimetres consequently avoiding any practical fabrication of fiber Bragg grating in POF by this method. Experimental setup of single beam internal technique is shown in figure (2.8) [3].
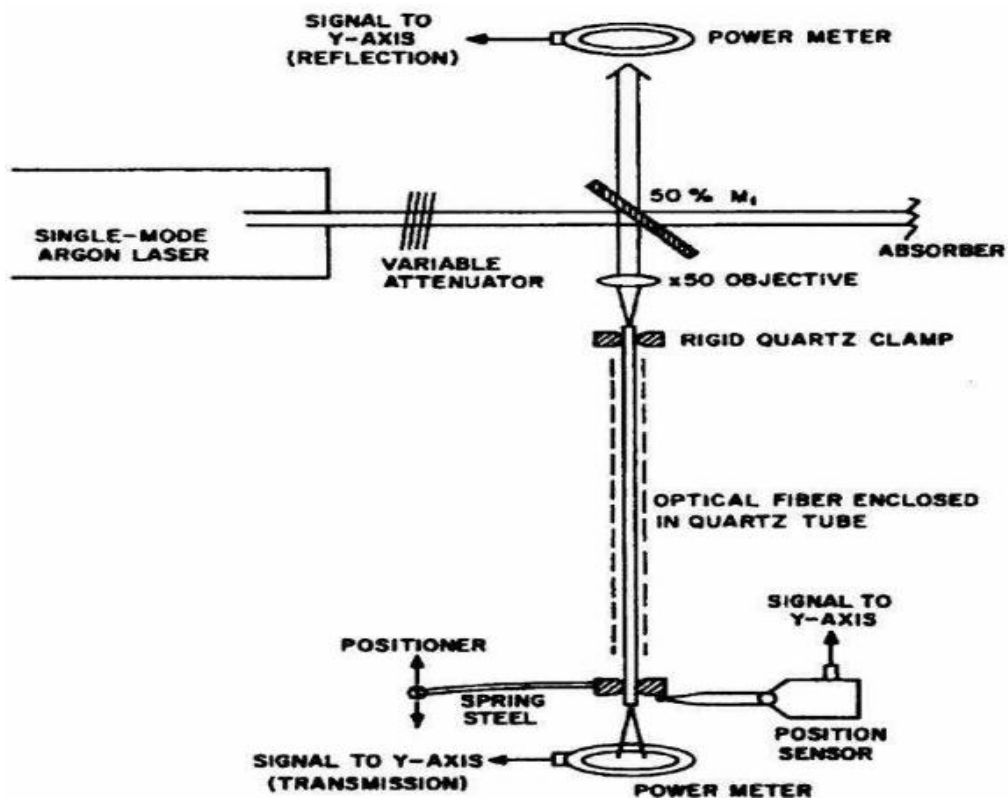
Figure (2.8): Experimental setup of single beam internal technique [3].

2.5.2. Externally Inscription FBGs Techniques

To produce a FBG in silica or POF, a periodic variation of the index of refraction is necessary along the core of the optical fiber, frequently formed optically by an interference pattern. Although in recent times the periodic variation of the refractive index also has been fabricated with pulsed type laser which produce each grating plane separately. There are four various externally fabrication techniques of FBGs: amplitude splitting interferometry, wavefront splitting interferometry, phase mask inscription and point by point inscription [27].

2.5.2.1 Amplitude Splitting Interferometry Technique [4]

This technique was first used by Meltz et. al. who proved FBG fabrication results when the fiber exposed with UV interference pattern vertically on its axis. This fabrication was done as a result of splitting the UV inscription beam into two equal intensity UV beams, and these two UV beams recombined generating UV interference pattern. Then this interference pattern was focussed using a cylindrical lens into the fiber core , using a cylindrical lens effect on increasing the pattern intensity and this improves the fabrication.

Figure (2.9) shows an example of typical amplitude splitting interferometer technique. In this figure UV laser beam is guided to a beam splitter, this will split the UV laser beam into two equal intensity laser beams. Both are reflect by the mirrors and heading for the fiber core where the two UV beams are recombined. This leads to formation of UV interference pattern in the core of the fiber. At the high intensity of this pattern, the index of refraction of the core of the optical fiber is permanently varied, thus forming Bragg grating planes.
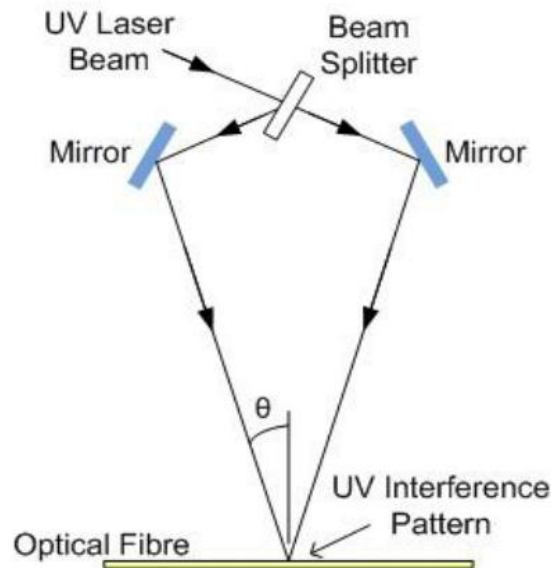
Figure (2.9): A typical arrangement of amplitude splitting interferometer technique [27].

19

The period (Λ) between the grating planes is known via the inscripting laser wavelength (λ_{UV}) and half the angle separation (θ) between the two recombining UV laser beams and it's given as follow:

$$\Lambda = \frac{\lambda_{UV}}{2 \times \sin(\theta)} \qquad\qquad 2.13$$

Combining Equation 2.7 and Equation 2.13 the Bragg wavelength (λ_B) of the fabricated FBG can be known via the inscription laser wavelength (λ_{UV}) and half the angle separation (θ) between the two recombining UV laser beams and it's given as follow:

$$\lambda_B = \frac{n_{eff} \times \lambda_{UV}}{\sin(\theta)} \qquad\qquad 2.14$$

The choice of the UV inscription laser beam is known by the photosensitivity of the used fiber core (silica or polymer). This inscription wavelength is restricted to a small region of the UV wavelength range, which limits its control on the Bragg reflected wavelength (λ_B). This makes half the angle separation between the two recombining UV beams (θ) controls the Bragg reflected wavelength (λ_B). This feature has no limit and can be used to determine the Bragg reflected wavelength which considered as advantage when this technique is used. The disadvantage of this technique is the susceptibility of the optical components to mechanical vibrations . Any slightest movements of the optical components could effect on the generated interference pattern of the two recombining UV laser beams, causing a poor quality response of FBG.

2.5.2.2 Wavefront Splitting Interferometry Technique

This technique has two typical arrangements shown in figure (2.10) for FBGs in optical fibers: the prism interferometer arrangement [39] and the Lloyd's mirror interferometer arrangement [40].

The principle of this technique is as follow, if a UV collimated beam is incident on any reflective surface like a prism edge or a mirror, thus half of the beam is reflected through the incident beam path. Interference occurs in the region where both the reflected beam and unreflected beam are interfering by overlapping. The fringe pattern generated from the interference is focused by a cylindrical lens to the fiber core. Using this technique makes the grating quality is affected fewer by the surrounding environment due to the reduced optical components used in this system this will lead to the reduction of the optical path when using this technique. It is easy to fabricate FBG at a tuneable wavelength; nevertheless the tuneable wavelength range limited by the used interferometric arrangement. Additionally, the length of the fabricated Bragg grating with this technique is limited to the half of the incident UV laser beam width.
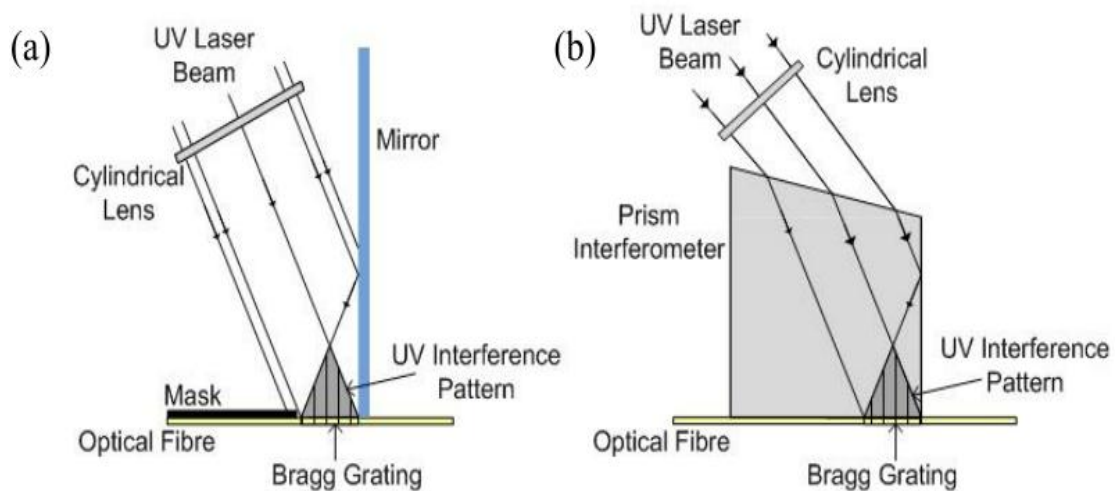
Figure (2.10): (a) Lloyd's mirror wavefront splitting interferometer technique arrangement (b) prism wavefront splitting interferometer technique arrangement [27].

2.5.2.3 Phase Mask Technique

It's a very common technique as a result of the high dependability and simplicity of FBGs fabrication. This technique was first reported in 1993[41-42] and since that time has exceeded the amplitude and the wavefront splitting interferometry techniques. This technique involves of launching an inscription UV laser into a phase mask (which is a single diffracting optical element), this results in the formation of an interference fringe pattern similar to that obtained in previous techniques.
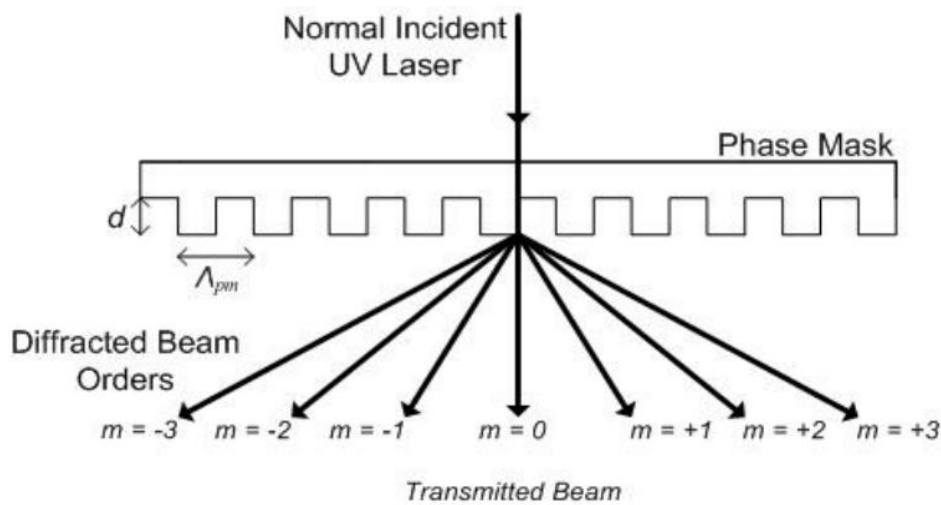
Figure (2.11): A UV laser beam launching into a phase mask, representing different orders of the splitted laser [27].

Phase mask is plate made from a fused silica; this plate is transparent to the inscription UV laser. Surface relief pattern is on one side of the mask with a square wave profile which has been impressed into the surface by electron beam lithography or holographically. When UV laser directed from the top surface of a phase mask , the light is diffracted on the bottom surface of the mask by the periodic relief pattern. The UV beam is diffracted and split into various laser beams and then these splitted beams travel in different directions, identified as orders, precisely $m = 0, \pm1, \pm2, \pm3$ and so on as presented in figure (2.11). The diffraction angle (θ_m) can be obtained for each order as follow:

$$m \times \lambda_{UV} = \Lambda_{PM} \times (sin\theta_m + sin\theta_i) \qquad\qquad 2.15$$

where (λ_{UV}) is UV inscription laser beam wavelength, (Λ_{PM}) is the relief pattern period and (θ_i) is angle of incident the UV beam to the top phase mask surface. When the incident angle (θ_i) of the UV beam is perpendicular to the top phase mask surface as presented in figure (2.11), Equation 2.15 simplifies as follow:

$$m \times \lambda_{UV} = \Lambda_{PM} \times sin\theta_m$$

$$\therefore \ \Lambda_{PM} = \frac{m \ \times \ \lambda_{UV}}{sin\theta_m} \qquad\qquad 2.16$$

While the incident angle (θ_i) is perpendicular to the phase mask the diffraction angle (θ_m) for positive orders and negative orders ($\pm m$) is equal. For FBG fabrication majority, the diffracted light is limited to the following orders $m = 0$ and ± 1. Also for FBG fabrication, the intensity pattern is produced from the diffracted ± 1 orders. Hence to maximize the intensity pattern, the zeroth order requires to be repressed. This is done through the careful design of the periodic profile of the phase mask surface relief pattern. The produced interference fringe pattern from the diffracted ± 1 orders is considered similar to that produced from the two divided beams in the amplitude splitting interferometry technique [43].

As shown in figure (2.12), the phase mask is placed parallel to the surface of the fiber as near as possible without really touching it for the protection of the phase mask surface relief pattern from damage. The pattern of the intensity is usually focussed using a cylindrical lens along the fiber core length. Like the previous techniques, the high points of the intensity of the pattern leads to a permanent index of refraction variation inside the fiber core [44].
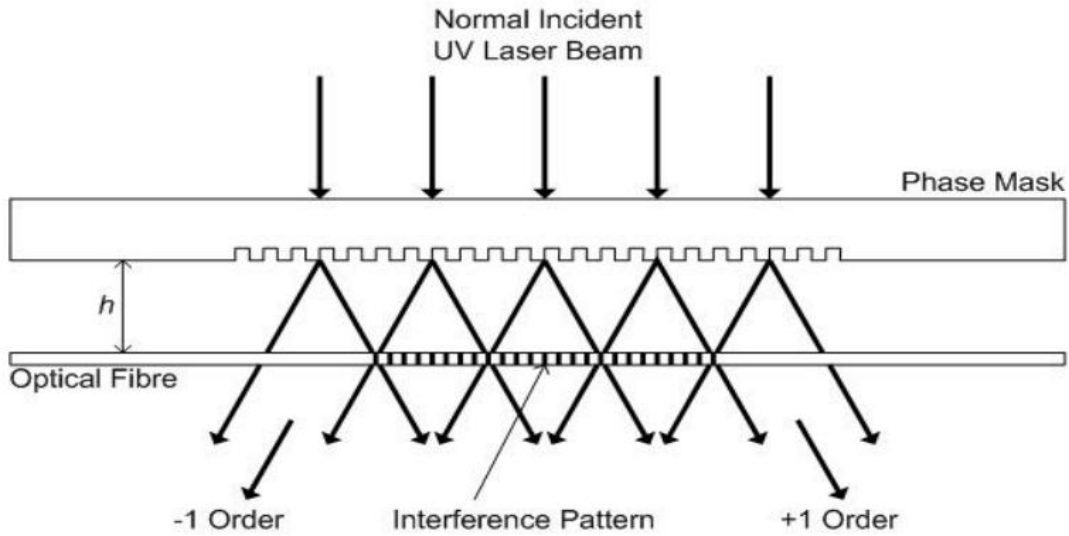
Figure (2.12): Interference pattern generated from −1 and +1 diffraction orders of the phase mask [27].

The advantage of this technique over the two previous techniques is the higher mechanical stability. Also the diffracted beams have to travel only a small distance from the relief pattern of the mask to the fiber. Moreover, the simplicity of using one optical component adds stability to this setup, at the same time it permits for a simpler and reliable technique. However, This technique has a major disadvantage which is that a new phase mask is necessary for each designed FBG with a various Bragg reflected wavelength as shown by combining Equation 2.7 and Equation 2.16, where the Bragg reflected wavelength (λ_B) is relies on the phase mask period (Λ_{PM}):

$$\lambda_B = n_{eff} \times \Lambda_{PM} \hspace{3cm} 2.17$$

This may lead to expensive tooling, mainly if wavelength division multiplexing (WDM) sensors are needed where a new phase mask would be required for each FBG with a various Bragg reflected wavelength [44].

2.5.2.4 Point by Point Inscription Technique

This technique was first described by Malo et. al. [45]. A UV pulse laser or a femtosecond laser is used to inscript grating planes separately, each step at a time along the core of the optical fiber. A single pulse light directed through a slit then it focused on the fiber core. After the refractive index is varied at the irradiation point , the fiber is translated from its original place using a precision translation stage to a distance equal to Λ, which is Bragg grating period. This process is repeated till the desired FBG fabrication is achieved. The grating parameters can be adjusted flexibly (such as grating period, grating length, etc.) which considered as advantage when using this technique. However, control accurateness of the movement of the translation stage is critical [45].

2.6 Olive Oil

Olive oil can be categorized as an organic dye compound; it has good nonlinear optical properties with high coefficient of nonlinearity, high damage threshold and good transparency at short wavelengths that candidate to be applied in nonresonant photonic applications. Olive oil is made of many organic compounds such as cholesterol, phospholipids, fatty acids, and glycolipids, which are able to act as lyotropic liquid crystal (which is one of liquid crystal determined by changing the temperature or concentration when an appropriate concentration of material is dissolved in some solvent). Therefore, these compounds are characterized by varied photonic applications [46].

2.7 Capillary Action

In the capillary action, a capillary tube is immersed into the liquid and then the liquid usually rises to a certain height in the tube. The height of the liquid in the

capillary tube is related proportionally to the surface tension and it is obtained by the formula [47]:

$$h = \frac{2.\sigma.cos\theta_C}{\rho.g.r_C} \qquad\qquad 2.18$$

where h is the height of the liquid, σ is the surface tension, θ_C is the contact angle, ρ is density of liquid, g is acceleration gravity, r_C is the capillary radius.

Maximum velocity V_0 of the liquid in the capillary tube is related inversely proportional to the coefficient of viscosity is calculated by [48]:

$$V_0 = \frac{r_C{}^2.\rho.h}{8.\eta} \qquad\qquad 2.19$$

where η is the coefficient of viscosity

The time (T) that the liquid takes to rise inside the capillary tube is obtained by:

$$T = \frac{h}{V_0} \qquad\qquad 2.20$$

Capillary tube volume (V_C) is calculated by equation (2.21):

$$V_C = \pi.r_C{}^2.h \qquad\qquad 2.21$$

2.8 FBG Magnetic Field Sensor

Fiber Bragg gratings have confirmed as highly efficient sensors for strain, temperature and chemicals. Using these primary measured secondary parameters such as acceleration [49], tilt [50], pressure [51], shear force [52], vibration [53], and chemical species [54] have been sensed. Sensing magnetic field is essential in situations such as defence, geophysics, medicine and industries. Techniques for measuring magnetic field

are search-coil magnetometer, flux-gate magnetometer, Hall-effect sensor, fiber-optic magnetometer and magnetooptical sensor [55]. Fiber optics based magnetic field sensors primarily exploit variations in the intensity, phase, polarization and wavelength of the guided electromagnetic wave as a result of the magnetic field.

Measurement of magnetic field has been established with the optical fiber using Faraday Effect [56], Lorentzian force [57], and magnetostrictive effects [58], [59], [60] in an interferometric configuration. Typically, the information encoded as the perturbed polarization state of the light is changed to intensity based data which can then be easily sensed using a photodetector. Since the Verdet constant (which is an optical constant that refer to the strength of the Faraday effect for a particular material and it can be determined using equation (2.22) [61]) of the optical fibers is small, more fiber length has to be exposed to the magnetic field when Faraday Effect sensors are used. Consequently, long fibers present birefringence (i.e., different refractive index) and increased transit time. In order to reduce the fiber length, multiple reflections [62] of the light is used.

$$\varphi = V_{Constant} \times B \times L \qquad\qquad 2.22$$

where φ is the rotation angle of the polarized light measured in (radian), L is the path length where the light and magnetic field interact measured in (meter), B is the magnetic field component in the direction of the light propagation measured in (Tesla) and $V_{Constant}$ is Verdet constant measured in (radian / Tesla . meter).

CHAPTER THREE

Experimental Preparation and Arrangement of Bragg Infiltrated Materials Inside PCFs

This chapter describes the optical properties and the experimental preparation of the liquid mixture infiltrated inside four hollow core photonic crystal fibers with different concentrations of the liquid mixture for each fiber. It also describes the experimental arrangement that is used to fabricate FBGs inside the PCFs, FBG testing setup for output detection and data recording, microscopic images of inscription PCFs, optical properties and the simulation of Bragg reflected wavelength is then presented.

3.1 Preparation for Fabrication FBG

Figure (3.1) shows the flow chart for the preparation of the infiltrated materials in order to fabricate fiber Bragg grating for four hollow core photonic crystal fibers.
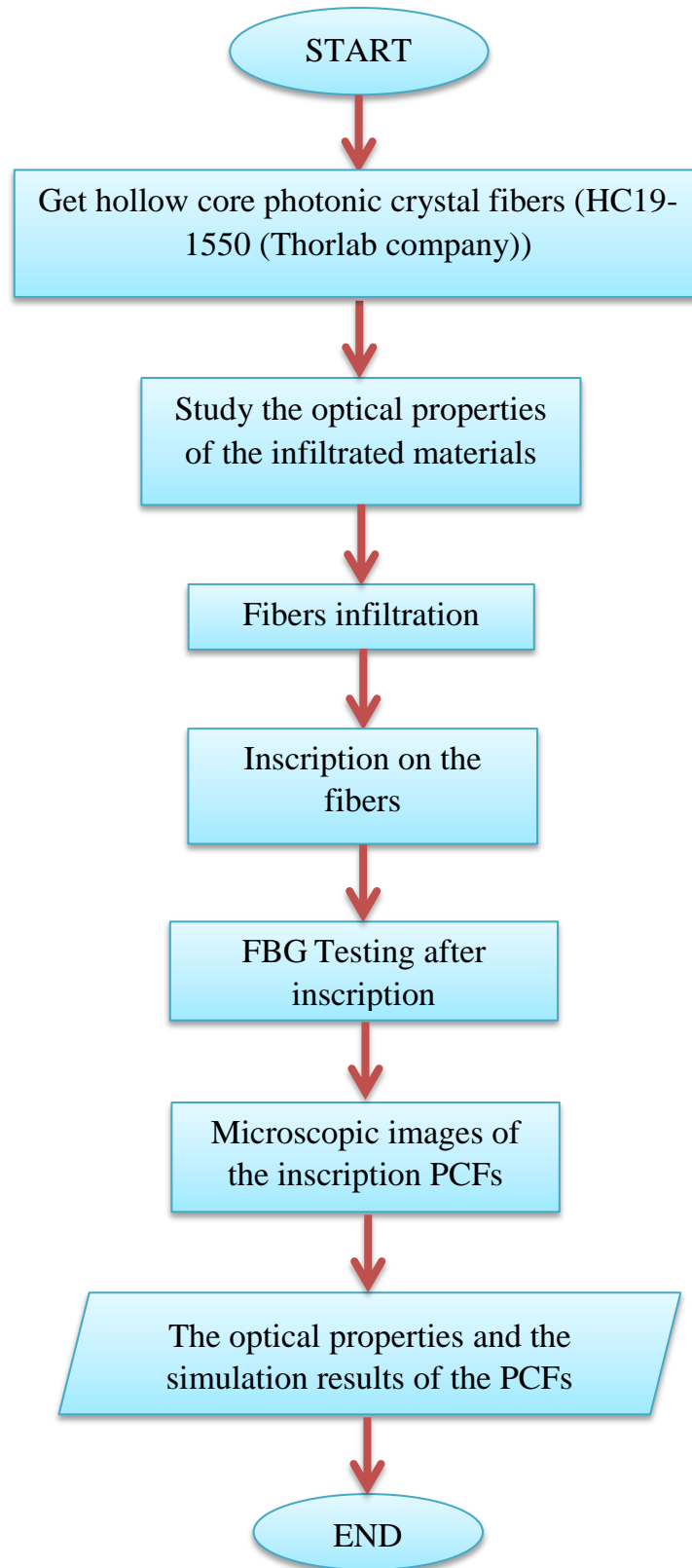
Figure (3.1): The flow chart of preparation to fabricate FBG.

29

3.2 Photo Polymer Adhesive Photosensitive Material

The key step used in this research is the chemical reaction of laser light effects on the photosensitive material (polymer adhesive material). The cure process of polymer adhesive depends on the intensity and the wavelength of the laser. This reaction causes optical variation in the properties of the adhesive material as well as in the index of refraction. The adhesive resin is in liquid state because the monomers and photoinitiators will not react chemically with each other before laser light irradiation , but when exposing to laser radiation, then photoinitiators subject to the variation process which create free radicals that is chemically react with monomers, creating chains of monomers. Monomer chains are changed to chains of cross linked polymer at the cured state. The material used in this process is star line Glass Mechanix adhesive, it is a colourless, clear liquid photo polymer adhesive and it has medium viscosity for bonding glass. This material is affected by the UV irradiation in a process termed "curing process", which is a converting process from liquid state into solid material state.

Ultraviolet-Visible-Infrared (UV-VIS-IR) spectrophotometer is used to obtain the absorption spectrum of star line Glass Mechanix adhesive material which is shown in figure (3.2).
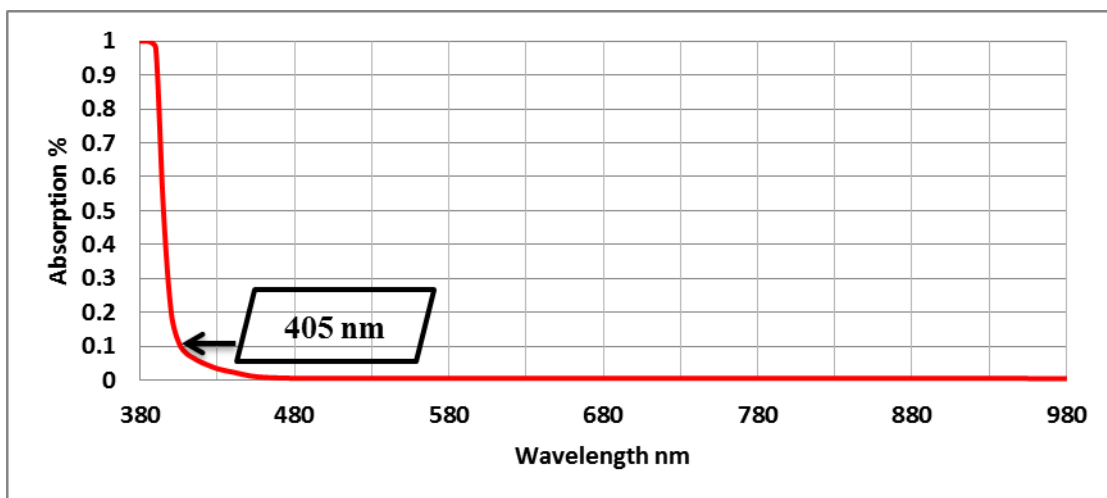
Figure (3.2): Illustrate the absorption of the polymer star line.

Figure (3.2) shows that the adhesive material star line Glass Mechanix gives maximum absorption till 385 nm wavelength. i.e. the fastest curing occurs at such maximum wavelength. Also the process of curing requires more time after 385 nm wavelength. Hence, the time of cure depends on the material absorption. So, the nearest and appropriate laser at wavelength 405 nm is usedfor the fabrication . Laser diode transmittance spectrum that used in the process of curing is given in figure (3.3).
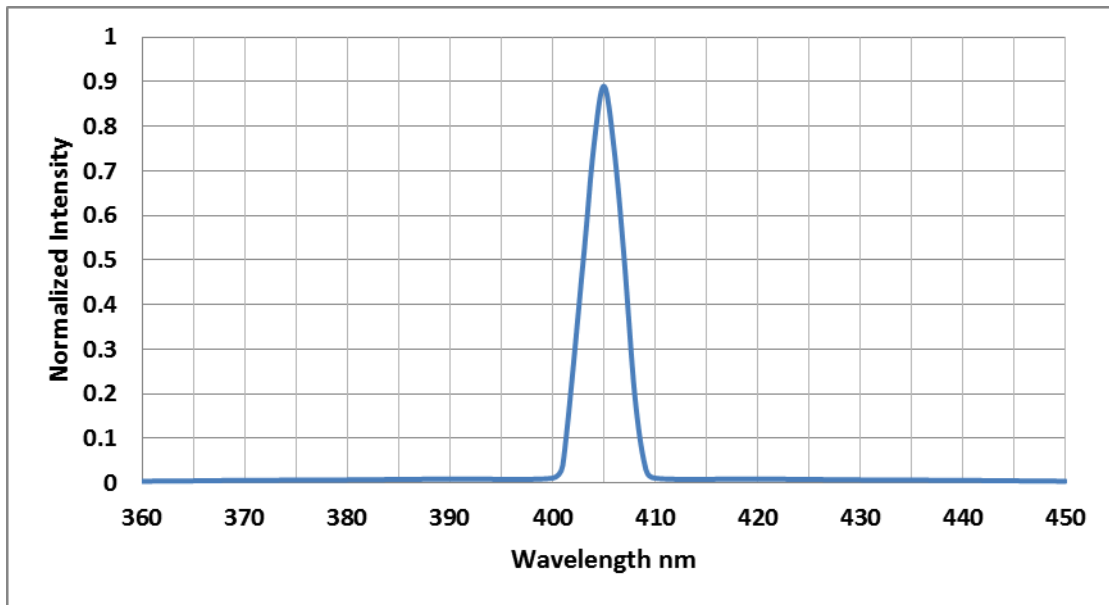
Figure (3.3): Laser diode spectrum of 405 nm.

As given in figure (3.2), the adhesive material has 10% absorption at a laser wavelength 405 nm which makes it functional in this project but it needs extra time for cure. Additionally, the star line optical adhesive has a medium viscosity.

3.3 Olive Oil

It is an organic composite, it candidates to be used in photonics applications because it has a good nonlinear optical properties [46]; It is used as a mixture with star line optical adhesive material. In this research, the type of olive oil is virgin.

UV-VIS-IR spectrophotometer is used for measuring the optical transmission of olive oil. Figure (3.4) shows olive oil transmission spectrum.
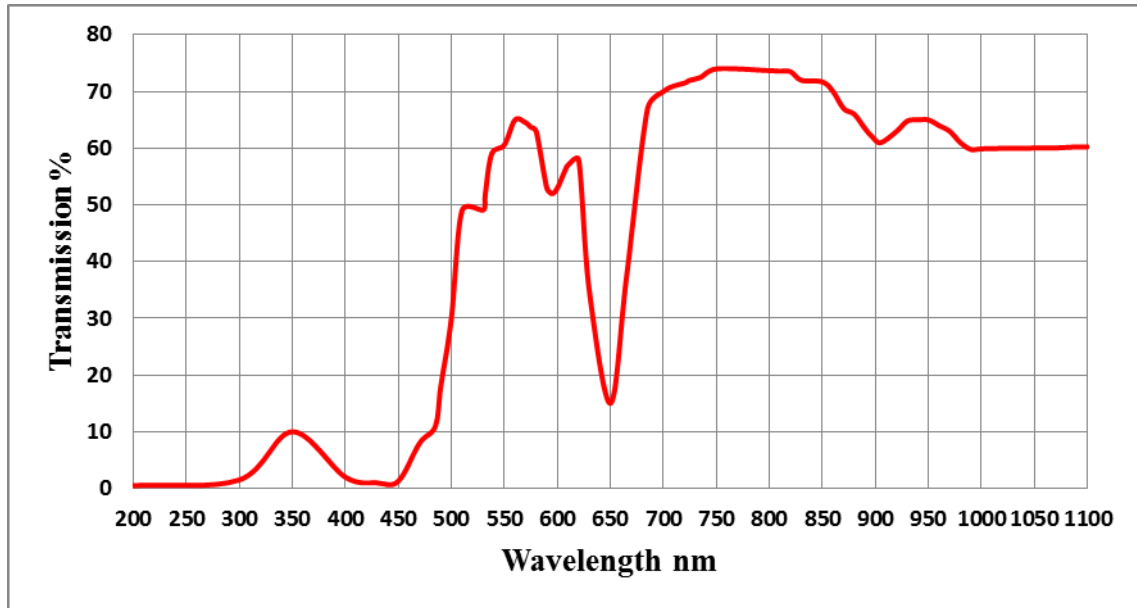
Figure (3.4): Olive oil transmission spectrum.

3.4 Fiber Infiltration

The next step after choosing the star line adhesive for making Bragg gating, a PCF (HC19-1550 (Thorlab company)) hollow core type has been used. This PCF consists of fiber core diameter about ($20\pm2\mu m$), and there are air holes surrounding this fiber core, each hole has a diameter around ($70\pm5\mu m$) and cladding diameter of ($115\pm3\mu m$) as shown in Appendix (A). Bragg grating is made by exposing the PCF (which is infiltrated with liquid mixture of adhesive material, olive oil and ethanol) to blue laser. Olive oil has higher viscosity as compared with the star line Glass Mechanix adhesive material and it must be diluted to mix with it. Therefore, ethanol is used with the liquid mixture because of the hydrophobic interactions between the hydrocarbon chains in olive oil and ethanol causes the one with higher viscosity to dissolve. The olive oil is diluted with ethanol before being added to the photo adhesive material. Capillary action technique is being used for infiltration the fiber in this research.

3.4.1 Theoretical Calculations for Infiltration Liquid Mixture Inside the Air Holes of the PCF

Theoretical calculations have been done for the infiltration of liquid mixture (olive oil, star line Glass Mechanix and ethanol) inside the optical fiber:

The density and viscosity of the liquid mixture were measured by densitometer and viscometer and are equal to (2787.114 Kg/m^3), (0.08994385604 Kg/m.s) at (20°C) respectively. Assumed that PCF core radius range from 5 µm to 25 µm (the radius of the hollow core PCF (HC19-1550 (Thorlab company)) that is used in this research equal to (10±1 µm), i.e. its within the range of the assumption), then the velocity of liquid mixture was calculated by applying equation (2.19) as shown in figure (3.5)
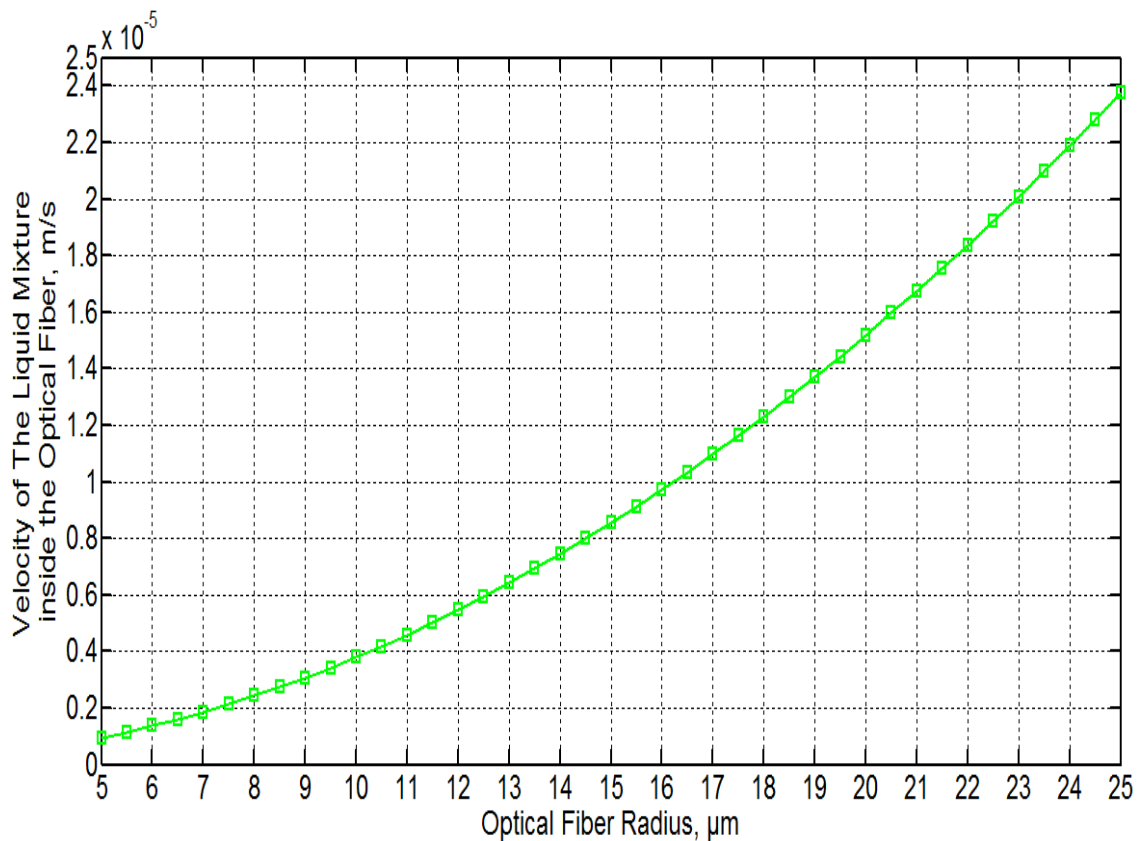
Figure (3.5): The velocity of liquid mixture inside the optical fiber.

Assuming that the height of the liquid mixture would rise from 10 cm to 50 cm, and by knowing the velocity of the liquid mixture from the previous calculations, then the time that liquid mixture takes to rise inside the optical fiber was calculated by applying equation (2.20) and is shown in figure (3.6):
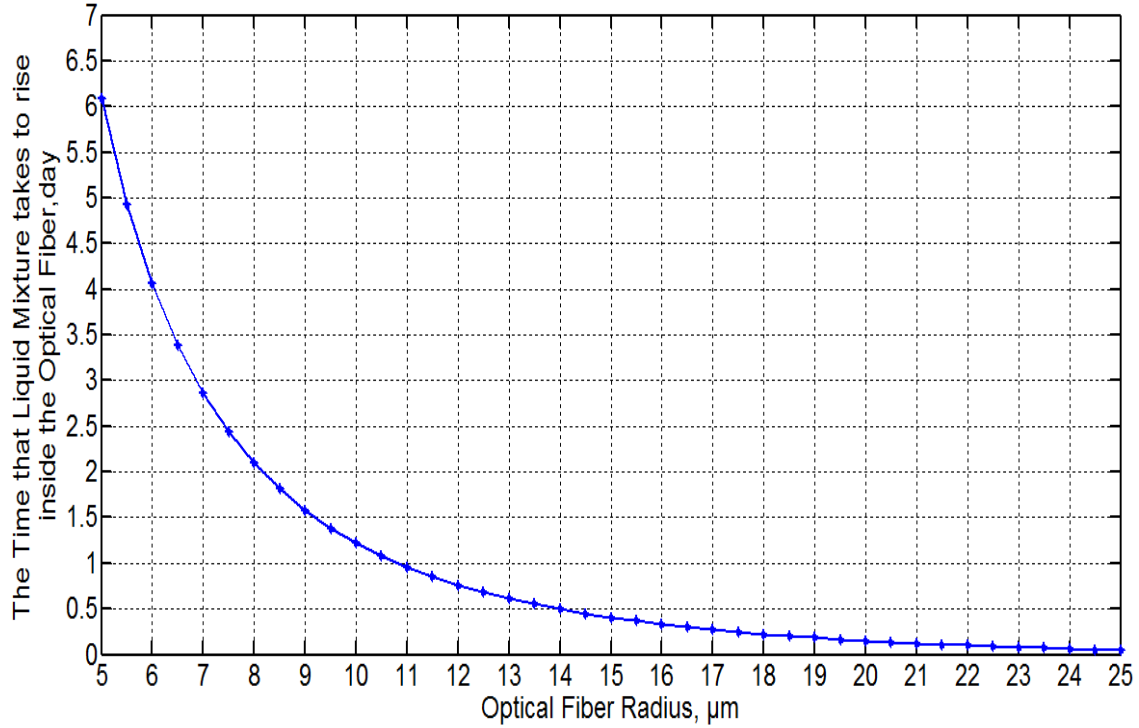
Figure (3.6): The Time that liquid mixture takes to rise inside the fiber.

In this research the average radius of the optical fiber core is equal to 10 μm and the optical fiber length (which is considered as the height of the liquid mixture inside a PCF) was choosed to be 15 cm, this length was choosed because a large angle (which separate the two interfering blue laser beams) is needed to fabricate FBG at the required wavelength. By applying equations (2.19) and (2.20), the average velocity of the liquid mixture inside this fiber is equal to (3.798260325 μm/s) and the average time that liquid mixture takes to rise inside this fiber is equal to (10.969934 hours) respectively. The average volume of the liquid mixture for this fiber was also calculated by applying equation (2.21) and it's equal to (4.71238898 * 10^{-5} ml).

Four hollow core photonic crystal fibers were used.

- **PCF (A):** was infiltrated with only star line Glass Mechanix adhesive material of volume (0.12 ml/cc).

- **PCF (B):** was infiltrated with a volume (0.12 ml/cc) of liquid mixture consists from (0.06 ml/cc) star line Glass Mechanix adhesive material, (0.03 ml/cc) olive oil and (0.03 ml/cc) ethanol.

- **PCF (C)**: was infiltrated with a volume (0.12 ml/cc) of liquid mixture consists from (0.04 ml/cc) star line Glass Mechanix adhesive material, (0.04 ml/cc) olive oil and (0.04 ml/cc) ethanol.

- **PCF (D):** was infiltrated with a volume (0.12 ml/cc) of liquid mixture consists from (0.03 ml/cc)star line Glass Mechanix adhesive material, (0.06 ml/cc) olive oil and (0.03 ml/cc) ethanol.

As it's seen the volume of the liquid mixture of four fibers is greater than the required volume because it's the smallest scale available.

3.5 Inscriptions on the Fiber

The experimental setup depends on Amplitude splitting interferometric technique, which is used to fabricate Fiber Bragg grating at Bragg wavelength ($\lambda_B = 651.3$ nm) reflected from the core of the PCF. (405 nm) blue laser will be used instead of UV laser for the fabrication process.

Half the angle separation between the interference of the two beams of blue laser 405 nm (θ) is affected by the reflected Bragg wavelength (λ_B). This wavelength is obtained theoretically using equation (2.14). Therefore, the value of (θ) between the interference of the two blue laser beams must be (65°) in order to reflect a wavelength of (651.3) nm from the core of the PCF. Figure (3.7) shows the flow chart of inscription on the fiber.
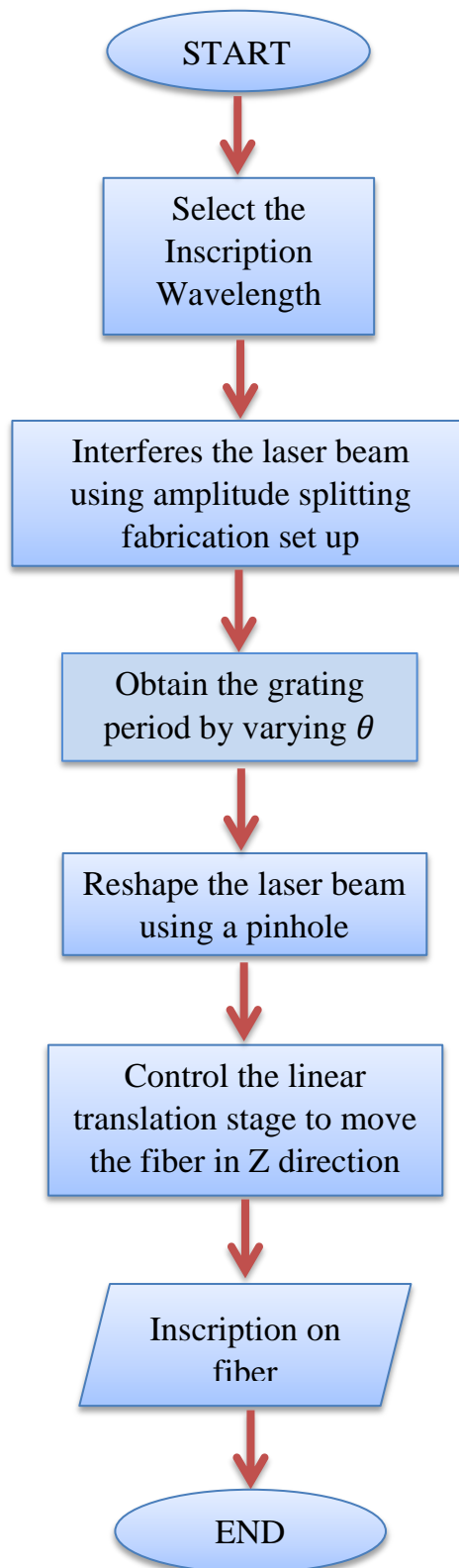
Figure (3.7): The flow chart of inscription on the fiber.

36

3.5.1 Experimental Arrangement of the Fabrication Process

The diagram for the experimental arrangement of fiber Bragg grating fabrication shown in figure (3.8) and it consisting of three parts:
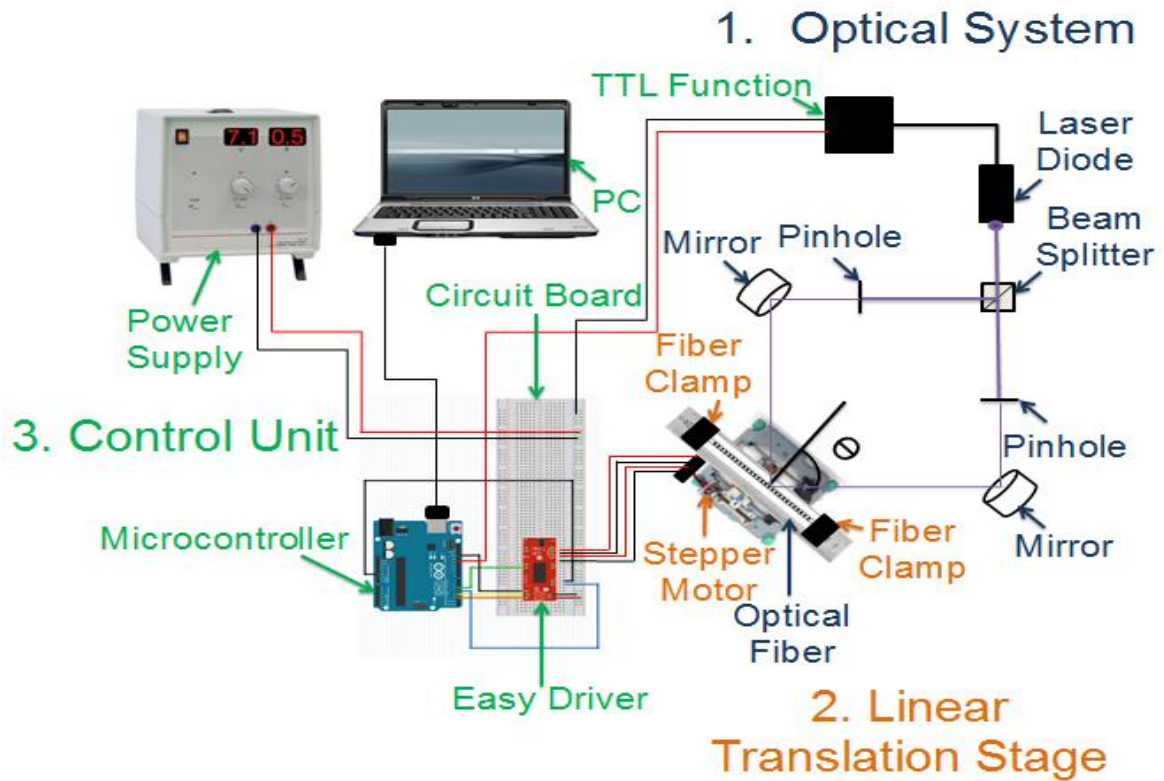
Figure (3.8): Experimental Arrangement diagram.

1. Optical system, which consists of:

− Laser diode 405 nm used for fabricating Bragg grating in the fiber.

− Beam splitter used for splitting the laser beam into two beams.

− Two pin holes used for changing laser spot shape from elliptical to circular shape.

− Two mirrors to reflect the laser beams at certain point on the fiber with specific angle (θ).

– Optical fiber, hollow core photonic crystal fiber type is used for fabricate Bragg grating inside it.

2. Linear translation stage, which consists of:

– Two fiber clamps used to hold the fiber.
– Bipolar stepper motor used for moving the fiber on a movement base in specific steps and direction.

3. Control unit, which consists of:

– Circuit board with easy driver A3967 and microcontroller used for controlling bipolar stepper motor steps and direction.
– Power supply used for supplying the circuit with power.
– Personal computer (PC) used for programming the circuit.

3.5.2 Experimental Set up of the Fabrication Process

The experimental setup of the fabrication process is classified mainly into stages: the linear translation stage, the control unit and the optical system; It will be explained later in details. The experimental fabrication setup is shown in figure (3.9).
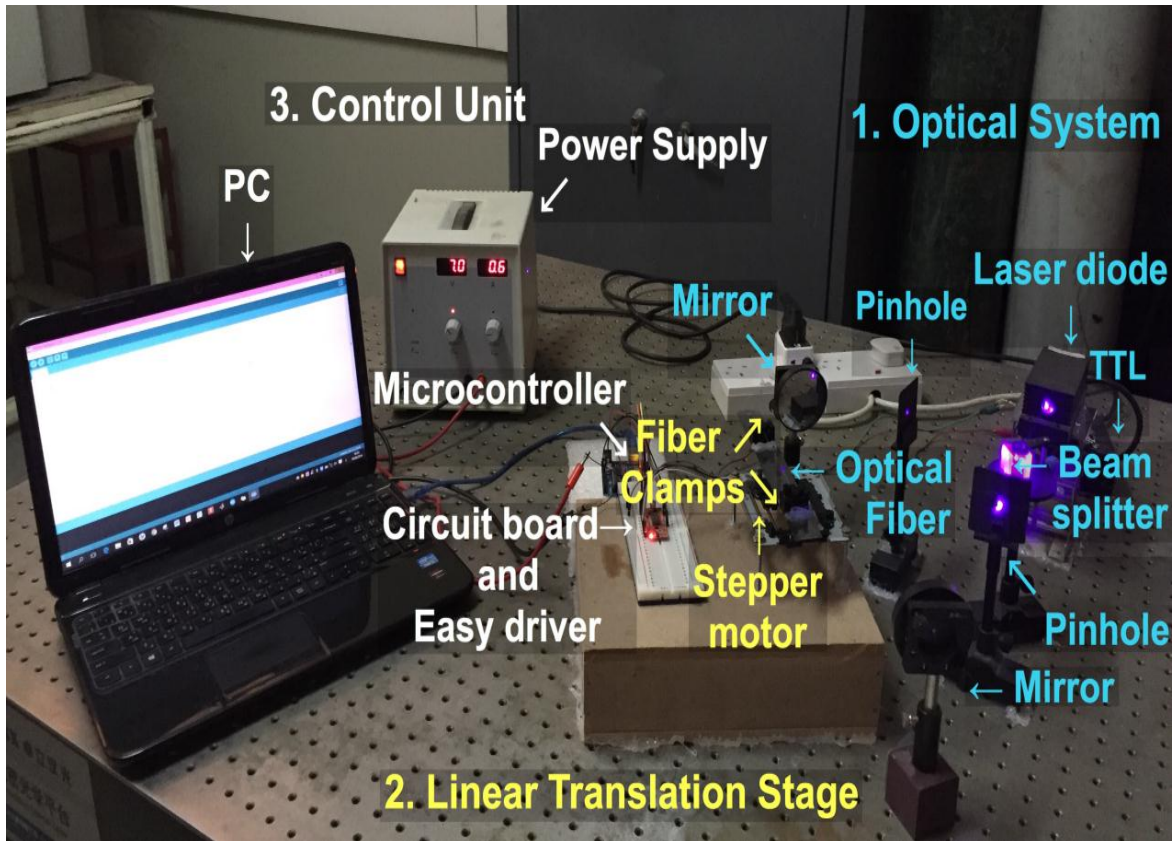
Figure (3.9): Experimental Fabrication set up.

3.5.2.1 The Optical System

This system consists of an optical source, two pinholes, two mirrors and beam splitter, as given in figure (3.10). Each component has an exceptional importance for FBG fabrication.
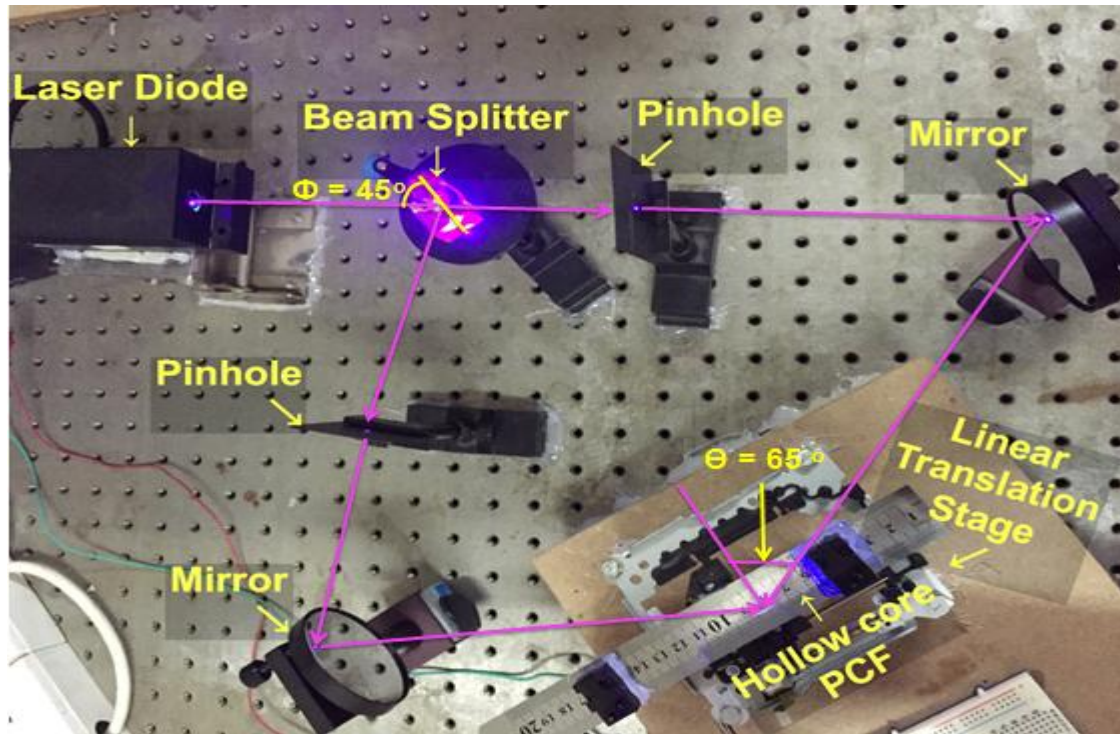
Figure (3.10): The path of the laser beam in the optical setup.

The optical source used for fabrication fiber Bragg grating is a continuous wave diode laser type (SDL-405-100T) emitting at 405 nm wavelength and 100 mW output power as shown in Appendix (B). It has a control unit used to switch it ON/OFF.

The purpose of choosing this wavelength depends on the photosensitivity of the infiltrated material inside the hollow core photonic crystal optical, i.e. this laser wavelength nearly matched the spectrum of absorption of the star line adhesive that was infiltrated in the PCF.

The profile beam of the laser diode source used has elliptical shape. So, focusing this laser beam required reshaping the laser beam into circular shape.

If the laser source is switched on, the path of the laser beam is followed through the optical elements as shown in figure (3.10).

The laser beam is directed to a beam splitter, where it is splitted into two laser beams of the same power. The beam splitter that is used has an incident angle about 45° in order to split the laser beam.

40

After that these beams are directed to a dielectric mirrors to be reflected. These dielectric mirrors control the paths of the beams by adjusting these mirrors in x and in y axes. Then, these beams are recombined and creating interference fringes pattern inside the PCF core as presented in figure (3.11).
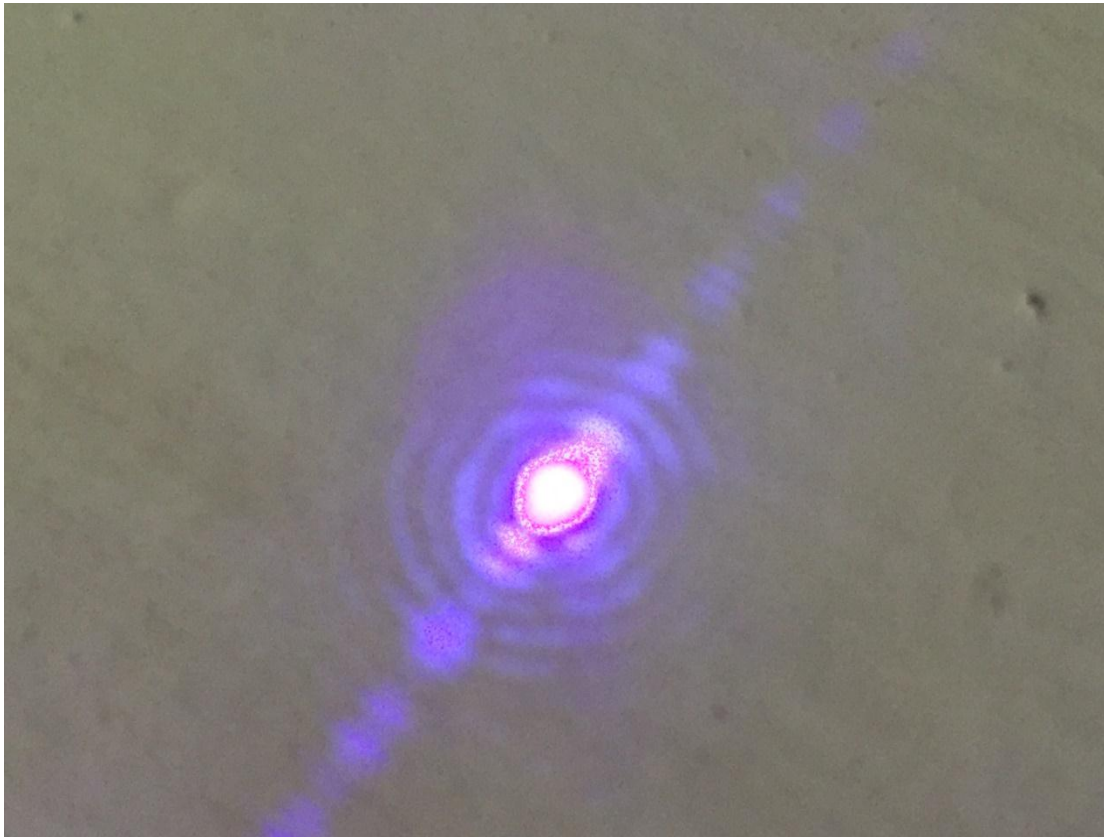
Figure (3.11): The two laser beams are interfering to make the fringes pattern.

3.5.2.2 The Linear Translation Stage

It is a stage moves linearly in z-axis only and it's consists of two fiber clamps and bipolar stepper motor as given in figure (3.12).
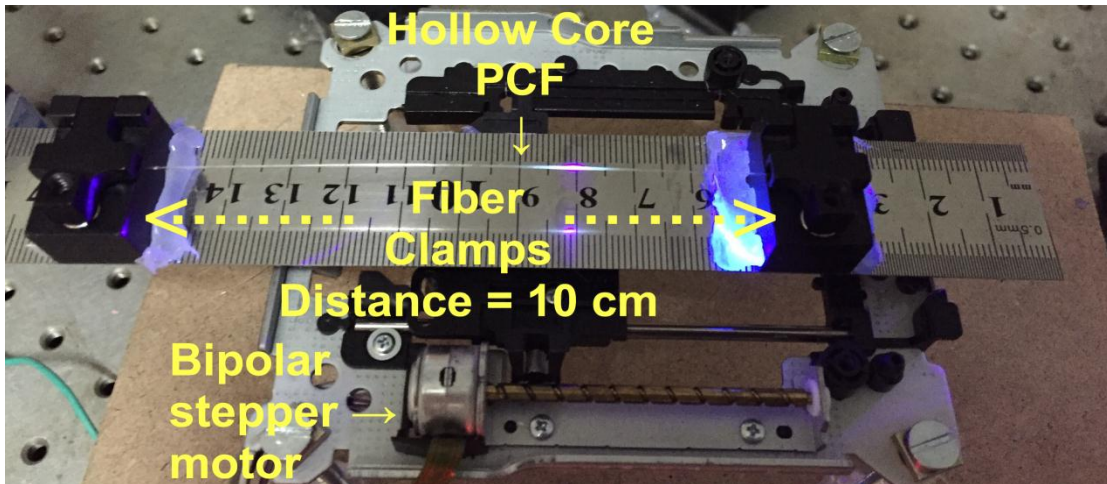
Figure (3.12): A translation stage that is moves linearly in z-axis.

The fiber is fixed on the stage and held by the fiber clamps. The distance separation between these clamps is 10 cm.

The motor used in this stage is a bipolar Micro stepper motor, its two phase four wire hybrid type, this motor requires dc voltage supplier about 4-6 volt. The motor has a 15 mm diameter with SM15DD screw type and 9 mm height. The rod diameter and length are 3 mm and 52.5 mm respectively as shown in Appendix (C). The total distance of the movable stage is 3.8 cm in one direction and the motor is moved 158 full steps to complete this distance. Motor resolution is 240 μm for each step of the stepper motor. Stepper motor is shown in Figure (3.13).
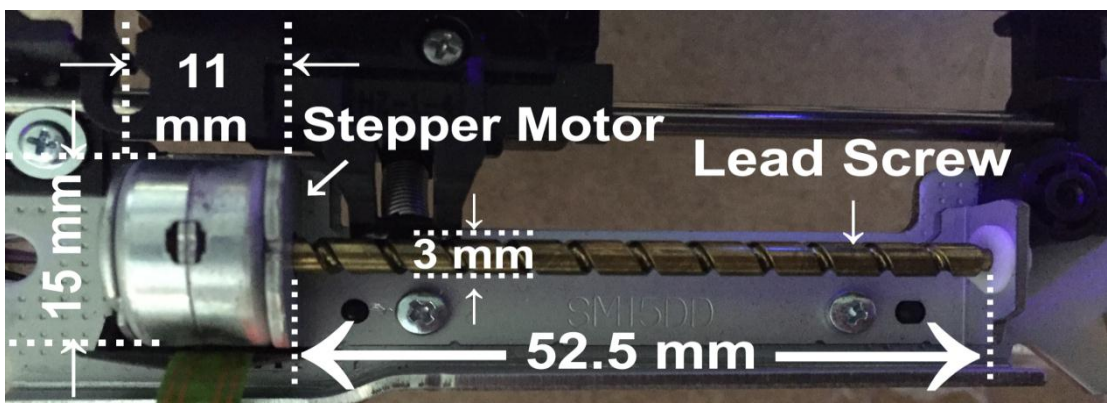
Figure (3.13): The bipolar stepper motor and the lead screw.

3.5.2.3 The Control Unit

The control unit consists of motor driver board, microcontroller board, power supply and personal computer as shown in figure (3.14).
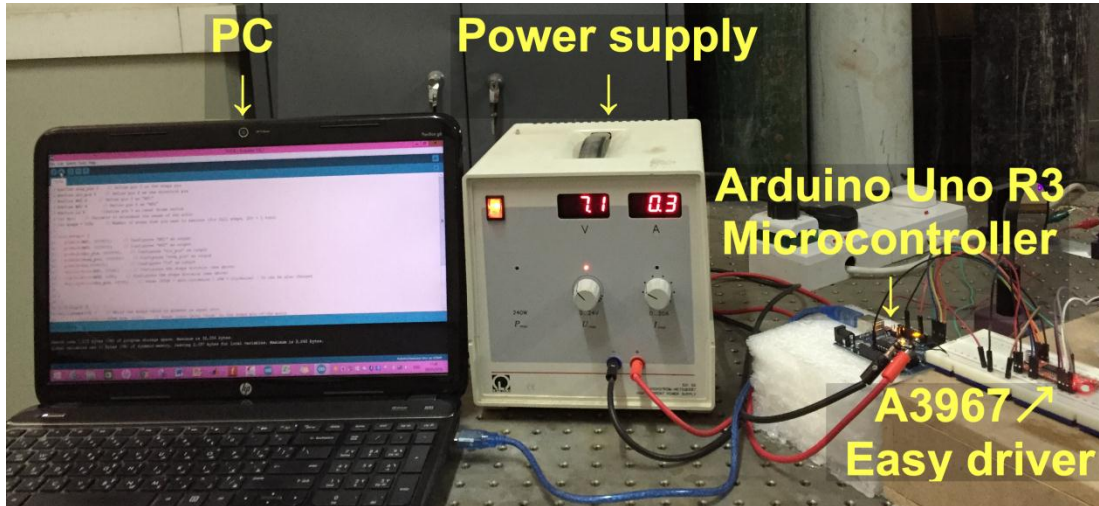
Figure (3.14): The control unit of the system.

A3967 micro stepping easy driver V4.4 board is a stepper motor controller as shown in figure (3.15).
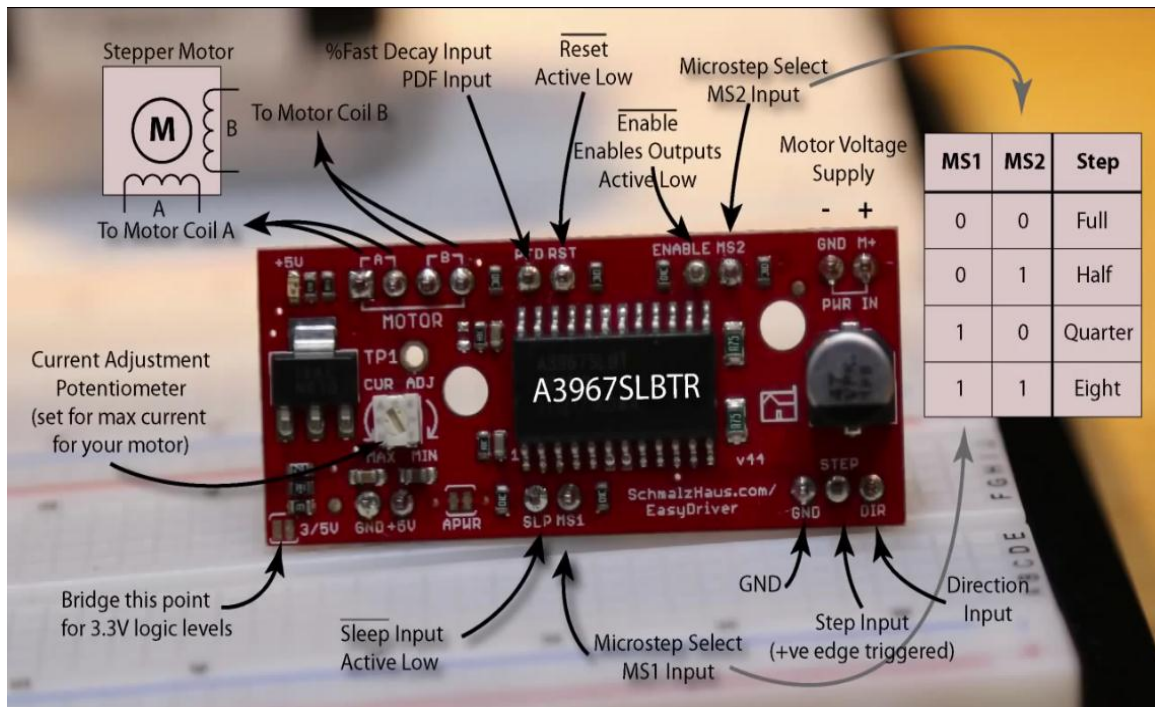
Figure (3.15): A3967 micro stepping easy driver board.

It's a simple and compatible with anything that can output a digital pulse (from 0 to 5V) pulse or (from 0 to 3.3V) pulse. A3967 easy driver drives bipolar stepper motors, and motors wired as bipolar (4, 6, or 8 wired stepper motors), it has four ports (A1, A2, B1, and B2) that can be connected directly to the bipolar stepper motor.

This driver requires operation voltage (from 7V to 30V) to power the stepper motor at any voltage. The higher voltage means the higher torque at high speeds. The easy driver has voltage regulator on the board for the digital interface that can be set to (5V) or (3.3V) and has adjustable current control (from 150mA/phase to 750mA/phase).

The direction pin (dir.) controls the direction of the stepper motor and step pin (step) controls the number of steps of the motor. The microstep select (MS1 and MS2) pins of the A3967 can change micro stepping resolution to full, half, quarter and eighth steps. This Easy Driver version provides much more flexibility and control over the stepper motor, when compared to older versions; also in this version the silk error on the min/max adjustment was fixed.

The main advantage of using the A3967 easy driver is for the protection of the microcontroller since the current quantity needed to supply a stepper motor passes the quantity of the supply current limit of the microcontroller. Figure (3.16) shows the microcontroller board.
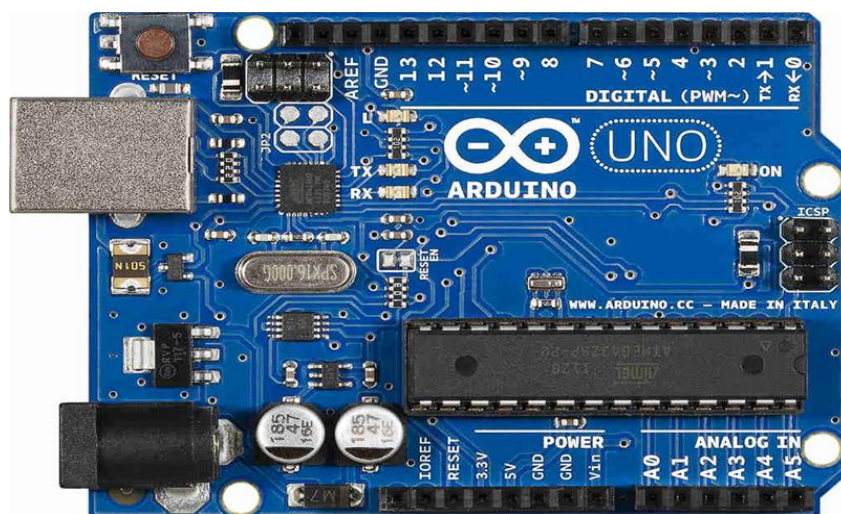
Figure (3.16): Arduino Uno R3 microcontroller board.

44

The Arduino Uno R3 is a microcontroller board based on the ATmega328 chip. It has a fourteen digital input/output pins (six of it can be used as pulse width modulation PWM outputs), a six analog inputs, a sixteen megahertz crystal oscillator, a USB connection and a reset button. Simply it can be connected to a computer with a USB cable or power it with an AC-to-DC adapter or battery to start. It's programmed using C/C++ software language.

The power supply is used for supplying the Easy driver with 7 volts. The personal computer (PC) is used for supplying the microcontroller through the USB connection and for software programming of the easy driver and microcontroller in order to specify the steps, direction and speed of the stepper motor. Figure (3.17) shows the schematic of the control unit circuit.
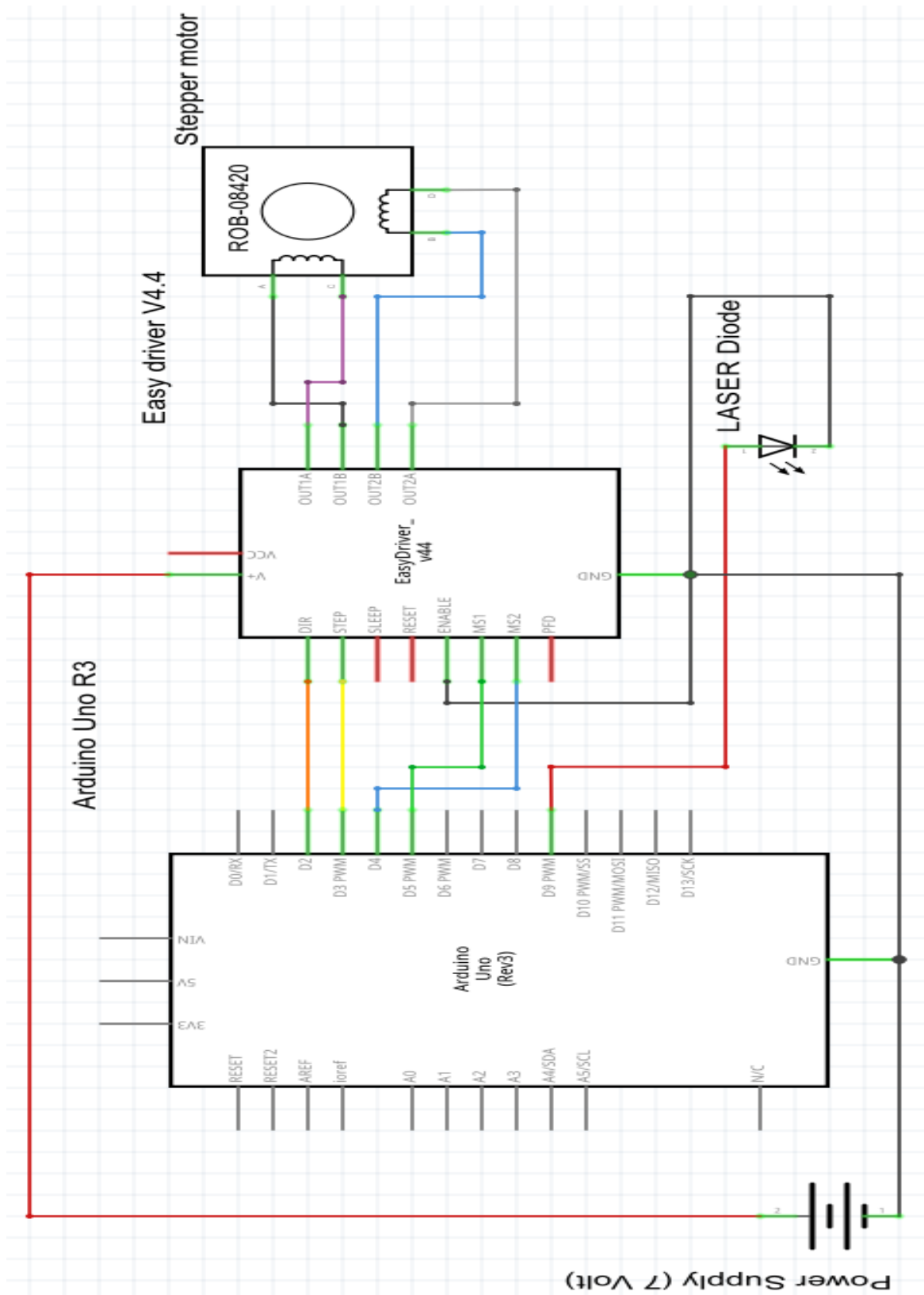
Figure (3.17): The schematic of the control unit circuit.

The Arduino is programmed to switch the laser diode ON and OFF by TTL function of the laser drive and to control a bipolar stepper motor by sending signal to the bipolar stepper motor through A3967 easy driver. These signals control the stepper motor speed, steps, and direction. After sending these signals to the A3967 easy driver input signal port, then these signals pass from A3967 easy driver to the input ports bipolar stepper motor (A1, A2, B1, B2).

Arduino Uno R3 is programmed to do the following sequence:

1. The laser is switched on by TTL function to script on the fiber for 3 minutes. To ensure that no movement or vibration occurs in place, the fiber is held firmly during this time.

2. The laser is switched OFF to stop the inscription process.

3. The fiber is moved by step resolution 240 μm. Then, the laser is switched ON again.

This procedure is repeated again until it covers the distance of 3.8 cm. The laser is still off for two seconds after each step to make sure that no additional inscription on the fiber happens through the steps movement. The total time of the inscription process of four fibers is about 32:30 hours. Appendix (D) shows more information about the programming language.

3.6 FBG Testing Setup for Output Detection and Data Recording

It is essential to detect and record the output data of Bragg reflected response from the PCFs to makes sure if the inscription of the FBG is completed correctly and also to obtain the value of reflected Bragg wavelength. The setup that is used to test the FBG is presented in figure (3.18). It consists of a laser of 651.3 nm, an accurate metric ruler, two fiber clamps, optical signal analyzer (OSA) and PC.
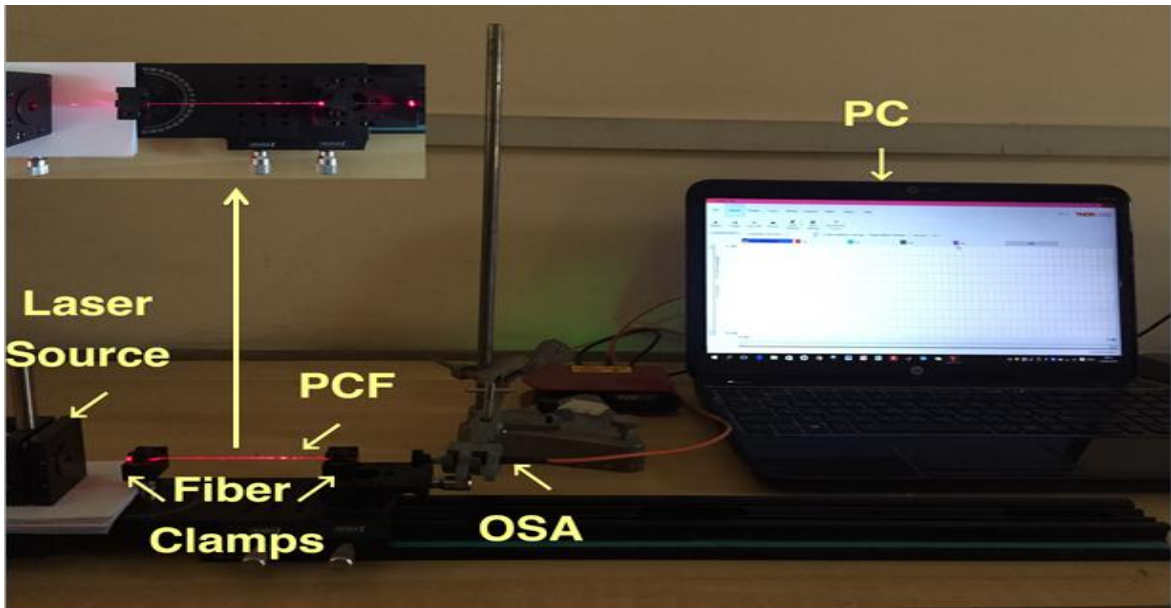
Figure (3.18): Setup to test FBG.

Each component has its own function in this setup. The 651.3 nm laser source is used for testing the functionality of the PCF. The end of the PCF is placed in front of the laser source and the other end in front of an OSA (Thorlabs-CCS200) for data analysis and recording.

The OSA (Thorlabs-CCS200) is a wavelength scanning device that can record the output detected power for each wavelength. It has internal charge coupled device (CCD) line array with 3648 pixel. It is also auto compensated for dark current noise and amplitude corrected. This OSA (Thorlabs-CCS200) is sensitive to wavelengths ranges from 200 nm to 1000 nm. Different parameters can be varied for optimizing the output detected power. The output power of the desired wavelength before and after FBG fabrication has been measured using OSA (Thorlabs-CCS200). The resolution of this OSA gives the reflection of the FBG.

When the light from the laser source entered the PCF, The fabricated Bragg grating in the PCF will reflect the desired Bragg wavelength, so the OSA (Thorlabs-CCS200) from the other end of the PCF will show the exact amount of power that is transmitted from these Bragg grating; therefore Bragg reflected wavelength can be obtained from the transmission spectrum.

48

3.7 Microscopic Images of the Inscription PCFs

The next step after the process of inscription is to check PCFs visually, typically through an optical microscope. The images of the microscope shows different essential information about the PCFs properties, for example the optical examination shows if the process of inscription is completed successfully. Furthermore, it displays the defects that might occur during the process of inscription. The inscription results on the four PCFs are illustrated in figures (3.19-3.22).The Bragg grating appears in the cores of the four PCFs.

Figure (3.19) shows PCF (A) with a 40X microscope image of fabricated FBG. It shows that PCF (A) didn't experience any break through the process of inscription. If any break happened, it could be presented in the section of the fiber core. The image that is magnified displays a nearer view of PCF core. It shows the regions that are exposed to blue light successfully. These regions illustrate the fabricated Bragg grating inside the fiber core which is resulted from the interference of the two blue laser beams.
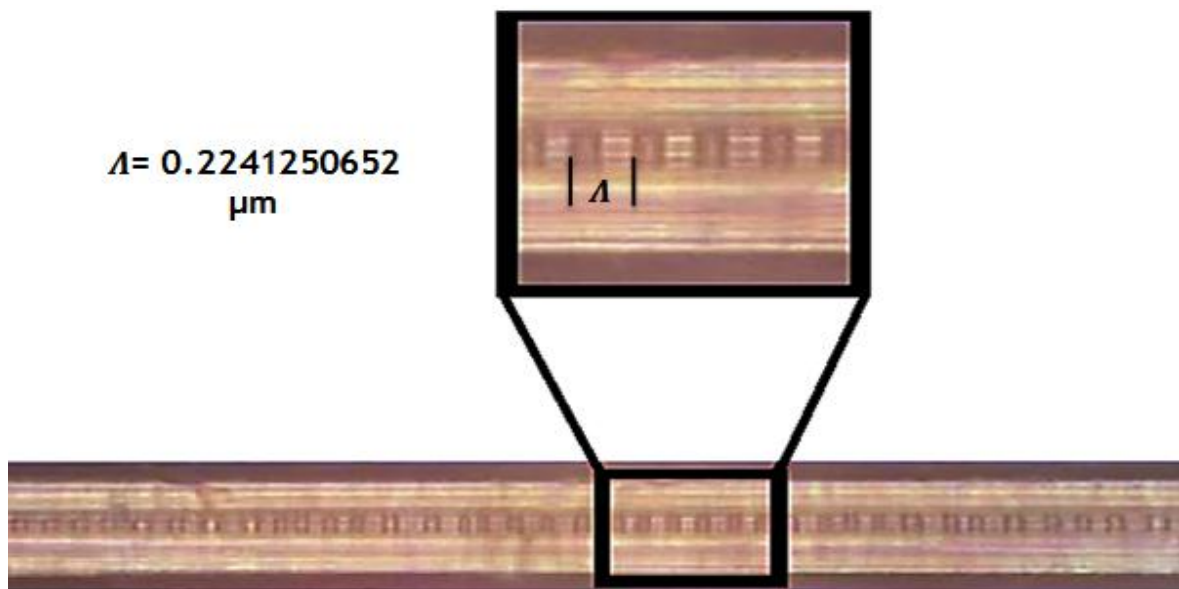
$\varLambda = 0.2241250652$ μm

Figure (3.19): FBG of PCF (A) under optical microscope with average grating period 0.2241250652 μm.

Figure (3.20) shows PCF (B) with a 40X microscope image of fabricated FBG. It shows that PCF (B) core didn't experience any break. It displays the regions that exposed to blue light gives less clear view than PCF (A) due to the density of olive oil.
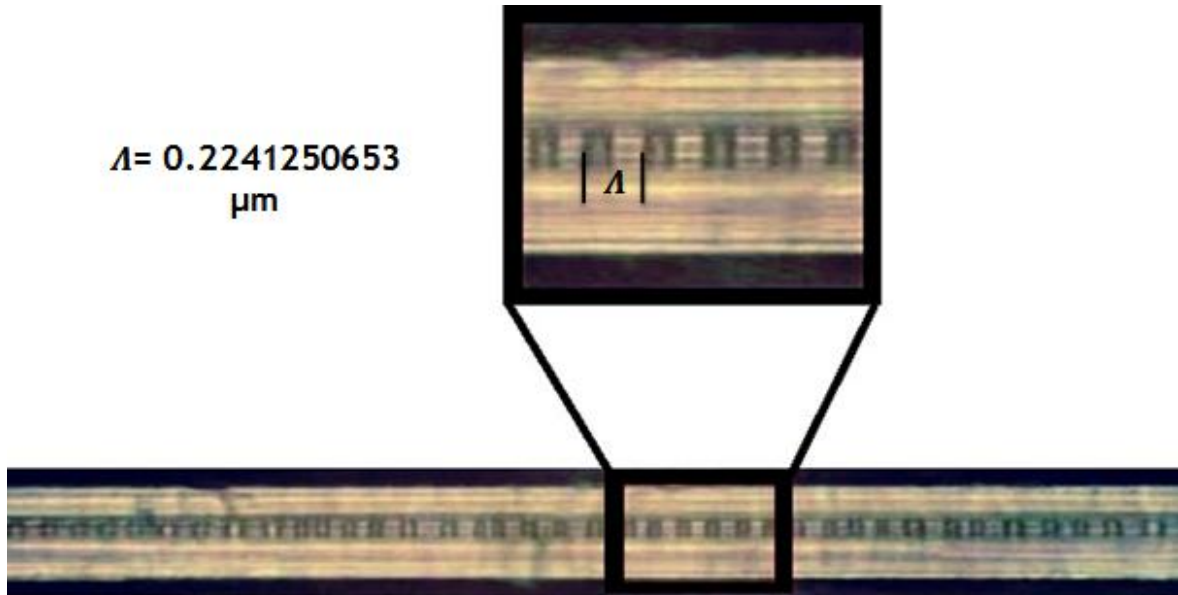
$\varLambda$= 0.2241250653 µm

Figure (3.20): FBG of PCF (B) under optical microscope with average grating period 0.2241250653 µm.

Figure (3.21) shows PCF (C) with a 40X microscope image of fabricated FBG. It show the regions that are cured by blue light are recognized hardly due to the higher density of olive oil than PCF (A) and PCF (B).
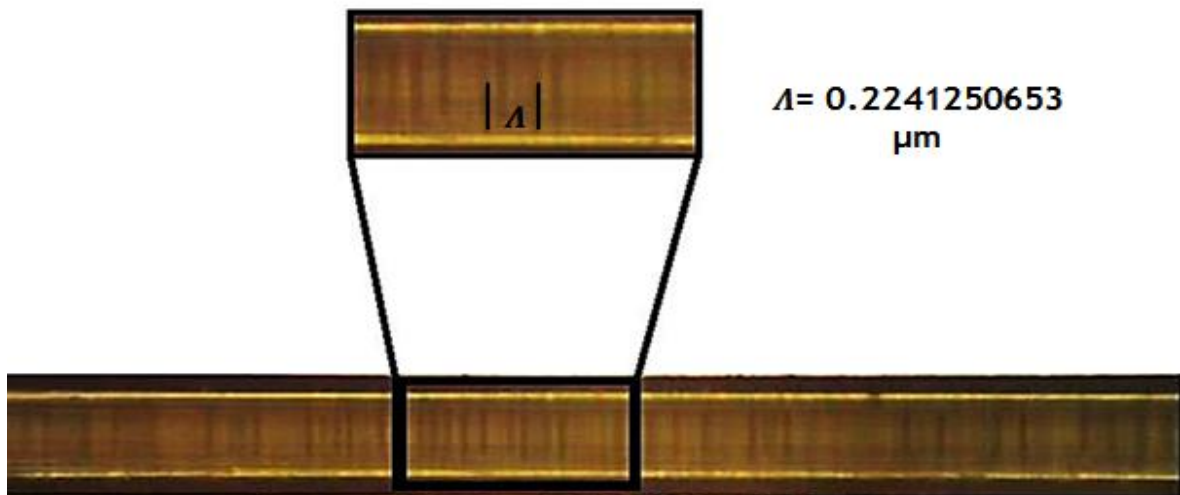
$\Lambda = 0.2241250653$ μm

Figure (3.21): FBG of PCF (C) under optical microscope with average grating period 0.2241250653 μm.

Figure (3.22) shows PCF (D) with a 40X microscope image of fabricated FBG. It shows the regions that are cured by blue light are most hardly recognized due to the higher density of olive oil than PCF (A), PCF (B) and PCF (C).
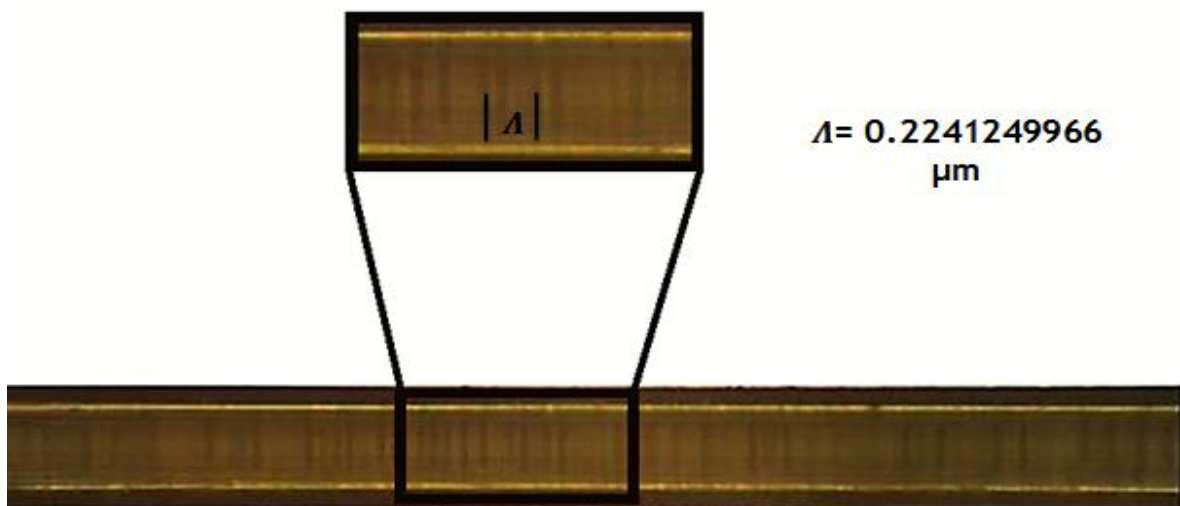
$\Lambda = 0.2241249966$ μm

Figure (3.22): FBG of PCF (D) under optical microscope with average grating period 0.2241249966 μm.

51

PCF (A) shows clearer grating period than PCF (D) because the photosensitive material is higher in PCF (A).

3.8 The Optical Properties

It is a process that gives the wavelength bands of the tested FBG inside the PCF. This is done by directing the laser light inside the PCFs. In this research, laser at wavelength 651.3 nm is used for the testing process.

The output spectrum of a PCF without any grating inscription is shown in figure (3.23) . It shows that, the laser directed through the PCF without any variation laser spectrum i.e. no reflection happens. This result is very important for comparison with inscrpited PCFs spectrums.
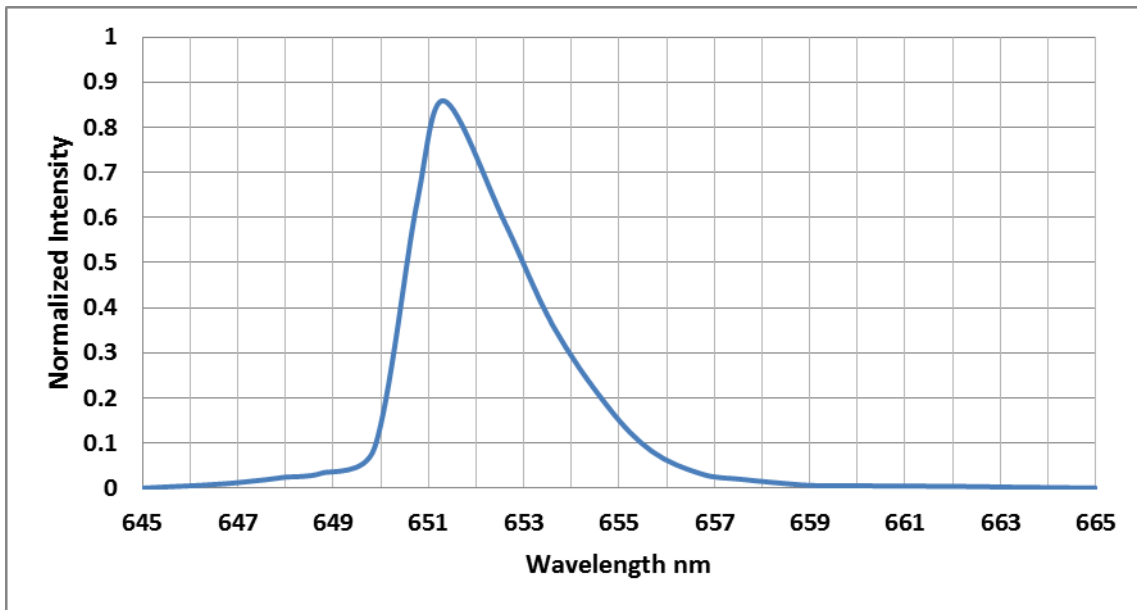
Figure (3.23): Transmission spectrum of 651.3 nm diode laser guided inside a hollow core PCF (HC19-1550 (Thorlab company)) without any infiltrated material.

3.8.1 FBG Inscribed on PCF (A) Optical Properties

The fabricated FBG using star line adhesive is verified by optical properties. The output of the fabricated PCF is presented in figure (3.24). FBG

length of all PCFs is 3.8 cm. As shown in figure (3.24) the output laser peak shifts and reduce at 653.3551 nm, this wavelength shift from the setting wavelength 651.3 nm with half angle separation $\theta = 65°$ is due to the setting error of the half angle separation (θ) between two interfering blue laser (405 nm) correctly about 0.588 % calculated from the following equation:

$$\% \, Error = \left| \frac{Theoretical \; \theta - Experimental \; \theta}{Theoretical \; \theta} \right| \times 100$$

The experimental half angle separation is about $\theta = 64.62°$, the theoretical half angle separation calculated using equation (2.14) by applying the values of the fabrication laser beam 405 nm, the effective refractive index of PCF (A), and the reflected Bragg wavelength of fiber (A). The effective refractive index of PCF (A) and the reflected Bragg wavelength are given in table (3.1) .

This reduction of Bragg wavelength is because of the reflection from the periodic Bragg grating layers in the PCF core.

As mentioned previously, the index of refraction and the grating period between layers determine the Bragg reflected wavelength. So, by changing the period, the peak of Bragg reflected wavelength can be blue shifted or red shifted. However, the grating period is obtained using equation (2.13) using the interference created by the two blue laser beams 405 nm that is used in FBG fabrication and using the half angle separation (θ) between two interfering blue laser (405 nm).

The FBG quality is obtained via the sharpness or the width of the reflected Bragg wavelength. Figure (3.24) shows a sharp drop at wavelength 653.3551 nm expressing a high precision reflection and FWHM about 0.5 nm.

Figure (3.24): The transmission spectrum of the laser diode after coupling with the fabricated FBG in PCF (A).

3.8.2 FBG Inscribed on PCF (B) Optical Properties

The second test of the fabricated FBG made from this liquid mixture shows a higher reflection from the periodic Bragg layers at 653.3555438 nm with more sharpness than the previous fabricated PCF and with FWHM about 0.53 nm as shown in figure (3.25).The strength of reflection resulting from the fact that liquid mixture is strongly cured when PCF core is irradiated by the blue laser.
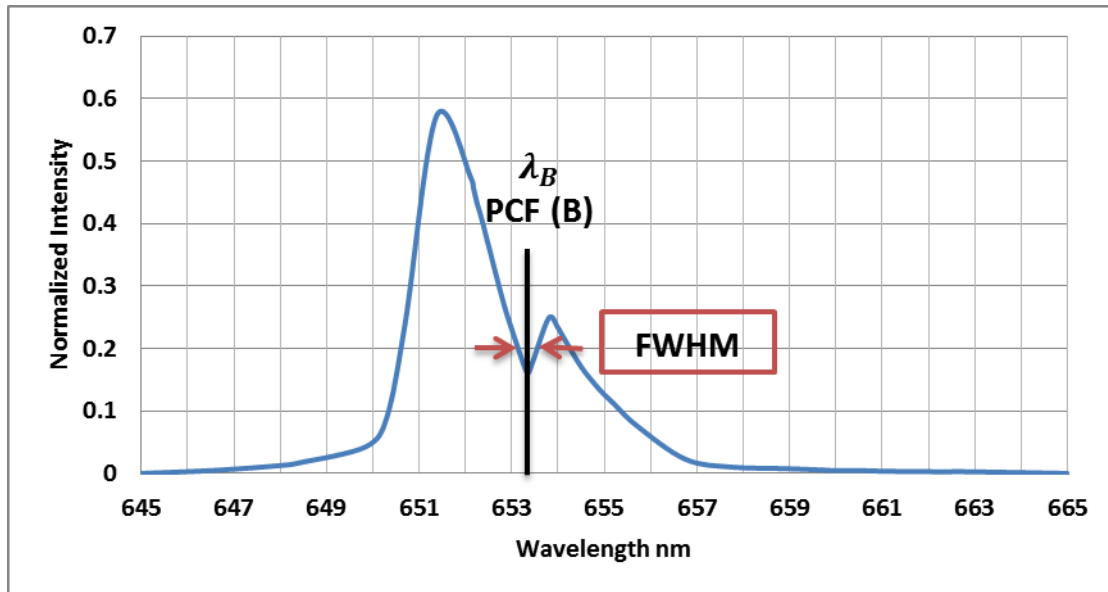
Figure (3.25): The transmission spectrum of the laser diode after coupling with the fabricated FBG in PCF (B).

3.8.3 FBG Inscribed on PCF (C) Optical Properties

The third test of the fabricated FBG made from this liquid mixture shows a higher reflection from the periodic Bragg layers at 653.3565367 nm with more sharpness than the previous two fabricated PCFs with FWHM about 0.7 nm as shown in figure (3.26).

The strength of reflection comes from the fact that this mixture is much strongly cured when PCF core is irradiated by the blue laser.
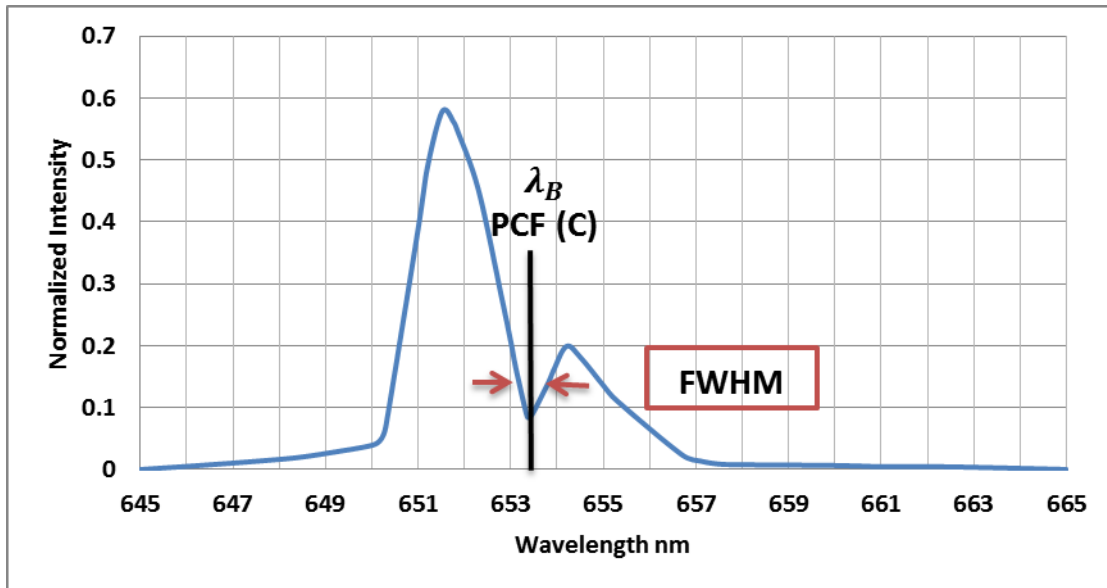
Figure (3.26): The transmission spectrum of the laser diode after coupling with fabricated FBG in PCF (C).

3.8.4 FBG Inscribed on PCF (D) Optical Properties

The fourth test of the fabricated FBG made from this liquid mixture shows the highest reflection from the periodic Bragg layers at 653.3582 nm with much more sharpness than the previous fabricated PCFs with FWHM about 0.74 nm as shown in figure (3.27).

The strength of reflection comes from the fact that this mixture is much morestrongly cured when PCF core is exposed to the laser irradiation.
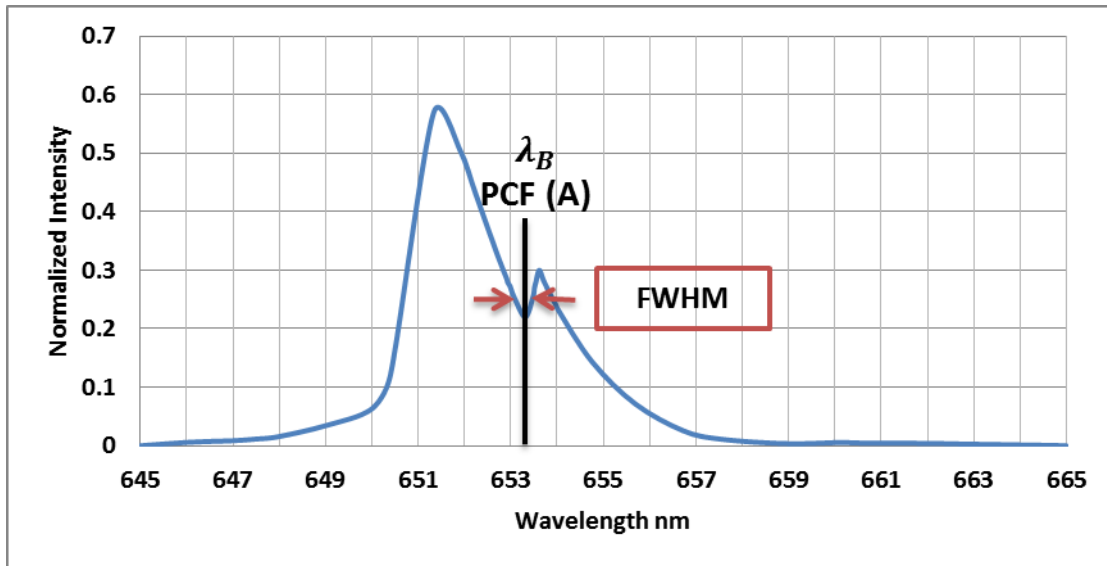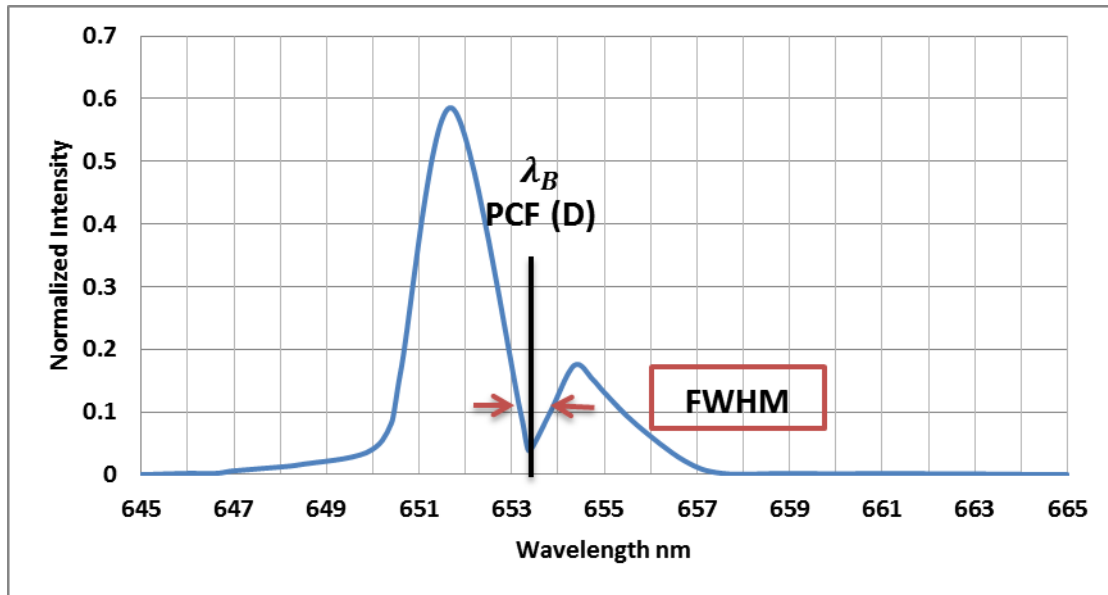
Figure (3.27): The transmission spectrum of the laser diode after coupling with fabricated FBG in PCF (D).

3.8.5 The Differences between the Four Graphs of Output Spectrums

The comparison between the spectrums of the fabricated FBGs in PCFs show that, using the PCF (D) gives an enhanced output spectrum , generating a sharpest output with greater reflection depth and widest FWHM. Hence, decreasing Bragg grating length is necessary for the process of inscription because this will decrease the cost. i.e. to get the same reflectivity results from PCFs (A, B, and C), Bragg grating length must be doubled or tripled and this effect on the cost and the time of the inscription process, because the reflectivity increases by the increasing of Bragg grating length as mensioned previously [29]. The four PCFs output spectrums are presented in figure (3.28).
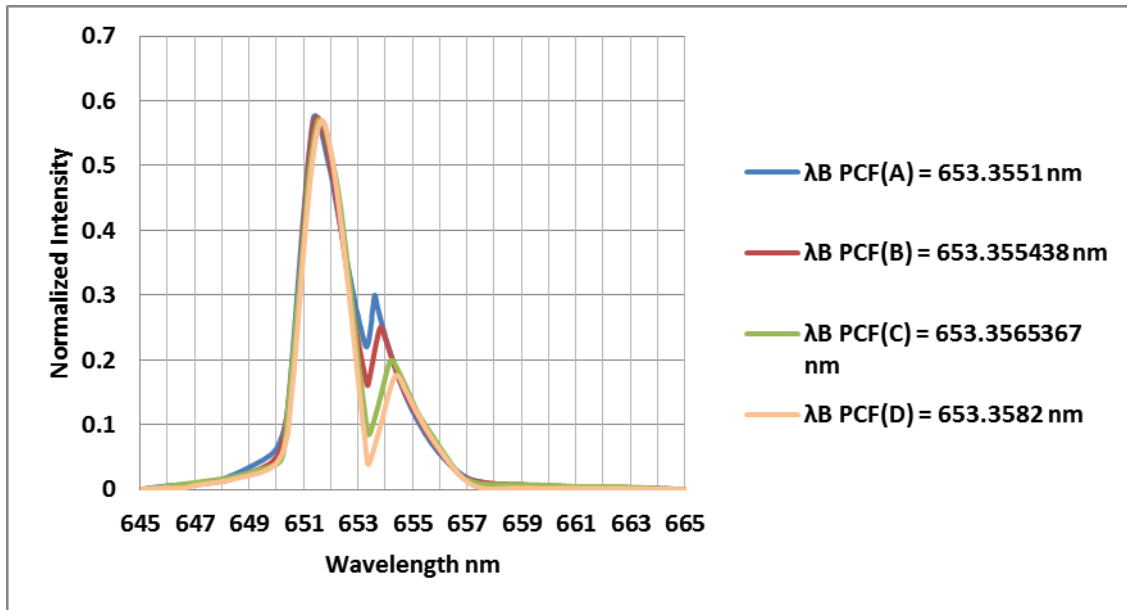
Figure (3.28): The transmission spectrums of the fabricated FBGs in four PCFs.

Table (3.1) gives the numerical examination of the four PCFs spectrums using the equations of the previous chapter. It's obvious that the Bragg reflected wavelength shift for the four PCFs are approximately similar with 0.001 nm difference. However, the variation of the indices of refraction is changes with little quantity for the four PCFs. The liquid mixtures FWHM is more than of the PCF (A).

Table (3.1): The variations between the four PCFs.

Injected material	λ_B (nm)	$\Delta n \times 10^{-6}$	n_{eff}	$\Delta\lambda$ (nm)	Reflectivity %	FWHM (nm)
PCF (A)	653.3551	7.623	1.45756812	2.0178723	76.20	0.5
PCF (B)	653.3555438	8.613	1.45756911	2.0183161	82.87532	0.53
PCF (C)	653.3565367	10.828	1.4575713250	2.019309	91.49684	0.7
PCF (D)	653.3582	14.985	1.457575482	2.0209723	96.09647	0.74

3.9 Reflected Bragg Wavelength Simulation

Investigating FBG further, a MATLAB program is used to simulate the reflection/transmission spectrum of Bragg reflected wavelength of PCF (A) using the same parameters that used in the process of inscription, the result of simulation is shown in figure (3.29).
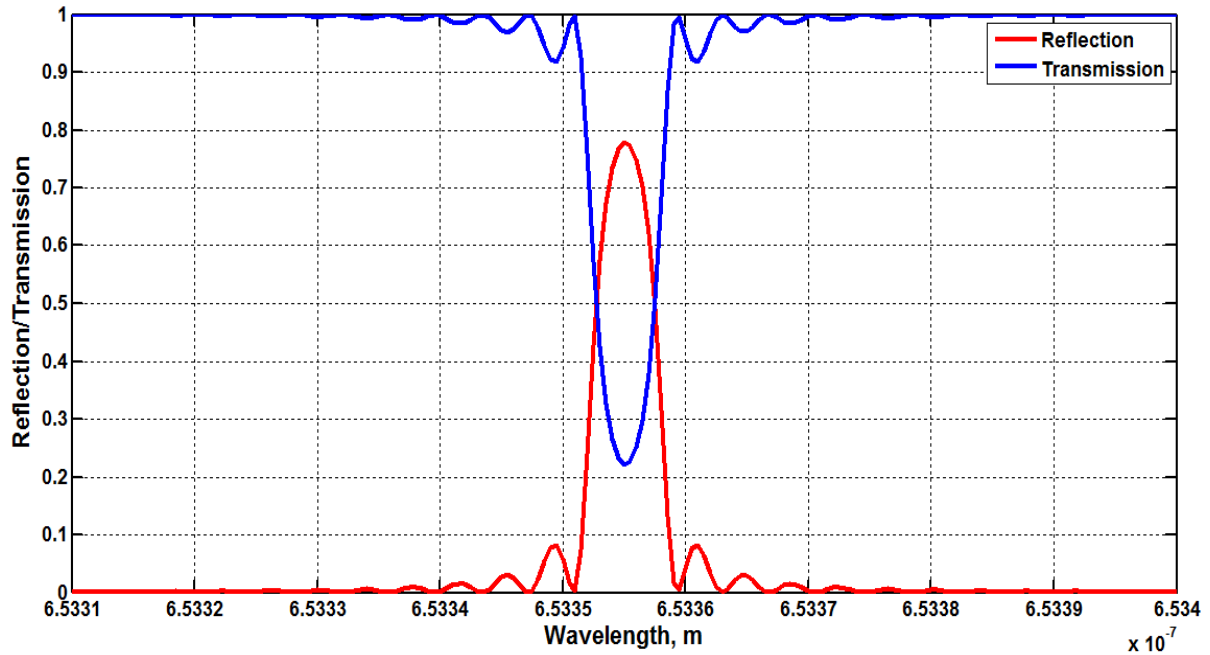
Figure (3.29): Reflection/Transmission of PCF (A) with grating length of 3.8 cm.

The figure displays the reflection/transmission spectrum of the FBG by the coupled mode theory and the transfer matrix method (TMM) using equation (2.10) [29]. It also displays that the center wavelength of the reflection/transmission is at 653.3551 nm. The effective index of refraction used in this code is very similar to that in table (3.1) which is obtained using experimental measurements. It also shows that, the reflectivity and transmissivity is about 77.81 % and 22.19 % respectively. Appendix (E) shows the simulation code to find the reflection/transmission spectrum of star line Glass Mechanix optical adhesive material. If the grating length is increased about 9.8 cm then the reflectivity of PCF (A) will reach 100 % as shown in figure (3.30). Appendix (F) shows the simulation code to find the

reflection/transmission spectrum of star line Glass Mechanix optical adhesive material with grating length 9.8 cm.
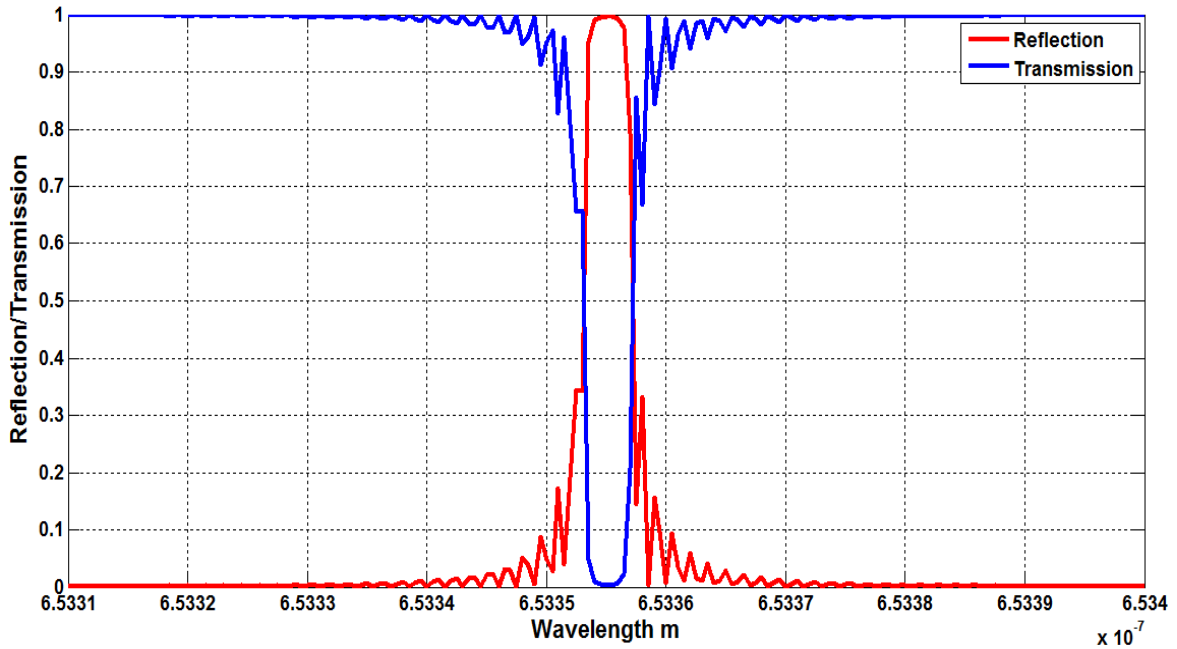
Figure (3.30): Reflection/Transmission of PCF (A) with grating length about 9.8 cm.

Figure (3.31) shows the reflection/transmission spectrum using the parameters of PCF (B).Simulation results show that Bragg reflected wavelength of the reflection/transmission is at 653.3555438 nm. The effective refractive index used in the simulation code is very similar to that given in table (3.1) which are obtained using experimental determinations. Figure (3.31) also shows that, the reflectivity and transmissivity is about 83.97 % and 16.03 % respectively for exact number of periods. Appendix (G) shows the simulation code to find the reflection/transmission of PCF (B).
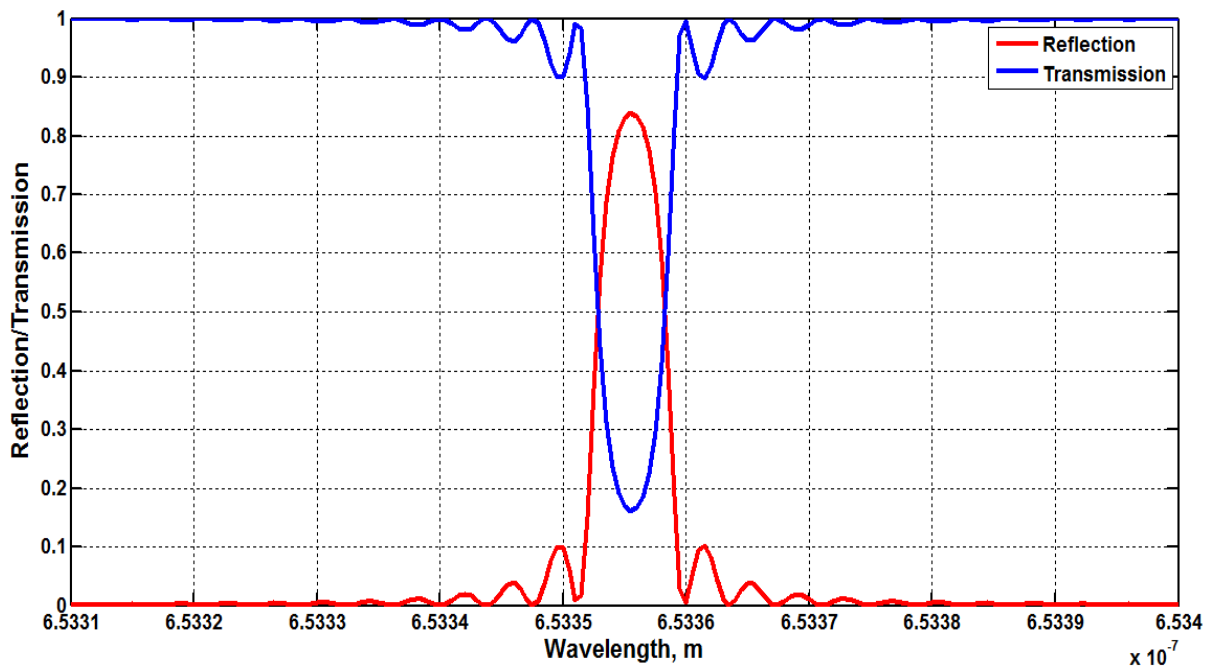
Figure (3.31): Reflection/Transmission of PCF (B).

Figure (3.32) shows the reflection/transmission spectrum using the parameters of the PCF (C). Simulation results show that Bragg reflected wavelength of the reflection/transmission is at 653.3565367 nm.

The effective refractive index used in the simulation code is very similar to that given in table (3.1) which is obtained by experimental determinations. It also shows that, the reflectivity and transmissivity is about 92.5 % and 7.5 % respectively for exact number of periods. Appendix (H) shows the simulation code to find the reflection/transmission of PCF (C).
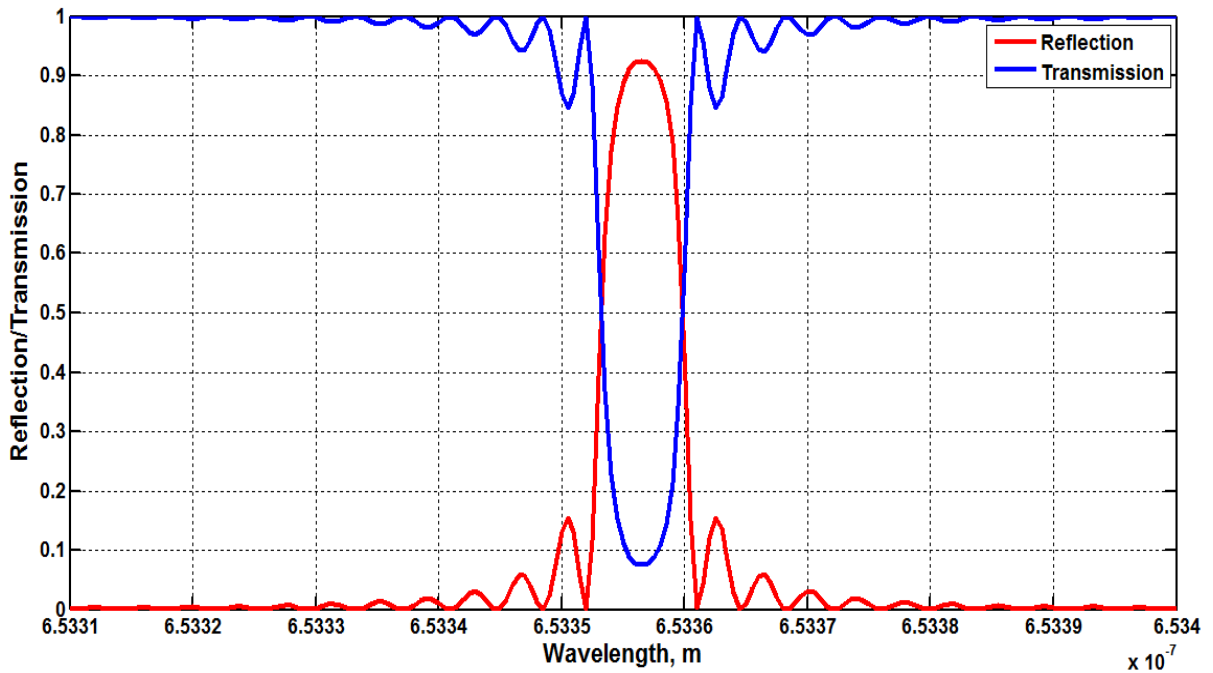
Figure (3.32): Reflection/Transmission of PCF (C).

Figure (3.33) shows the reflection/transmission spectrum using the parameters of the PCF (D). Simulation results show that Bragg reflected wavelength of the reflection/transmission is at 653.35582 nm.

The effective refractive index that is used in the simulation code is very similar to that given in table (3.1) which is obtained by by experimental determinations. It also shows that, the reflectivity and transmissivity is about 98.28 % and 1.72 % respectively for exact number of periods. Appendix (I) shows the simulation code to find the reflection/transmission of PCF (D).
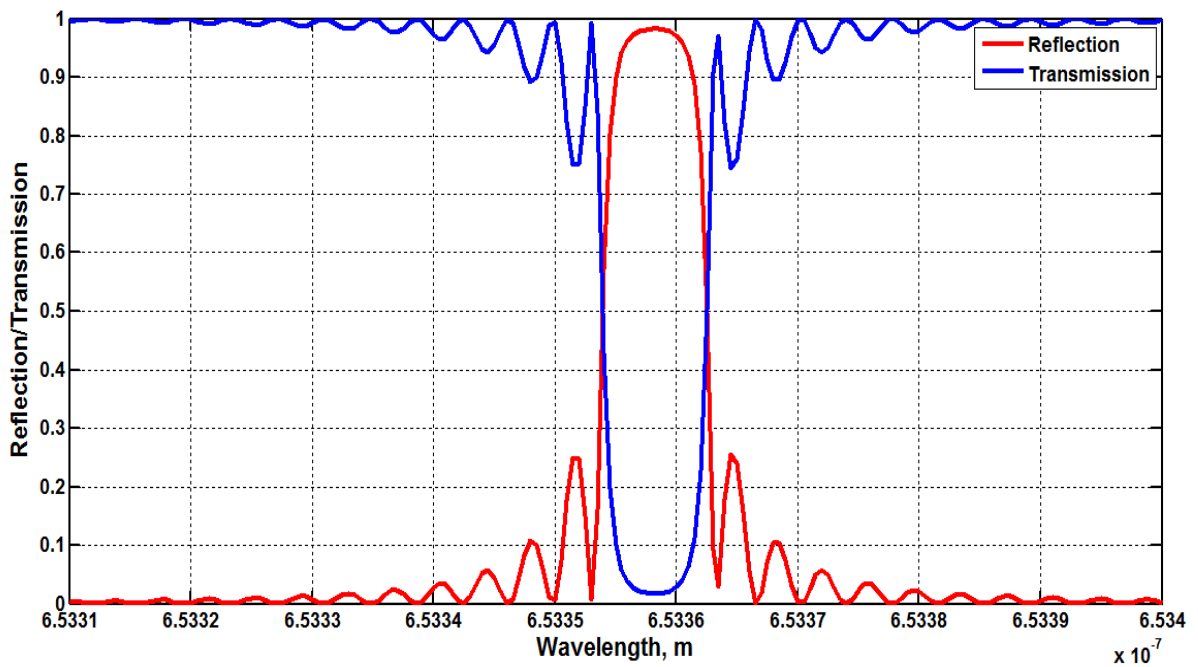
Figure (3.33): Reflection/Transmission of PCF (D).

It can be noticed from the previous results that PCF (D) has the highest reflection due the concetration of olive oil because the absorbance peak of olive oil appears at the reflected Bragg wavelength and its emission peak when the material excited at the same wavelength as shown in figure (3.34) [63].
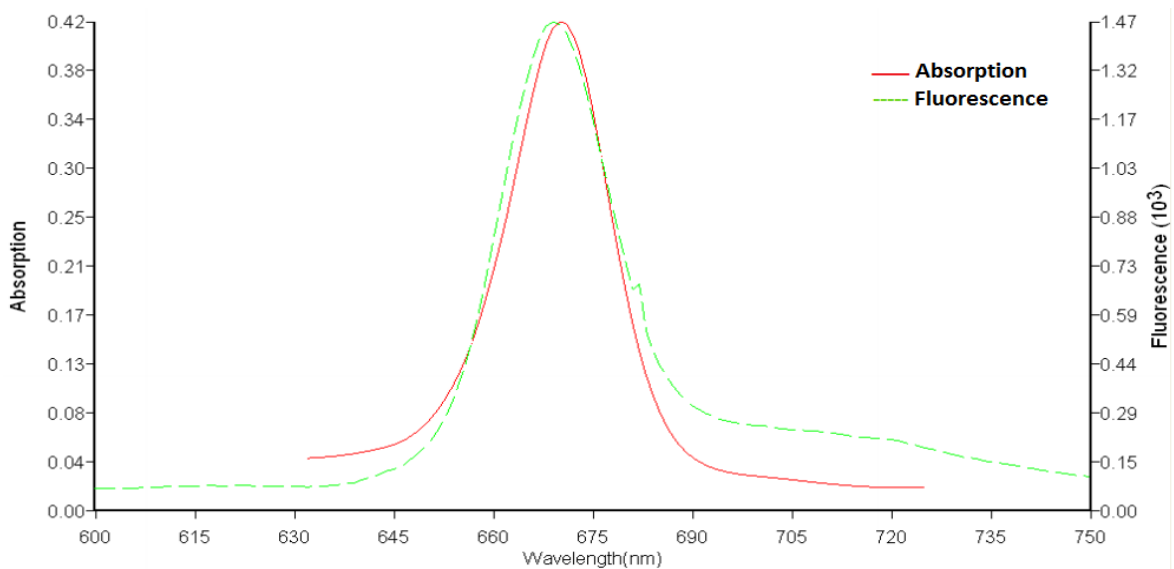
Figure (3.34): The absorbance peak of olive oil appears at wavelength 669 nm and its emission peak when the material excited at that wavelength [63].

CHAPTER FOUR

Application of Fiber Bragg Grating in Magnetic Sensing Technology

Many applications can be done on the FBG that would be constructed in previous chapter. One of these applications used FBG as magnetic field sensor.

This chapter describes the experimental setup and results of magnetic field sensing on three PCFs with different volumes of the liquid mixture.

4.1 Fiber Preparation

Three types of FBG are being prepared for magnetic field sensor:

- **PCF (B):** the first PCF with liquid mixture volume (0.12 ml/cc) consists of (0.06 ml/cc) Star line Glass Mechanix adhesive material, (0.03 ml/cc) Olive oil, (0.03 ml/cc) Ethanol.
- **PCF (C):** the second PCF with liquid mixture volume (0.12 ml/cc) consists of (0.04 ml/cc) Star line Glass Mechanix adhesive material, (0.04 ml/cc) Olive oil, (0.04 ml/cc) Ethanol.
- **PCF (D):** the third PCF with liquid mixture volume (0.12 ml/cc) consists of (0.03 ml/cc) Star line Glass Mechanix adhesive material, (0.06 ml/cc) Olive oil, (0.03 ml/cc) Ethanol.

4.2 Experimental Arrangement Diagram and Setup of Magnetic Field Sensor :

The experimental arrangement diagram and setup of the magnetic field sensor as shown in figures (4.1. a and 4.1. b) are used to test the magnetic field

sensing on fiber Bragg grating by measuring Bragg reflected wavelength shift of three types of PCFs.
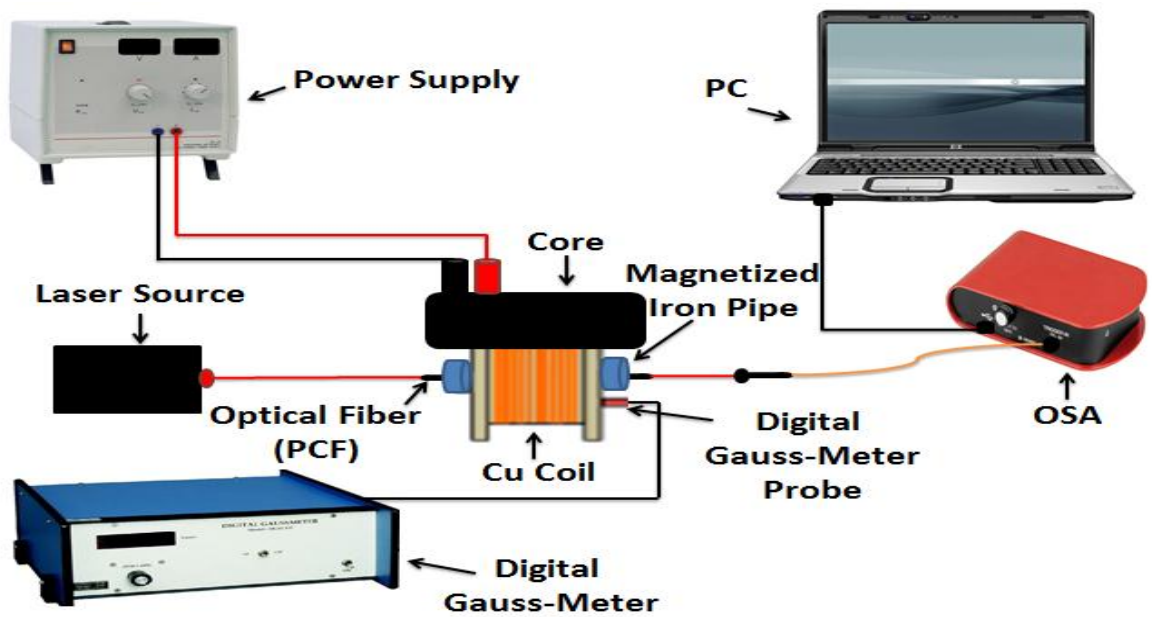
Figure (4.1. a): The experimental arrangement diagram of magnetic field sensor.
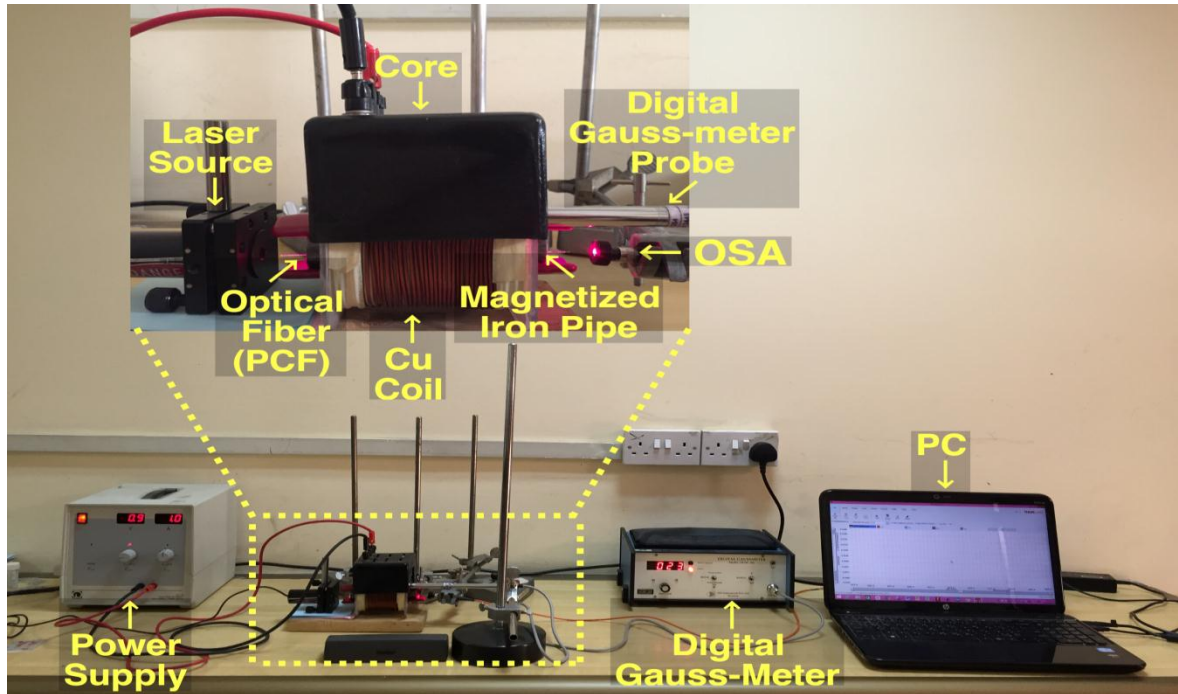
Figure (4.1. b): The experimental set up of magnetic field sensor.

The experimental set up shown in figure (4.1. b) consists of:

1. Laser diode source of 650 nm wavelength is used to pass the light inside hollow core photonic crystal fiber (HC19-1550 (thorlab company)) .

2. Magnetic field source:

   A. Power supply is used to provide the electrical current needed to generate the magnetic field by changing the electrical current values from 1A to 5 A at a certain voltages.

   B. Core with a copper coil is connected to the power supply in order to provide the electrical current needed to generate the the magnetic field inside an iron pipe of 10 cm length.

3. Hollow core photonic crystal fiber (HC19-1550 (thorlab company)) held inside the magnetized iron pipe is used to test magnetic sensitivity i.e. measuring Bragg reflected wavelength shift in the presence of the magnetic field.

4. Digital Gauss-meter (DGM-202) with an axial probe.

5. Optical spectrum analyzer (OSA) (Thorlabs-CCS200) is used for data analysis and recording.

6. PC is used to display the data analysis and recording.

First, the power supply was set at voltage value where the current reaches 1A, then the magnetic flux density value is measured with the digital Guass-meter axial probe, and then the light had coming out from PCF (B) was visualized by OSA to measure Bragg reflected wavelength. After that the current was set at values of (2, 3, 4, and 5 A) and the previous procedures of measuring the magnetic flux density and Bragg reflected wavelength shift for each current value were repeated for PCF (B). The two others PCFs (C) and (D) followed the same procedure of the PCF (B).

4.3 The Optical Properties Results of Bragg Reflected Wavelengths Shifts:

The experimental set up of magnetic field sensor in figure (4.1.b) was used to measure the optical properties of Bragg reflected wavelengths shifts spectrums by generating a magnetic field around the PCF as given in figures (4.2-4.4). These spectrums are obtained by changing the electrical current from 1 A to 5 A, where the magnetic flux density was measured for each current value within a range of (0-93) Gauss, more details in tables (4.1-4.3). The magnetic flux density and Bragg reflected wavelengths shifts were measured using axial probe and OSA respectively.

1. PCF (B)

Figure (4.2) shows the spectrums of different Bragg reflected wavelengths shifts of PCF (B). Table (4.1) gives more information about the numerical examination of these spectrums.

Figure (4.2): The spectrums of different Bragg reflected wavelengths shifts of PCF (B).

Table (4.1): The numerical examination of PCF (B).

Electrcal Current (A)	Magnetic Flux density (Gauss)	λ_B (nm)	Reflectivity %	FWHM (nm)
0	0	653.3555438	82.87532	0.53
1	21	653.3617	82.95165	0.5302
2	39	653.3714	83.07888	0.5305
3	60	653.3808	83.20611	0.5308
4	76	653.3894	83.50120	0.5312
5	92	653.3975	83.62341	0.5315

2. PCF (C)

Figure (4.3) shows the spectrums of different Bragg reflected wavelengths shifts of PCF (C). Table (4.2) gives more information about the numerical examination of these spectrums.
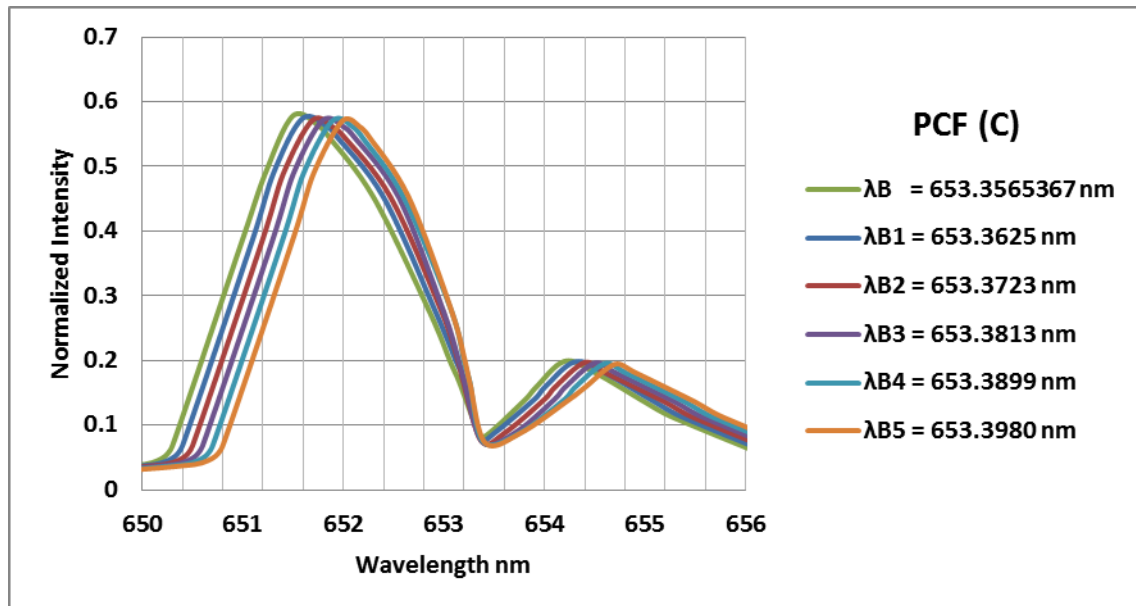
Figure (4.3): The spectrums of different Bragg reflected wavelengths shifts of PCF (C).

Table (4.2): The numerical examination of PCF (C).

Elecrtical Current (A)	Magnetic Flux density (Gauss)	λ_B (nm)	Reflectivity %	FWHM (nm)
0	0	653.3565367	91.49684	0.7
1	22	653.3625	92.13524	0.8
2	42	653.3723	92.4878	0.85
3	58.5	653.3813	92.54204	0.88
4	77	653.3899	92.58724	0.92
5	93	653.3980	92.67764	0.97

3. PCF (D)

Figure (4.4) shows the spectrums of different Bragg reflected wavelengths shifts of PCF (D). Table (4.3) gives more information about the numerical examination of these spectrums.
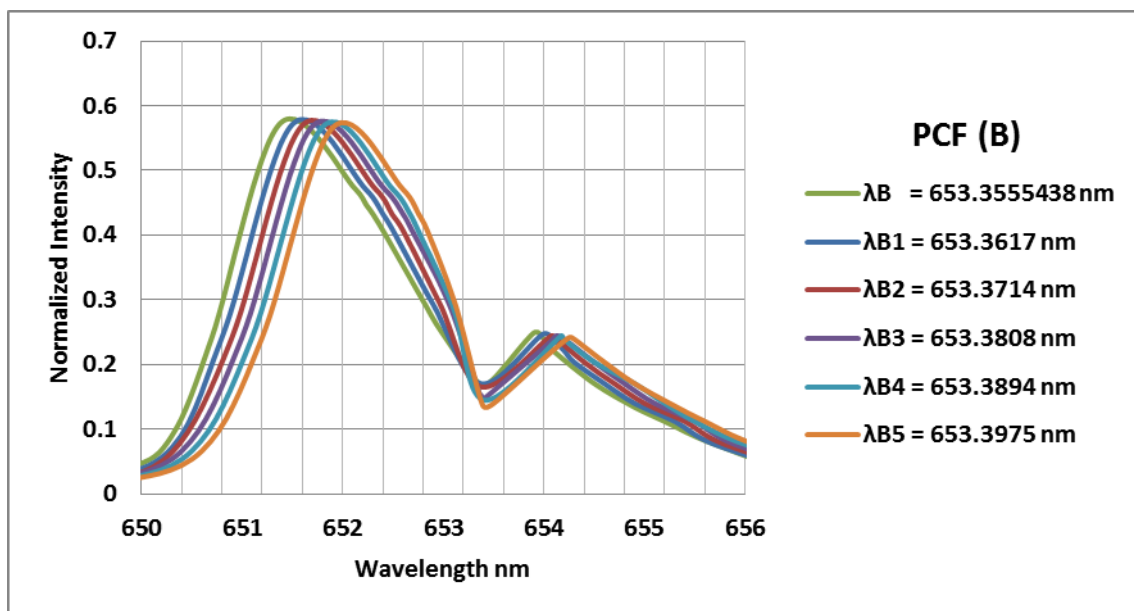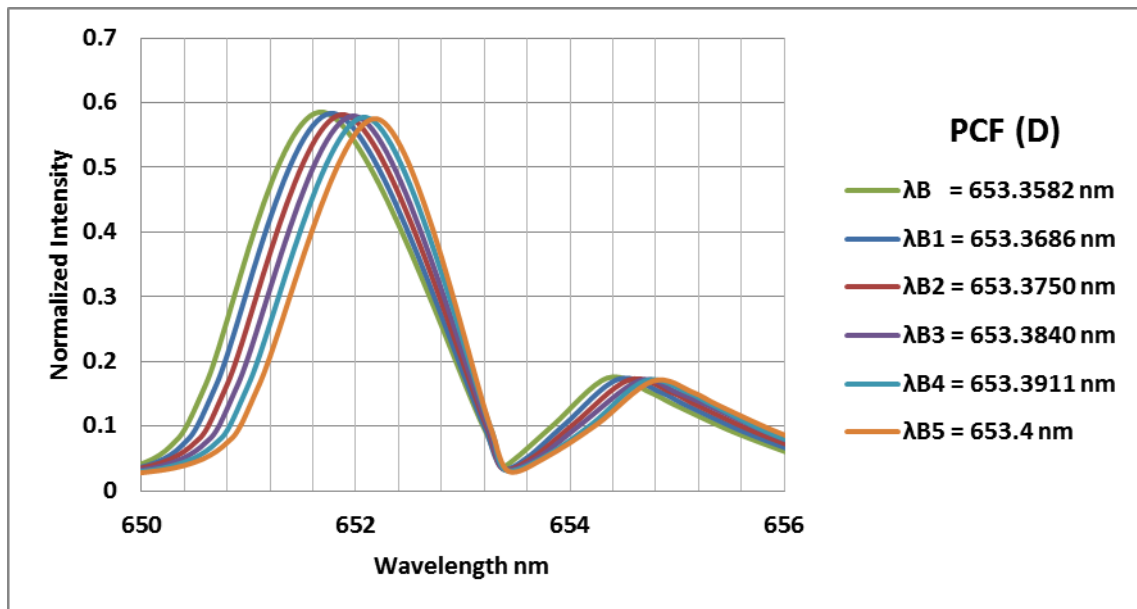

Figure (4.4): The spectrums of different Bragg reflected wavelengths shifts of PCF (D).

Table (4.3): The numerical examination of PCF (D).

Electrical Current (A)	Magnetic Flux density (Gauss)	λ_B (nm)	Reflectivity %	FWHM (nm)
0	0	653.3582	96.09647	0.74
1	22	653.3686	96.50737	0.83
2	41	653.3750	96.61009	0.86
3	60	653.3840	96.71282	0.89
4	78	653.3911	96.81554	0.94
5	93	653.4	96.91827	0.98

The curves between the electrical current and magnetic flux density of three PCFs (B, C, and D) were determined from tables (4.1-4.3) are shown in figure (4.5). These curves show how the magnetic flux density increases in a linear relation with the electrical current.
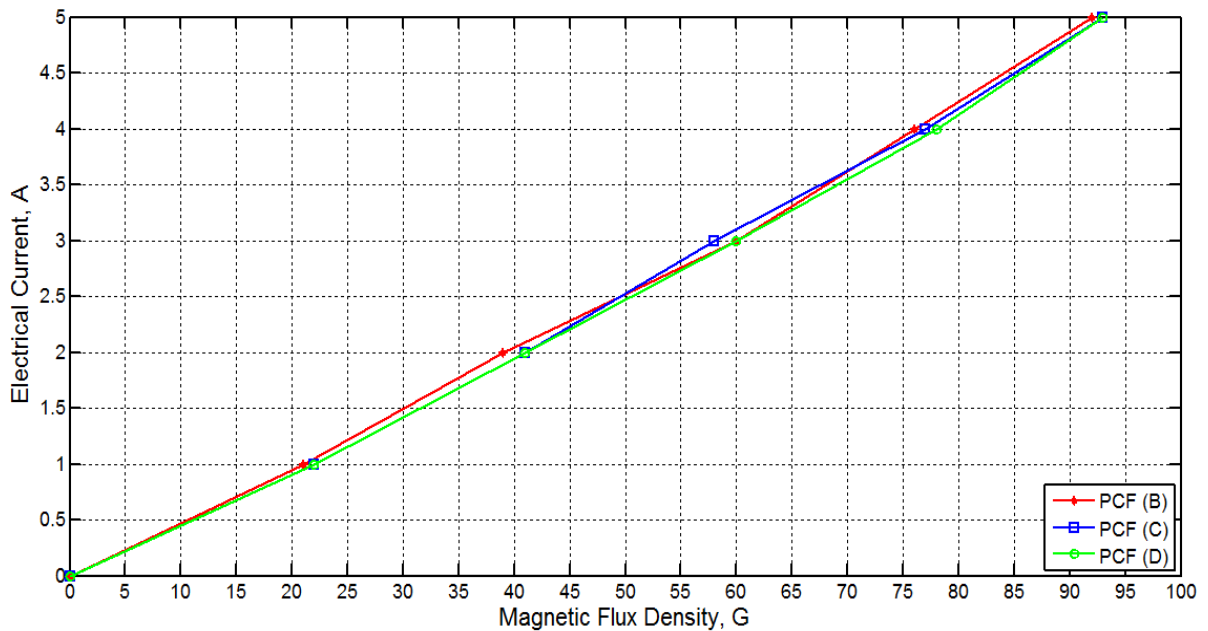
Figure (4.5): Comparison curves of the electrical current versus magnetic flux density of three PCFs (B, C, and D).

70

Figure (4.5) shows that there is a small variation in the measured magnetic field density for all PCFs; fiber (D) has the largest average magnetic flux density about 18.6 Gauss, fiber (C) has average magnetic flux density about 18.5 Gauss, while fiber (B) has the smallest average magnetic flux density about 18.4 Gauss.

The curves between the magnetic flux density and Bragg reflected wavelengths shifts of three PCFs (B, C, and D) were determined from tables (4.1-4.3) are shown in figure (4.6).
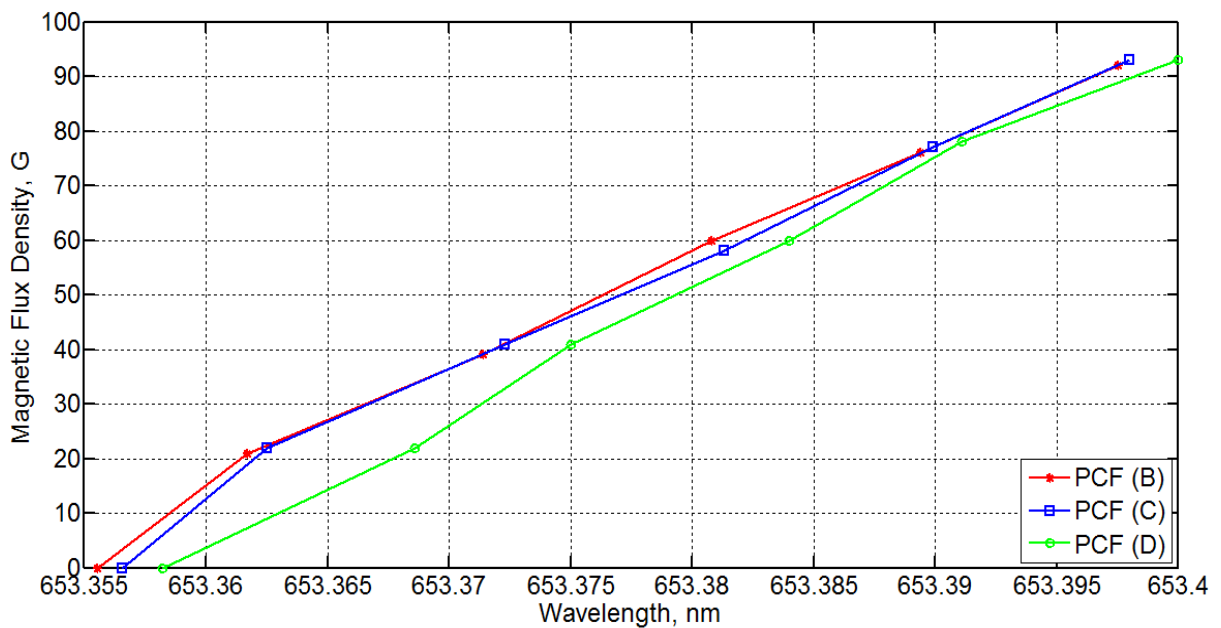
Figure (4.6): Comparison curves of the magnetic flux density versus Bragg reflected wavelengths shifts of three PCFs (B, C, and D).

The curves in figure (4.6) above show that increasing in the magnetic flux density is due to the linear relation with the electrical current leads to shifting the Bragg reflected wavelengths of the three PCFs to NIR range and not to UV range, this is happened because olive oil has a positive Verdet constant equals to (98.6808 rad/T. m) at the Bragg reflected wavelength [61].

As seen in figure (4.6) the PCF (D) has the greatest average wavelength shift per magnetic flux density sensitivity (0.000494623656 nm/ Gauss) than the

PCFs (B and C) which are of average wavelength shift per magnetic flux density sensitivity (0.0004560456522 nm/Gauss) and (0.000482518919 nm/Gauss) respectively, this is happened due to the different concetrations of olive oil in the three PCFs. Since olive oil is a photonic crystal material, therefore a PCF with larger concetration of olive oil has the greatest sensitivity.

CHAPTER FIVE

Conclusions and Future Work

5.1 Conclusions

The important facts concluded from the obtained results of this work can be given as follow:

1. The fabrication setup is able to fabricate Bragg grating in four PCFs filled with liquids of different consetrations consisting of olive oil, star line Glass Mechanix adhesive material and ethanol using amplitude interferometric technique with Bragg reflected wavelength (λ_B) of 653.3 nm and reflectivity ranges equal to (PCF(A)=76.20 %, PCF (B) =82.87532 %, PCF (C) =91.49684 %, PCF (D) = 96.09647 %). It is designed and implemented successfully comparable to the fabricated FBG using two PCFs filled with mixture of olive oil and optical adhesive material and acetone or with only optical adhesive material using the same technique with Bragg reflected wavelength (λ_B) of 806 nm and reflectivity ranges approximately equal to 50 % and 80 % respectively [21].

2. Increasing the concentration of olive oil in the liquid mixture that infiltrated inside PCFs gives a remarkable shift in the fabricated Bragg reflected wavelength due to the nonlinearity of olive oil [63].

3. The results show that increasing the concentration of olive oil in the liquid mixture that infiltrated inside PCFs giving the highest reflectivity because olive oil has an absorption and an emission peaks when it excited at the fabricated Bragg reflected wavelength (653.3 nm) [63].

4. The Bragg fibers that fabricated can be used as magnetic sensor.

5. The results of applying FBG in magnetic field sensing show that increasing the magnetic flux density will increase the shift of Bragg reflected wavelength. As well

as increasing olive oil concentration in the liquid mixture that infiltrated inside PCFs giving a remarkable wavelength shift to NIR range because olive oil at this fabricated Bragg wavelength has positive Verdet constant equals to (98.6808 rad/T. m) [61], so PCF (D) is more sensitive compared to other PCFs (B and C).

6. Increasing olive oil concentration in the liquid mixture that infiltrated inside PCF (D) gives a noticeable wavelength shift sensitivity about (0.000494623656 nm/ Gauss).

7. The sensitivity of the three PCFs (B, C, and D) is higher compared to the sensitivity of a PCF without Bragg grating and filled with only olive oil about (0.0003509 rad/Gauss) at 650 nm wavelength by dividing the rotation angle per the magnetic flux density [61].

8. The FWHM is increased linearly with the increasing of Bragg reflected wavelength for all PCFs due to their direct proportional relation [28].

9. The shift in wavelength due to the magnetic field is a linear shift.

10. The reflectivity increases linearly with the increasing in magnetic flux density.

5.2 Future Work

A number of future works can be proposed relying on the practical results of this thesis as follows:

1. Using a higher resolution translation stage to produce more precise Bragg grating for the same fiber length.

2. Fabricating multi functionality sensors on the same fiber such as pressure, strain, temperature, acceleration sensors.

3. Use UV grating instead of interferometric technique to fabricate FBG.

REFERENCES

[1] **A. Othonos,**" Review of Scientific Instruments: Fiber Bragg Gratings", Vol. 68, No. 12, PP. 4309-4341, December 1997.

[2] **K.O. Hill, Y. Fujii, D.C. Johnson and B.S. Kawasaki,** "Photosensitivity in Optical Fiber Waveguides: Application to Reflection Filter Fabrication", Applied Physics Letters, Vol. 32, No. 10, PP. 647-649, May 1978.

[3] **B. S. Kawasaki, K. O. Hill, D. C. Johnson, and Y. Fujii,** "Narrow-Band Bragg Reflectors in Optical Fibers", Optics Letters, Vol. 3, No. 2, PP. 66-68, 1978.

[4] **G. Meltz, W.W. Morey and W. H. Glenn,** "Formation of Bragg Gratings in Optical Fibers by a Transverse Holographic Method", Optics Letters, Vol. 14, No. 15, PP. 823-825, Aug 1989.

[5] **K. O. Hill, B. Malo, F. Bilodeau, and D. C. Johnson,** "Photosensitivity in Optical Fibers", Annu. Rev. Mater. Sci.,Vol. 23, PP. 125-157 ‹1993.

[6] **R. J. Campbell and R. Kashyap,** "The Properties and Applications of Photo Sensitive Germanosilicate Fiber", Int. J. Optoelectron, Vol. 9, No. 1, PP. 33-57, 1994.

[7] **R. KASHYAP,** "Photosensitive Optical Fibers: Devices and Applications", Opt. Fiber Technol, Vol. 1, No.1, PP.17–34, Oct 1994.

[8] **M. Green, And S. J. Madden,** "Low Loss Nematic Liquid Crystal Cored Fiber Waveguides", Appl. Opt., Vol. 28, No. 24 PP. 5202–5203, 1989.

[9] **Abby Juhl,**"Holographic Polymer Dispersed Liquid Crystal", Braun Group People, University of Illinois, Site:http://braungroup.beckman.illinois.edu/AbbyGriffith.html.

[10] **F. Bruyneel, H. De Smet, J. Vanfleteren, A. Van Calster,** "Cell Gap Optimization and Alignment Effects in Reflective PDLC Microdisplays", Liquid Crystals, Vol. 28, No. 8, PP. 1245-1252 ‹2001.

[11] **Y. J. Liu and X. W. Sun,** "Holographic Polymer-Dispersed Liquid Crystals: Materials, Formation, and Applications", Hindawi Publishing Corporation, Advances in OptoElectronics, Vol. 2008, 2008.

[12] **E. Wikszak, J. Thomas, J. Burghoff, B. Ortaç, J. Limpert, S. Nolte,** "Erbium Fiber Laser Based on Intracore Femtosecond-Written Fiber Bragg Grating", Optics Letters Vol. 31, No.16, PP. 2390-2392, 2006.

[13] **Y. Lai, K. Zhou, K. Sugden, and I. Bennion,**" Point-by-point Inscription of First Order Fiber Bragg Grating for C-Band Applications", Optics Express, Vol. 15, No. 26, Dec 2007.

[14] **B. Guan, D. Chen, Y. Zhang, H. Wang, H. Tam,** "Bragg Gratings in Pure-Silica Polarization Maintaining Photonic Crystal Fiber", IEEE photonics technology letters, Vol. 20, No. 23, December 2008.

[15] **Y. Wang, H. Bartelt, M. Becker, S. Brueckner, J. Bergmann, J. Kobelke, M. Rothhardt,** "Fiber Bragg grating Inscription in Pure-Silica and Ge-Doped Photonic Crystal Fibers", Applied Optics, Vol. 48, No. 11, April 2009.

[16] **Z. Zhang, C. Zhang, X. Tao, G. Wang, and G. Peng,**" Inscription of Polymer Optical Fiber Bragg Grating at 962 nm and Its Potential in Strain Sensing", IEEE Photonics Technology Letters, Vol. 22, No.21, Nov 2010.

[17] **Y. Wang, H. Bartelt, W. Ecke, R. Willsch, J. Kobelke,** "UV-Laser-Inscribed Fiber Bragg Gratings in Photonic Crystal Fibers and Sensing Applications", Proc. SPIE 8201, International Conference on Optical Instruments and Technology: Optoelectronic Measurement Technology and Systems, .Vol 8201, November 2011.

[18] **C. M. Rollinson, S. A. Wade, B. P. Kouskousis, D. J. Kitcher, G. W. Baxter, and S. F. Collins,**" Variations of the Growth of Harmonic Reflections in Fiber Bragg Gratings Fabricated Using Phase Masks", J. Opt. Soc. Am. A, Vol. 29, No. 7, July 2012.

[19] **T. Elsmann, T. Habisreuther, A. Graf, M. Rothhardt, and H. Bartelt,** "Inscription of First-Order Sapphire Bragg Gratings Using 400 nm Femtosecond Laser Radiation", Optics Express, Vol. 21, No. 4, Feb 2013.

[20] **I. Bundalo, K. Nielsen, C. Markos, O. Bang,** "Bragg Grating Writing in PMMA Microstructured Polymer Optical Fibers in Less Than 7 Minutes ", Optics Express, Vol. 22, No. 5, 10 March 2014.

[21] **A. Engad, H. M. Ahmed and A. A. Al- Dergazly,**" Photonic Crystal Fiber Bragg grating Using Olive Oil as Liquid Photonic Crystal and Adhesive Material for Construction", IJISET - International Journal of Innovative Science, Engineering & Technology, Vol. 2, No. 3, March 2015.

[22] **D. Marcuse,** "Loss Analysis of Single-Mode Fiber Splices", the Bell System Technical Journal, Vol. 56, No. 5, PP. 703-718, 1977.

[23] **S. Arismar Cerqueira,** "Recent Progress and Novel Applications of Photonic Crystal Fibers", Reports on Progress in Physics, Vol. 73, No. 2, 2010.

[24] **M.Yasin, S.W. Harun, and H. Arof,** "Recent Progress in Optical Fiber Research", InTech, PP. 3-25, 2012.

[25] **T. Ritari,** "Novel Sensor and Telecommunication Applications of Photonic Crystal Fibers", Ph.D thesis, Helsinki University of Technology, Department of Electrical and Communications Engineering,Optics and Molecular Materials, 2006.

[26] **A. Othonos and K. Kalli**, "Fiber Bragg Gratings: Fundamentals and Applications in Telecommunications and Sensing", Artech House, Norwood, MA, 1999.

[27] **I. P. Johnson,** "Grating Devices in Polymer Optical Fibre", Aston University, August 2011.

[28] **R. C. S. B. Allil, Marcelo M. Werneck, B. A. Ribeiro, F. V. B. de Nazaré,** "A Guide to Fiber Bragg Grating Sensors", PP. May 15, 2013.

[29] **D. K. W. Lam and B. K. Garside,** "Characterization of Single-Mode Optical Fiber Filters", Appl. Opt., Vol. 20, No.3, PP. 440-445, 1981.

[30] **V. Mizrahi and J. E. Sipe,** "Optical Properties of Photosensitive Fiber Phase Gratings", J. Light wave Technol., Vol. 11, No. 10, PP. 1513-1517, 1993.

[31] **T. Erdogan, J. E. Sipe,** "Tilted Fiber Phase Gratings", J. Optical Society of America A, Vol. 13, No.2, PP. 296-313, 1996.

[32] **D.J. Dunn,** "Adhesives and Sealants: Technology, Applications and Markets", Rapra Technology Limited, 2003.

[33] **H. Liu, F. Lin, M. Chen, and K. Xu,** "Preparation and Properties of New UV-curable Naphthyl Epoxy Acrylates", Journal of Functional Polymers, Vol. 19, No. 3، March 2010.

[34] **P. Cognard,** "Handbook of Adhesives and Sealants: General Knowledge, Application of Adhesives, New Curing Techniques", Elsevier Science, 2006.

[35] **S. Ebnesajjad,** "Handbook of Adhesives and Surface Preparation: Technology, Applications and Manufacturing", Elsevier Science, 2010.

[36] **P. Glöckner,** "Radiation Curing: Coatings and Printing Inks; Technical Basics, Applications and Trouble Shooting", Vincentz Network, 2008.

[37] **R. Sutherland, V. Tondiglia, L. Natarajan, P. Lloyd, and T. Bunning,** "Liquid Crystal Bragg Gratings for High-Brightness Spatial Light Modulators",

78

Proceedings of the society of photo-optical instrumentation engineers (SPIE) Newsroom, November, 2007.

[38] **R.L. Sutherland, V.P. Tondiglia, L.V. Natarajan, P.F. Lloyd, T.J. Bunning,** "Coherent Diffraction and Random Scattering in Thiol-Ene Based Holographic Polymer-Dispersed Liquid Crystal Reflection Gratings," Journal of Applied Physics, Vol. 99, No. 12, June 2006.

[39] **R. Kashyap, J. R. Armitage, R. W. Wyatt, S. T. Davey, and D. L. Williams,** "All-Fibre Narrow-Band Reflection Gratings at 1500 nm", Electron. Lett., Vol. 26, No. 11, PP. 730-731, 1990.

[40] **R. Kashyap**, "Fiber Bragg Gratings", Academic Press, 1999.

[41] **K. O. Hill, B. Malo, F. Bilodeau, D. C. Johnson, J. Albert,** "Bragg Gratings Fabricated in Monomode Photosensitive Optical Fiber by UV Exposure through a Phase Mask", Applied Physics Letters, Vol. 62, No. 10, PP. 1035-1037, 1993.

[42] **D. Z. Anderson, D. Z. Anderson, V. Mizrahi, T. Erdogan, A. E. White,** "Production of In-Fiber Gratings Using A Diffractive Optical-Element", Electronics Letters, Vol. 29, No.6, PP. 566-568, 1993.

[43] **Z. Xiong, G. D. Peng, B. Wu, and P. L. Chu,** "Effects of the Zeroth-Order Diffraction of a Phase Mask on Bragg Gratings", Journal of Lightwave Technology, Vol. 17, No. 11, PP. 2361-2365, Nov 1999.

[44] **Q. Zhang, D. A. Brown, L. Reinhart, T. F. Morse, J. Q. Wang, G. Xiao,** "Tuning Bragg Wavelength by Writing Gratings on Prestrained Fibers", IEEE Photonics Technology Letters, Vol. 6, No. 7, PP. 839-841, 1994.

[45] **B. Malo, K. O. Hill, F. Bilodeau, D. C. Johnson, and J. Albert,** "Point-by-Point Fabrication of Micro-Bragg Gratings in Photosensitive Fiber Using Single Excimer Pulse Refractive Index Modification Techniques", Electron. Let., Vol. 29, No. 18, PP. 1668-1669, 1993.

79

[46] **A. Al-dergazly, A. Fadhel,** "Investigation of Olive Oil as a New Photonic Liquid Crystal for Optical Communication Systems", World Scientific and Engineering Academy and Society (WSEAS) Stevens Point, Wisconsin, USA, 2010.

[47] **S. Serpil, S. G. Sumnu,**" Physical Properties of Food", Journal of Food Processing and Preservation, Vol. 31, No. 1, February 2007.

[48] **N. Siddiqui and A. Ahmad,** " A Study on Viscosity, Surface Tension and Volume Flow Rate of Some Edible and Medicinal Oils", International Journal of Science, Environment and Technology, Vol. 2, No. 6, 2013.

[49] **T. A. Berkoff and A. D. Kersey,** "Experimental Demonstration of a Fiber Bragg Grating Acceleration sensor", IEEE Photon. Technol. Lett., Vol. 8, No. 12, PP. 1677-1679, 1996.

[50] **B. Guan, H. Tam, S. Liu,** "Temperature- Independent Fiber Bragg Grating Tilt Sensor", IEEE Photon. Technol. Lett., Vol. 16, No.1, PP. 224-226, January 2004.

[51] **H. Sheng, M. Fu, T. Chen, W. Liu, and S. Bor,** "A Lateral Pressure Sensor Using a Fiber Bragg Grating", IEEE Photon. Technol. Lett., Vol. 16, PP. 1146-1148, April 2004.

[52] **S. C. Tjin, R. Suresh, and N. Q. Ngo,** "Fiber Bragg Grating Based Shear-Force Sensor: Modeling and Testing", IEEE J. Lightwave Technol., Vol. 22, No. 7, PP. 1728-1730, July 2004.

[53] **W. Thongnum, N. Takahashi, S. Takahashi,** "Temperature Stabilization of Fiber Bragg Grating Vibration Sensor", 15th Int. conf. on Optical Fiber Sensors, PP. 223-226, 2002.

[54] **A. N. Chryssis, S. M. Lee, S. B. Lee, S. S. Saini, M. Dagenais,** "High Sensitivity Evanescent Field Fiber Bragg Grating Sensor", IEEE Photon. Technol. Lett., Vol. 17, No. 6, PP. 1253-1255, June 2005.

[55] **J. E. Lenz,** "A Review of Magnetic Sensors", Proc. of the IEEE, Vol. 78, No. 6, PP. 973-989, 1990.

[56] **G. W. Day, D. N. Payne, A. J. Barlow and J. J. Ramskov-Hansen,** "Faraday Rotation in Coiled, Monomode Optical Fibers: Isolators, Filters, and Magnetic Sensors", Opt. Lett., Vol. 7, No.5, PP. 238-240, May 1982.

[57] **H. Okamura,** "Fiber-Optic Magnetic Sensor Utilizing the Lorentzian Force", IEEE J. Lightwave Technol, Vol. 8, No. 10, PP. 1558-1560, October 1990.

[58] **A. Yariv, H. V. Winsor,** "Proposal for Detection of Magnetic Fields Through Magnetostrictive Perturbation of Optical Fibers" Opt. Lett., Vol. 5, No. 3, PP. 87-89, March 1980.

[59] **N. Hartman, D. Vahey, R. Kidd, and M. Browning,** "Fabrication and Testing of a Nickel-Coated Single-Mode Fiber Magnetometer", Electron. Lett., Vol. 18, No. 5, pp. 224-226, 1982.

[60] **A. Dandridge, A. B. Tveten, G. H. Sigel, E. J. West and T. G. Giallorenzi,** "Optical Fiber Magnetic Field Sensors", Electron. Lett., Vol. 16, PP. 408-409, 1980.

[61] **A. Shakir, R.D. AL-Mudhafa and A. Al-Dergazly,** "Verdet Constant Measurement of Olive Oil for Magnetic Field Sensor ", International Journal of Advances in Electrical & Electronics Engineering, Vol. 2, No. 2, PP. 362-368, 2013.

[62] **Y. N. Ning, B. C. Chu and D. A. Jackson,** "Miniature Faraday Current Sensor Based on Multiple Critical Angle Reflections in a Bulk-Optic Ring", Optics Letters, Vol. 16, No. 24, PP. 1996-1998, 1991.

[63] **O. N. Mohammed and A. A. AL – Dergazly,**" Measurement the Fluorescence Parameters of the Olive Oil and Comparing it with Some Laser Dye Materials", Baghdad university, Journal of Engineering, Vol. 16, No.1, PP. 4527-4534, March 2010.
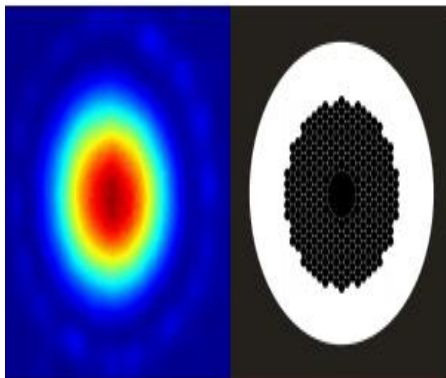
APPENDIX (A)

HCI9-I550

Hollow Core Photonic Bandgap Fiber

- < 3% of optical power located in silica
- Negligible bend loss
- Gaussian like fundamental mode

Hollow core Photonic Bandgap Fibers guide light in a hollow core, surrounded by a microstructured cladding of air holes and silica. Since only a small fraction of the light propagates in silica, the effect of material nonlinearities is insignificant and the fibers do not suffer from the same limitations on loss as conventional fibers made from solid material alone.

Specifications

Optical

Design wavelength	1550 nm
Attenuation @ 1550 nm	< 20 dB/km
Mode field diameter @ 1550 nm [1]	13 ± 2 μm
Operating wavelength [2]	1520-1600 nm

Applications

- Fiber optic gyroscopes
- Pulsed lasers (delivery and/or compression)
- Gas spectroscopy
- Low latency communication

Physical

Core diameter	20 ± 2 μm
Air filling fraction of the holey region	≥ 90 %
Diameter of the holey region	70 ± 5 μm
Outer cladding diameter	115 ± 3 μm
Coating diameter	220 ± 30 μm
Coating material	Single layer acrylate

1. Full $1/e^2$-width of the near field intensity distribution
2. Over which the attenuation is < 30 dB/km

A

APPENDIX (B)

405nm Purple Lasers
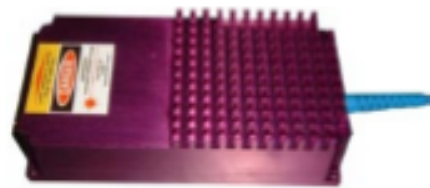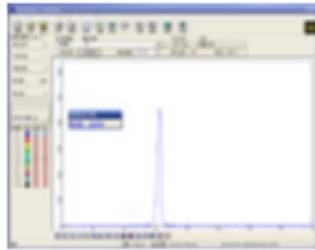
Specifications :

Model	SDL-405-XXXT
Wavelength (nm)	405±5nm
Output Power	1-100mW
Energy distributuon	Even
Beam spot	Round
Operating Mode	CW
Power Stability after warm-up	<1%, <3%, <5% (over 2/4/8 hours)
Warm-up time	< 5 minutes
Beam divergence, full angle (mrad)	8. 0mrad
Beam diameter at the aperture	2. 0mm
Beam height from base plate	24.8mm
Pointing stability after warm-up (mrad)	<0.05
Operating temperature (℃)	10~35℃
Power Supply	90-264VAC, 50/60Hz
Modulation	TTL Modulation or Analog Modulation
Expect life time	>10000 hours
Warranty time	1 year

APPENDIX (C)

2PCDC 4-6V hybrid 2 phase 4 wire Micro stepper motor diameter 15MM with screw SM15DD

Description

Motor diameter: 15 MM

Height: 9 MM motor

Secretary rod diameter: 3 MM

Secretary rod length: 52.5 MM

Motor type: 2 phase 4wire (hybrid)

voltage: DC 4-6V

C

APPENDIX (D)

```
#define step_pin 3
#define dir_pin 2
#define MS1 5
#define MS2 4
#define ld 9
int dir;
int steps =158 ;

void setup() {
  pinMode(MS1, OUTPUT);
  pinMode(MS2, OUTPUT);
  pinMode(dir_pin, OUTPUT);
  pinMode(step_pin, OUTPUT);
  pinMode(ld,OUTPUT);
  digitalWrite(MS1, LOW);
  digitalWrite(MS2, LOW);
  digitalWrite(dir_pin, HIGH);
}
void loop() {
while(steps>=0) {
     digitalWrite(step_pin, HIGH);
     delay(1000);
     digitalWrite(step_pin, LOW);
     delay(1000);
     digitalWrite(ld,HIGH);
     delay(180000);
     digitalWrite(ld,LOW);
     steps--;
  }
}
```

D

APPENDIX (E)

```
clear all; clc; close all
lamda_Bragg = 653.3551e-9;
L=0.038;
deltan=7.623e-6;
bitch=2.241250653e-7;
neff=1.45756812;
j(v)=0.995086161;
%      A=lamda_Bragg/(2*neff); neff=lamda_Bragg/(2*bitch);
lambda=(653.31e-9:0.0005e-9:653.4e-9);
%lambda=(1.0:0.1:1.5);
for i = 1:length (lambda);
%      beta(i)=(2*pi*neff)/lambda(i);
%      deltab(i)=beta(i)-(pi/bitch);
deltab(i) = 2*pi*neff*(1/lambda(i) - 1/lamda_Bragg) ;
k(i)=(pi/lambda(i))*deltan*j(v); gamma(i)=sqrt(k(i)^2-deltab(i)^2);
sinhp=sinh(gamma(i)*L);
coshp=cosh(gamma(i)*L);
% R(i)=abs(sinhp^2/(coshp^2-(deltab(i)^2/k(i)^2)));
R(i)=sinhp^2/(coshp^2-deltab(i)^2/k(i)^2);
end;
plot (lambda,R);
axis( [653.31e-9, 653.4e-9, 0, 1]);
hold on
plot (lambda,(1-R));
axis([653.31e-9, 653.4e-9, 0, 1]);
```

E

APPENDIX (F)

```
clear all; clc; close all
lamda_Bragg = 653.3551e-9;
L=0.098;
deltan=7.623e-6;
bitch=2.241250653e-7;
neff=1.45756812;
j(v)=0.995086161;
%       A=lamda_Bragg/(2*neff); neff=lamda_Bragg/(2*bitch);
lambda=(653.31e-9:0.0005e-9:653.4e-9);
%lambda=(1.0:0.1:1.5);
for i = 1:length (lambda);
%       beta(i)=(2*pi*neff)/lambda(i);
%       deltab(i)=beta(i)-(pi/bitch);
deltab(i) = 2*pi*neff*(1/lambda(i) - 1/lamda_Bragg) ;
k(i)=(pi/lambda(i))*deltan*j(v); gamma(i)=sqrt(k(i)^2-deltab(i)^2);
sinhp=sinh(gamma(i)*L);
coshp=cosh(gamma(i)*L);
% R(i)=abs(sinhp^2/(coshp^2-(deltab(i)^2/k(i)^2)));
R(i)=sinhp^2/(coshp^2-deltab(i)^2/k(i)^2);
end;
plot (lambda,R);
axis( [653.31e-9, 653.4e-9, 0, 1]);
hold on
plot (lambda,(1-R));
axis([653.31e-9, 653.4e-9, 0, 1]);
```

F

APPENDIX (G)

```
clear all; clc; close all
lamda_Bragg = 653.3555438e-9;
L=0.038;
deltan=8.613e-6;
bitch=2.241250653e-7;
neff=1.45756911;
j(v)=0.9950867987;
%      A=lamda_Bragg/(2*neff); neff=lamda_Bragg/(2*bitch);
lambda=(653.31e-9:0.0005e-9:653.4e-9);
%lambda=(1.0:0.1:1.5);
for i = 1:length (lambda);
%      beta(i)=(2*pi*neff)/lambda(i);
%      deltab(i)=beta(i)-(pi/bitch);
deltab(i) = 2*pi*neff*(1/lambda(i) - 1/lamda_Bragg) ;
k(i)=(pi/lambda(i))*deltan*j(v); gamma(i)=sqrt(k(i)^2-deltab(i)^2);
sinhp=sinh(gamma(i)*L);
coshp=cosh(gamma(i)*L);
% R(i)=abs(sinhp^2/(coshp^2-(deltab(i)^2/k(i)^2)));
R(i)=sinhp^2/(coshp^2-deltab(i)^2/k(i)^2);
end;
plot (lambda,R);
axis( [653.31e-9, 653.4e-9, 0, 1]);
hold on
plot (lambda,(1-R));
axis([653.31e-9, 653.4e-9, 0, 1]);
```

G

APPENDIX (H)

```
clear all; clc; close all
lamda_Bragg = 653.3565367e-9;
L=0.038;
deltan=10.828e-6;
bitch=2.241250653e-7;
neff=1.4575713250;
j(v)=0.9950882248;
%       A=lamda_Bragg/(2*neff); neff=lamda_Bragg/(2*bitch);
lambda=(653.31e-9:0.0005e-9:653.4e-9);
%lambda=(1.0:0.1:1.5);
for i = 1:length (lambda);
%       beta(i)=(2*pi*neff)/lambda(i);
%       deltab(i)=beta(i)-(pi/bitch);
deltab(i) = 2*pi*neff*(1/lambda(i) - 1/lamda_Bragg) ;
k(i)=(pi/lambda(i))*deltan*j(v); gamma(i)=sqrt(k(i)^2-deltab(i)^2);
sinhp=sinh(gamma(i)*L);
coshp=cosh(gamma(i)*L);
% R(i)=abs(sinhp^2/(coshp^2-(deltab(i)^2/k(i)^2)));
R(i)=sinhp^2/(coshp^2-deltab(i)^2/k(i)^2);
end;
plot (lambda,R);
axis( [653.31e-9, 653.4e-9, 0, 1]);
hold on
plot (lambda,(1-R));
axis([653.31e-9, 653.4e-9, 0, 1]);
```

H

APPENDIX (I)

```
clear all; clc; close all
lamda_Bragg = 653.3582e-9;
L=0.038;
deltan=14.985e-6;
bitch=2.241249966e-7;
neff=1.457575482;
j(v)=0.9950909022;
%      A=lamda_Bragg/(2*neff); neff=lamda_Bragg/(2*bitch);
lambda=(653.31e-9:0.0005e-9:653.4e-9);
%lambda=(1.0:0.1:1.5);
for i = 1:length (lambda);
%      beta(i)=(2*pi*neff)/lambda(i);
%      deltab(i)=beta(i)-(pi/bitch);
deltab(i) = 2*pi*neff*(1/lambda(i) - 1/lamda_Bragg) ;
k(i)=(pi/lambda(i))*deltan*j(v); gamma(i)=sqrt(k(i)^2-deltab(i)^2);
sinhp=sinh(gamma(i)*L)
coshp=cosh(gamma(i)*L);
% R(i)=abs(sinhp^2/(coshp^2-(deltab(i)^2/k(i)^2)));
R(i)=sinhp^2/(coshp^2-deltab(i)^2/k(i)^2);
end;
plot (lambda,R);
axis( [653.31e-9, 653.4e-9, 0, 1]);
hold on
plot (lambda,(1-R));
axis([653.31e-9, 653.4e-9, 0, 1]);
```

الخلاصة

تم في هذا البحث تصنيع أربعة ألياف براك المحززة وذلك بحقنها بمختلف الاحجام من السوائل (المادة الصمغية البصرية star line Glass Mechanix ، زيت الزيتون مذوب مع الايثانول) بداخل الجوف لتلك الالياف البلورية الفوتونية ((Thorlab company) HC19–1550). تقنية تداخل تقسيم السعة مع منصة انتقالية مصممة خصيصاً وبدقة عالية أستخدمت في عملية التصنيع. التصنيع تم بأستخدام ليزر أزرق يعمل عند الطول الموجي ٤٠٥ نانو متر. الألياف البلورية الفوتونية الأربعة المحقونة تم تعريضها لأشعة الليزر الأزرق ذو الطول الوجي ٤٠٥ نانو متر مُكونة اهداباً متكررة بشكل دوري لتوليد حزوز براك. هذه الأهداب تولدت من تداخل شعاعي الليزر الأزرق المنقسمين ذوي الطول الموجي ٤٠٥ نانو متر. طول البراك المصنع لليف يساوي ٣.٨ سم و معدل فترة الحزوز تساوي ٠,٢٢٤ مايكرو متر.

الألياف الأربعة تم تحليلها بوساطة المجهر البصري والذي أظهر المناطق التي تمت معالجتها بأستعمال الليزر الأزرق. الألياف المصنعة تم فحصها أيضاً عن طريق وضع ليزر عند احدى نهايتي الليف وقياس النفاذية عند النهاية الأخرى بأستخدام مُحلل الأشارة البصرية (Thorlabs–CCS200). ألياف براك المحززة صُنعت عند الطول الموجي ٦٥٣.٣ نانو متر. وكذلك أظهرت النتائج أن الليف ذي الحجم الأعلى من زيت الزيتون يمتلك أعلى قمة أنعكاسية حوالي ٩٦,٠٩٦٤٧% نانو متر و أكبر عرض كامل عند الحد الأعلى للمنتصف حوالي ٠,٧٤ نانو متر.

ثلاثة من الألياف المصنعة (PCF (B, C, and D والتي تحتوي على زيت الزيتون تم فحصها كمُتحسس للمجال المغناطيسي. أظهرت النتائج بأن كل الألياف تتحرك نحو الأشعة تحت الحمراء القريبة. وكذلك أظهرت النتائج بأن الليف ذي الحجم الأعلى من زيت الزيتون يمتلك أعلى تحسس مغناطيسي في الطول الموجي حوالي ٦٥٣.٤ نانو متر، أعلى الألياف حساسية بمقدار ٠.٠٠٠٤٩٤٦٢٣٦٥٦ نانو متر اجاوس،

أعلى قمة أنعكاسية حوالي ٩٦,٩١٨٢٧% نانو متر و أكبر عرض كامل عند الحد الأعلى للمنتصف حوالي

٠,٩٨ نانو متر .

وزارة التعليم العالي والبحث العلمي

جامعة النهرين/ كلية الهندسة

تصنيع ألياف براك المحززة بأستخدام الألياف البلورية الفوتونية المجوفة المحقونة

رسالة مقدمة

الى قسم هندسة الليزر والألكترونيات البصرية في جامعة النهرين

وهي جزء من متطلبات نيل شهادة ماجستير علوم

في

هندسة الليزر والألكترونيات البصرية

من قبل

فرح سالم حنش علي

(بكالوريوس، ٢٠١٤)

<table>
<tr><td>ربيع الثاني</td><td>١٤٣٨</td></tr>
<tr><td>كانون الثاني</td><td>٢٠١٧</td></tr>
</table>